Title
Design, Synthesis, and Evaluation of Next Generation Technologies in Stimulus-Responsive Materials and Organic Electronics

Author
Unruh, Jr, David Allen

Publication Date
2011

Peer reviewed|Thesis/dissertation

Design, Synthesis, and Evaluation of Next Generation Technologies in Stimulus-Responsive Materials and Organic Electronics

by

David Allen Unruh, Jr.

A dissertation submitted in partial satisfaction of the

requirements for the degree of

Doctor of Philosophy

in

Chemistry

in the

Graduate Division

of the

University of California, Berkeley

Committee in charge:

Professor Jean M. J. Fréchet, Chair
Professor Peter Vollhardt
Professor Costas Grigoropoulos

Fall 2011

Design, Synthesis, and Evaluation of Next Generation Technologies in Stimulus-Responsive Materials and Organic Electronics

by

David Allen Unruh, Jr.

Abstract

Design, Synthesis, and Evaluation of Next Generation Technologies in Stimulus-Responsive Materials and Organic Electronics

by

David Allen Unruh, Jr.

Doctor of Philosophy in Chemistry

University of California, Berkeley

Professor Jean M. J. Fréchet, Chair

Future advancements in technology are fundamentally limited by materials research and development. New materials are most often found by exploring new chemistries, but the nature of these chemistries can vary widely. This dissertation is a compilation of some of the chemical insights that can lead to the development of new stimulus-responsive materials and organic electronics.

For example, a tool that can consistently display specific, precise types of reactivity can have dramatic effects on the ability to make never-before seen materials. Chapter 1 discusses a multifunctional mixed monolayer resist for scanning probe nanolithography that can respond to two different electrochemical stimuli to produce two chemically different products, each with nanoscale resolution. The synthesis of a novel reductively active monolayer precursor, the preparation of this mixed monolayer surface, and its use in a proof-of-principle bottom-up assembly of complementary semiconductor components are described.

A combination of older chemistries can result in the development of new materials as well. In Chapter 2, the synthesis of a thermally-triggered single component epoxy monomer is described. A small library of these monomers is prepared, and structure-property relationships are established between monomer molecular structure and cure temperature, enthalpy of cure, and glass transition temperature. In addition, effects of cure on the production of voids in the fully cured thermosetting polymer are investigated.

New materials can also be made by altering the way other materials pack together, as commonly found in supramolecular chemistry. Chapter 3 discusses the pre-organization of small molecules into nanoscale crystalline domains as a means to establishing long range order in organic electronics. A small molecule previously used in bulk heterojunciton organic photovoltaics is shown to make high aspect ratio nanowires through solution-phase nanocrystal synthesis, and the degree of crystallinity and device performance in organic field effect transistors are compared to the same molecule cast as a thin film. In addition, different derivatives of the same molecule are evaluated for their ability to pack differently in the solid state.

Finally, new materials can be inspired by the limitations of existing materials and the challenges of an emerging technology. Chapter 4 introduces a new thienooxypyrroline acceptor

building block for donor-acceptor materials in organic photovoltaics and organic field effect transistors. The synthetic sequence to access this chromophore is described, and a small library of thienooxypyrroline monomers are prepared. Small molecules and polymers using these monomers are synthesized and shown to have promising device performance characteristics in preliminary testing of both OPVs and OFETs. Based upon the device data, possible next steps are presented for use of this building block in future materials for organic electronics.

Table of Contents

Acknowledgements

During my four years at UC Berkeley, I've grown substantially as a scientist. I don't think any other group could have offered me both the guidance and independence I needed to get where I am today. I would like to thank Professor Fréchet for seeing enough potential in me to allow me to join his group. His hands-off approach to running a group allowed me to develop as an independent scientist.

I would like to thank Marco Rolandi, Stefan Pastine, and Kyle Broaders for being my de facto mentors throughout my time at UC Berkeley. From Marco I learned how to formulate a research project. Stefan taught me how to work efficiently, and the importance of asking the seemingly obvious questions. Kyle was a constant reminder how critical intellectual curiosity is to a scientist's development.

I'd like to thank Mark Chen for his leadership and the work that we've accomplished together, much of which will carry on after I leave Berkeley. It wasn't until Mark Chen joined the group that I learned the benefits of working as a member of a team.

I'd also like to thank Jessie Moreton, my excellent undergraduate researcher, for her hard work, her enthusiasm, her fortitude, and her friendship.

I'd particularly like to thank my wife Callie for her unwavering support, love, faith, and patience.

I'd like to thank Kevin Cantrell, professor of chemistry at the University of Portland, for inspiring me to pursue a career in science.

Thanks to all the friends that I've gained over the past four years for their support, their camaraderie, and for giving me something to think about other than chemistry. I hope you can visit me in Arizona.

Finally, I'd like to thank my parents and my sister, who have helped shape me into the person I am today. My accomplishments are as much yours as they are mine.

Chapter 1
Bifunctional Patterning of Mixed Monolayer Surfaces using Scanning Probe Lithography for Multiplexed Directed Assembly

Abstract

The ability to pattern a surface multifunctionally with spatial resolution is of significant interest to a variety of fields. Herein we describe a scanning probe based patterning method where a dense electrochemically active mixed monolayer, through modulation of the applied surface bias, can be patterned to impart two different orthogonal surface-bound functional handles through two different electrochemical pathways. One such pathway results in localized patterns that exhibit chemistry typical of amines, and the other pathway coincides with the local anodic oxidation chemistry demonstrated in the literature. Each of these handles can be used individually to constructively interact with molecules and nano-objects to form regions of locally deposited materials. Used together, both patterns can be used to direct the assembly of complementary molecules to make complex nanoarchitectures.

Introduction

The development of methods for the production of substrates with different spatially-resolved functionalities is highly desirable as their impact may range from semiconductor fabrication to biology.[1,2] Surface-bound functionalities can serve as templates for the directed assembly of molecules or nano-objects, allowing the bottom-up fabrication of sensors, arrays, and devices. Several multicomponent patterning strategies have been reported including orthogonal solvent treatments, plasma treatments, photolithography, and capillary force lithography.[3-6] An issue with some of these techniques is that they may not extend to the sub-100 nm feature size regime or may require harsh treatments or complicated syntheses. The use of scanning probe lithography (SPL) for nanoscale patterning is attractive because it allows high resolution direct-write patterning,[7] real-time imaging of patterns, serial on-chip patterning of multiple functionalities, as well as mild processing conditions. We have previously reported a SPL technique for the local deprotection of surface-bound amines that utilized the electric field produced by a positively-biased sample and a grounded atomic force microscope (AFM) tip.[8,9] The ability to pattern a second functionality chemically distinct from amines in the same AFM patterning step would allow the assembly of complementary combinations of molecules with sub-100 nm features. Herein we report an electrochemically-based SPL method where depending upon the surface bias applied (Figure 1.1a), a redox-sensitive surface-bound molecule can be electrochemically reduced to yield an amine, or the surface can be locally oxidized to produce an oxygen-rich species.

It has long been established that the nanoscale water meniscus that forms between the surface and the tip of the scanning probe can mediate the controlled transfer of molecules from tip to surface,[10] the localized oxidation of both inorganic and organic surfaces,[11-14] and the electrochemical reduction of metals.[15] In comparison to oxidative methods, reductive SPL methods are not as extensively investigated. We envisioned that through careful monolayer design, we could use this water meniscus as a "nanoscale electrochemical cell," capable of performing local surface oxidation or reduction depending upon the patterning conditions. To this end, we designed a triethoxysilane derivative (**1**) featuring a redox-active trimethylbenzoquinone moiety. Benzoquinones have been exploited in a number of nonspecific

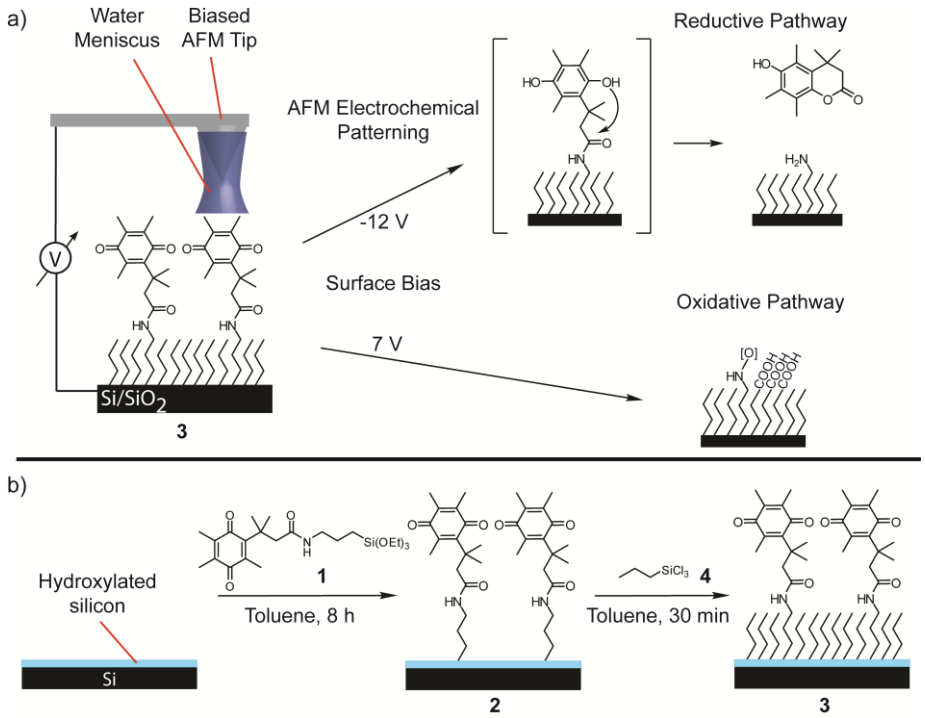

Figure 1.1. a) Schematic of orthogonal AFM patterning on the benzoquinone/propyltrichlorosilane mixed monolayer **3.** b) Syntheses of benzoquinone-modified surface **2** and mixed monolayer **3**. Reprinted with permission from Unruh et al. *J. Am. Chem. Soc.* **2010**, *132,* 6890. Copyright 2010 American Chemical Society.

surface reduction strategies.[16-18] Amine patterns could thus be generated in monolayers based on **1** via the local reduction and subsequent lactonization of the departing benzoquinone moiety under the stimulus provided by the AFM tip.

Results and Discussion

Figure 1.1b summarizes the reductively active surfaces used and their preparation. Benzoquinone-modified surface **2** had a typical thickness of 0.63 ± 0.27 nm as measured by ellipsometry, and a contact angle of 70 ± 4°. In line with the reduction of other trimethylbenzoquinone-based surfaces,[17] irreversible blanket reduction of **2** was demonstrated using cyclic voltammetry (CV, Figure 1.2). Support for this blanket modification was provided by surface contact angle measurements both before and after CV reduction. The contact angle after reduction (55°) approaches that of an amine-terminated monolayer (51°). The surface coverage of **1** on surface **2** calculated from CV data amounted to roughly 18% of available Si(100) surface binding sites. Such low coverage results from steric interactions between the relatively bulky trimethylhydroquinone groups of **1**.

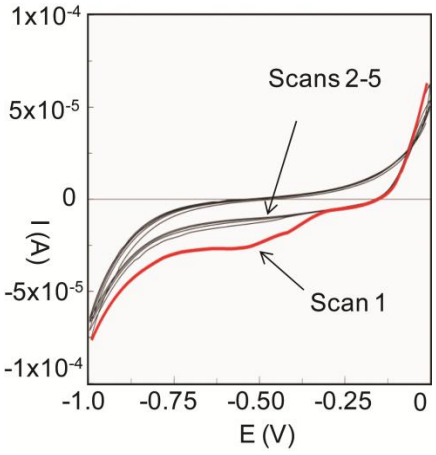

Figure 1.2. Cyclic voltammogram of **2**. 5 successive scans are shown, each at a rate of 100 mV/s with potentials relative to Ag/AgCl. Reprinted with permission from Unruh et al. *J. Am. Chem. Soc*. **2010**, *132,* 6890. Copyright 2010 American Chemical Society.

Having confirmed macroscopic reduction, we next investigated SPL on **2**. Patterning experiments were performed in contact mode with doped silicon tips in an

environment with 70 ± 5% relative humidity. The grounded tip was translated across the surface at a speed of 1–4 μm/s with a -12 V bias applied to the surface and lateral force microscopy was used to verify surface modification. The darkened vertical lines of Figure 1.3a have a width of about 80 ± 4 nm and correspond to the modified areas. The vertical deflection of the tip does not change while patterning and the corresponding post-patterned topography images do not show significant height changes; therefore, it is unlikely that the observed lines are due to scratching of the substrate. The difference in reduction bias between SPL and CV may be due to the lack of a supporting electrolyte in the water meniscus during SPL. The width of the patterned lines was found to depend upon several factors including relative humidity, applied surface bias, and patterning speed (Figure 1.4). In addition, microscale patterning was also achievable using electrically conductive copper grids,[19] and the lateral force microscopy image of Figure 1.3b clearly shows pattern transfer from the grid to the substrate. It is important to note that no evidence of patterning was observed under dry conditions (relative humidity < 5%). This suggests that an electrochemical process is responsible for patterning, in contrast to other high electric field-based SPLs on organic monolayers.[8,9,20]

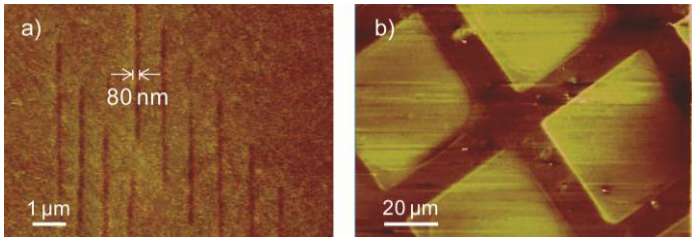

Figure 1.3. Lateral force microscopy images of a) SPL patterned, and b) copper grid patterned surfaces. Reprinted with permission from Unruh et al. *J. Am. Chem. Soc.* **2010**, *132,* 6890. Copyright 2010 American Chemical Society.

These patterned areas can act as templates for the direct assembly of various nano-objects through both ionic and covalent chemistries. For example, incubation of surfaces patterned either by SPL, shown in Figure 1.5, or on the microscale (Figure 1.6) in a solution of C_{60} provided raised regions ca. 0.8 nm in height, or close to the expected diameter of an amine-linked fullerene (1 nm). These assembled features withstood 3 days of Soxhlet extraction in toluene, as would be expected for covalent binding. Placing the patterned substrates in a solution of a pentathiophene butyric acid chloride **5** and a carboxyl-terminated generation-3 benzyl ether dendron **6** also resulted in raised lines corresponding roughly to the height of the newly attached molecule (Figure 1.5). The lines formed by assembly of the dendron onto the amine are stable to repeated washings with water, but they can be disrupted by immersion in a 1 M NaCl solution or removed entirely with 1 M aqueous acetic acid. Collectively, these results indicate that the electrochemically reduced regions display typical amine chemistry.

Having successfully demonstrated the ability to reductively pattern the benzoquinone-modified surface, we next turned our attention towards oxidative patterning of the same surface. Initial attempts with existing AFM-based oxidative methods[11,13] were unsuccessful as the underlying Si(100) was oxidized instead of the monolayer itself, resulting in SiO_2 patterns that are not amenable toward directed assembly. This observation was rationalized by the incomplete passivation of the underlying Si(100) due to the low coverage of the surface with **1**. To better passivate the surface, the initial benzoquinone-modified surface was treated with propyltrichlorosilane **4** to "backfill" the exposed Si(100) binding sites. Propyltrichlorosilane has a carbon chain length similar to that of the tether of **1**, thus, it was expected that a mixed monolayer consisting of **1** and **4** would be sufficiently dense to facilitate constructive oxidative patterning while still rendering the benzoquinone reductively active.

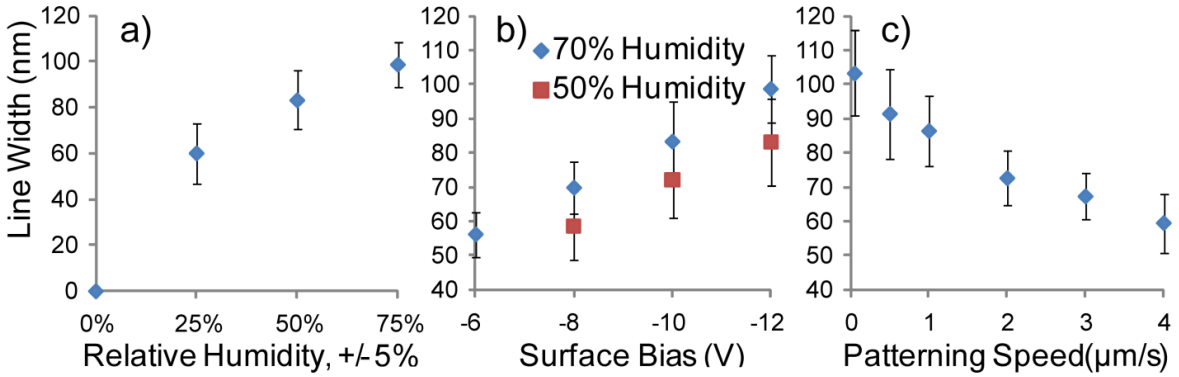

Figure 1.4. Influence of patterning parameters on line widths, measured by lateral force microscopy. a) Relative humidity, with surface bias = -12 V and tip speed = 1 μm/s; b) Surface bias, with tip speed = 1 μm/s; and c) Tip speed, with surface bias = -12 V and relative humidity = 70%. Reprinted with permission from Unruh et al. *J. Am. Chem. Soc.* **2010**, *132*, 6890. Copyright 2010 American Chemical Society.

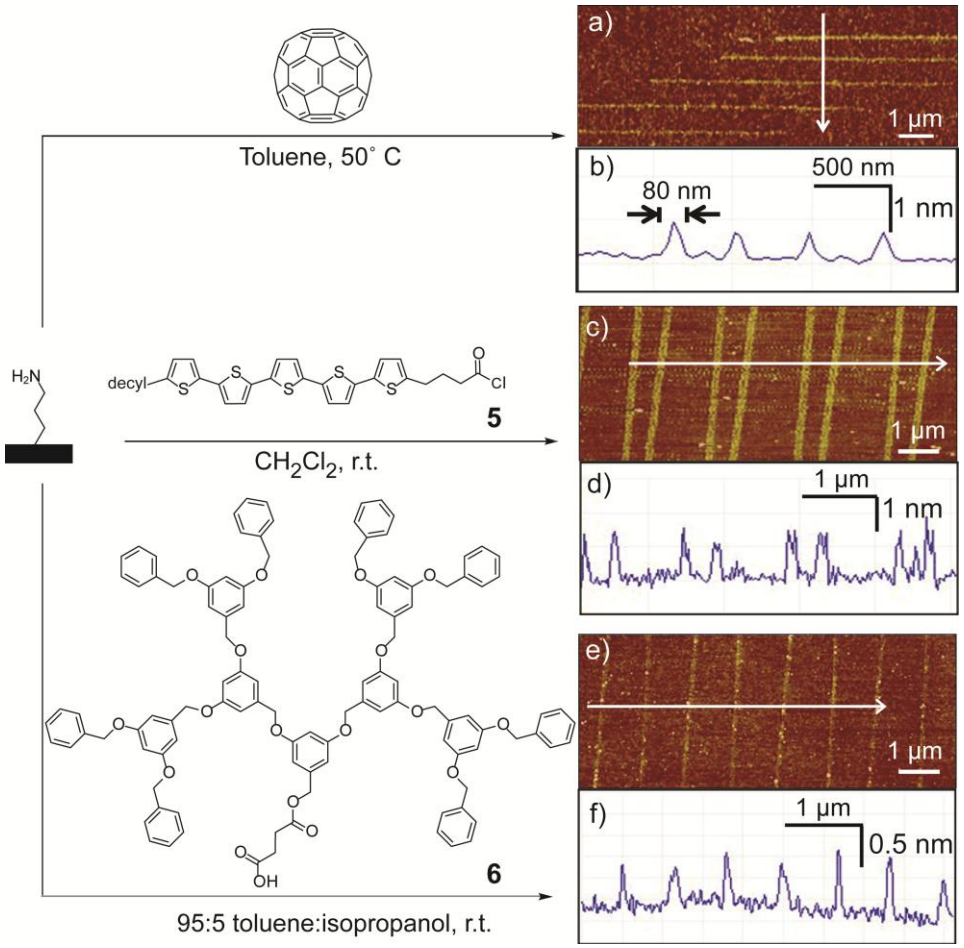

Figure 1.5. Directed assemblies of selected molecules onto the patterned amine. AFM topography images and line profiles of a) and b), C_{60}; c) and d), pentathiophene butyric acid chloride **5**; e) and f) generation 3 benzyl ether dendron **6**. White arrows on images correspond to region appearing on line profile. Reprinted with permission from Unruh et al. *J. Am. Chem. Soc.* **2010**, *132*, 6890. Copyright 2010 American Chemical Society.

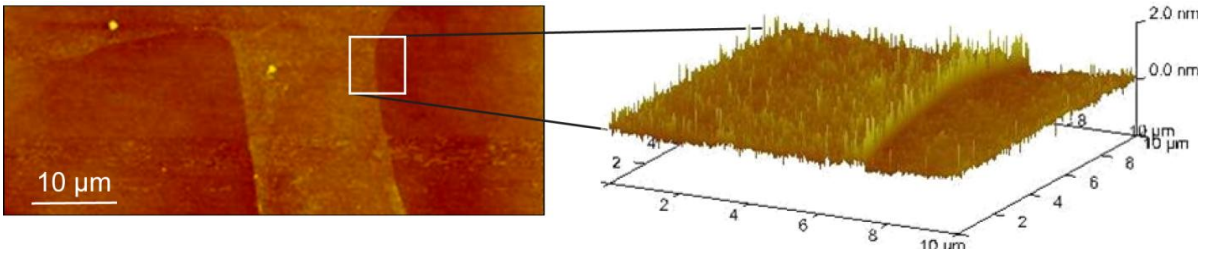

Figure 1.6. AFM topography image and 3D profile of **2**, patterned with copper grids and assembled with C_{60}. 3D profile corresponds to region within the white square of the topography image. Z axis of topography imgae = 10 nm. Reprinted with permission from Unruh et al. *J. Am. Chem. Soc.* **2010**, *132*, 6890. Copyright 2010 American Chemical Society.

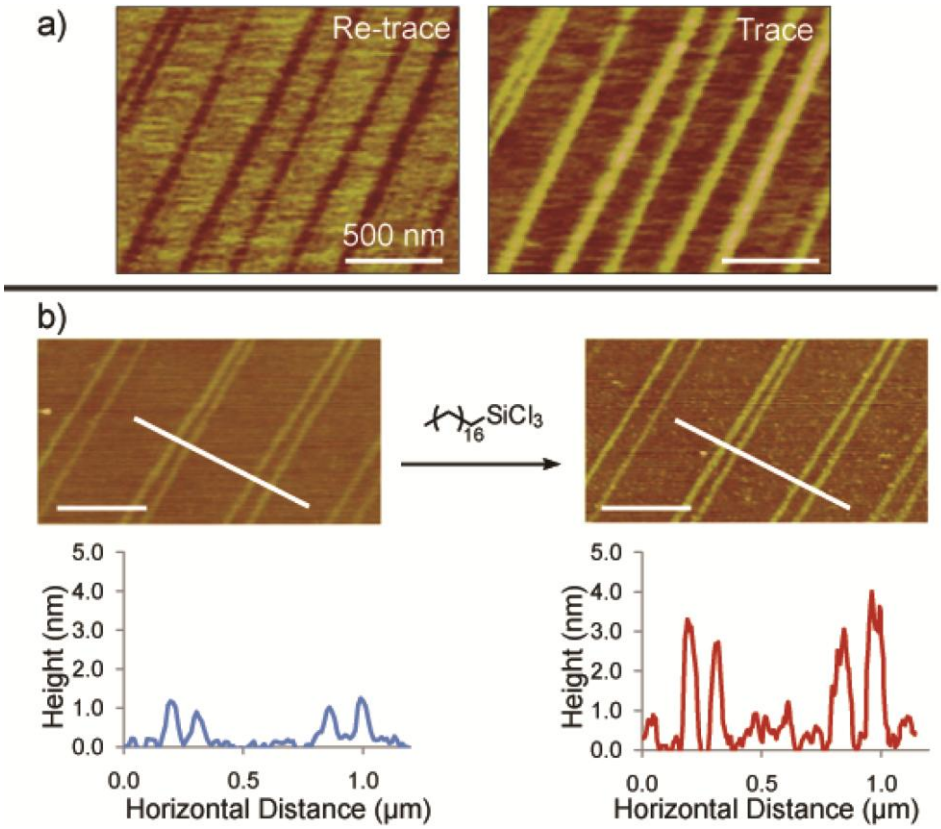

Figure 1.7. Oxidative patterning and directed assembly on mixed monolayer **3**. a) Contact mode height images of lines with re-trace and trace images taken simultaneously. Z-axis = 10 nm. b) Tapping mode height images of lines both before and after directed assembly with octadecyltrichlorosilane, with corresponding line profiles below. All lines drawn at 7 V, 1 µm/s tip speed, and 70% relative humidity. Reprinted with permission from Unruh et al. *J. Am. Chem. Soc.* **2010**, *132*, 6890. Copyright 2010 American Chemical Society.

Consistent with propyltrichlorosilane modification, the mixed monolayer **3** was thicker (0.75 ± 0.24 nm) and had a substantially increased contact angle (92 ± 4°) relative to surface **2**. Evidence for constructive oxidation of the alkane-based monolayer was provided by replication of a common contact mode imaging artifact encountered for oxidized organic monolayers (Figure 1.7a)[21] in addition to the reactivity of the oxidized patterns to chlorosilanes, which afforded raised lines roughly corresponding to the length of the molecule (Figure 1.7b). Together, these results indicate constructive oxidation of the alkane-based monolayer to oxygen-

rich functionalities such as carboxylic acids in preference to oxidation of the underlying silicon to SiO_2.

Because the combination of oxidative and reductive patterns on **3** generated two orthogonal functionalities on the same surface, the directed assembly of two different molecules through bifunctional patterning could be attempted as shown in Figure 1.8. Therefore, a pentathiophene dimethylchlorosilane **7** was assembled on the oxidized patterns, while C_{60} was assembled onto the reduced patterns. The observed height difference of ~2.5 nm between **5** and C_{60} corresponds to the difference in size of the two different objects. Directed assembly of both p-type and n-type materials on the same surface highlights the possibility of the surface assembly of complementary heterogeneous structures in the construction of more complex nanoarchitectures.

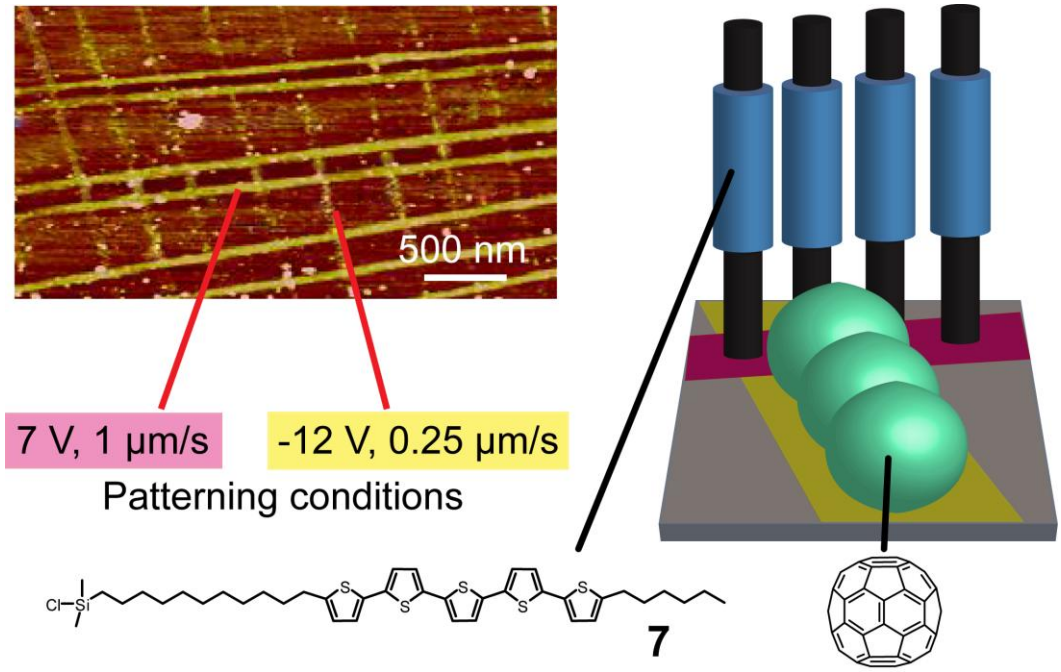

Figure 1.8. Multiplexed directed assembly onto bifunctionally patterned 3. Left: AFM height image, Z-axis = 10 nm. Right: graphical representation of assembled surface, where C_{60} is deposited on the reductive patterns (-12 V, 0.25 μm/s) and **7** is deposited on the oxidative patterns (7 V, 1 μm/s). All patterns drawn at 70% relative humidity. Reprinted with permission from Unruh et al. *J. Am. Chem. Soc.* **2010**, *132*, 6890. Copyright 2010 American Chemical Society.

Conclusions

We have developed a patterning methodology using SPL that enables the patterning in a single lithography session of two different functionalities into the same surface for subsequent use as separate templates in directed assembly. The sub-100 nm feature sizes of both the reductive and oxidative lines are some of the smallest to date for a bifunctional system. Bifunctional patterning strategies may provide a general platform for application in hybrid top-down/bottom-up fabrication, in the directed surface-based construction of elegant supramolecular assemblies,[22,23] or for the production of sensors and devices that may require complementary combinations of organic or inorganic materials.

Experimental

Materials. All reagents were obtained from commercial sources and used without further purification unless otherwise noted. All solvents used were reagent grade (99.9%) unless otherwise noted. THF was purchased from Fisher and vigorously purged with nitrogen for 1h. The solvent was further purified by passing it under nitrogen pressure through two packed columns of neutral alumina. Toluene and dichloromethane were purified under argon by passing through two columns of neutral alumina on a commercial apparatus. Thionyl chloride was distilled from a 5:1 mixture of thionyl chloride to quinoline to remove acidic impurities. All reactions were performed under dry N_2 unless otherwise noted. Water was purified using a Barnstead NANOpure Diamond purification system. All solutions to be used in surface modifications were filtered through Whatman Anotop 10 0.1µm membrane filters before use.

Characterization. Elemental analysis and high resolution fast atom bombardment mass spectroscopy (FAB-HRMS) were performed by the UC Berkeley mass spectroscopy and analytical facilities. ^{1}H and ^{13}C NMR measurements were conducted on a Bruker AVQ-400 nuclear magnetic resonance spectrometer. Surface contact angles were measured on a Krüss Model G10 goniometer at room temperature and ambient relative humidity. Ellipsometry measurements were performed with a Micro Photonics, Inc. PhE-101 Discrete Wavelength Ellipsometer. All atomic force microscopy was performed using a Digital Instruments (Veeco) Multimode AFM with a Nanoscope V controller and TAP 300 tips for tapping mode, and ESP tips for contact mode. Contact angle and ellipsometry values are reported as averages of 3 measurements. Cyclic voltammetry was performed with a Solartron 1285 potentiostat with CorrWare software. Surfaces were immersed in dry acetonitrile under inert environment with 1 M tetrabutylammonium tetrafluoroborate as a supporting electrolyte. Monolayer densities were calculated by integrating the area under the reduction curve in the cyclic voltammogram, converting to number of molecules through a stoichiometric ratio of 2 e- to 1 molecule, dividing by electrode surface area and normalized to the average experimental surface density of Si-OH (~4.8/nm^2).

Sample Preparation

General. A silicon (100) wafer was first cut into ca. 10x10 mm squares and microscopic markers were made using a diamond scribe in proximity of the patterns to allow realignment and imaging of the areas after the samples were patterned. The sample was then rinsed in toluene, acetone, and isopropanol, and blown dry with a stream of nitrogen. Native oxide was etched away with 48% HF, followed by two rinses and sonication in water. After drying the samples with a stream of nitrogen, the surface was functionalized using a Harrick Plasma PDC-32G plasma cleaner. The oxidized silicon substrate was then transferred to the corresponding solution for precursor deposition. Carboxyl-terminated third-generation benzyl ether dendron **6** and pentathiophene dimethylchlorosilane **7** were prepared according to previously published procedures.[24,25]

3-Aminotriethoxysilane (APTES). SAM formation was accomplished by chemical vapor deposition at room temperature, where hydroxylated samples were placed in a covered Petri dish with an uncovered cap containing ca. 5 mL APTES. After 30 min, the samples were removed, rinsed with acetone, isopropanol, and water, blown dry with a stream of nitrogen, and placed in a vial for characterization and patterning.

*Benzoquinone-modified surface **2**.* Hydroxylated samples were immersed in a 1 mg/mL solution of **1** in toluene under nitrogen at room temperature. After 8 hours, the surface was rinsed with

toluene, acetone, and isopropanol, blown dry with a stream of nitrogen, and placed in a clean vial for characterization/patterning.

*Benzoquinone/propyltrichlorosilane mixed monolayer **3***. Previously synthesized surfaces of **2** were immersed in a 5 mg/mL solution of propyltrichlorosilane in toluene at room temperature. After 30 minutes, the surface was sonicated in clean toluene, rinsed in toluene, and blown dry with a stream of nitrogen.

Patterning

AFM Nanopatterning. Reductive lines were drawn in contact mode, with a -12 V bias applied to the substrate and a grounded tip, at a tip speed of 1 μm/s. Humidity was controlled by monitoring the ratios of wet and dry nitrogen present within an atmospheric chamber which encased the AFM head. Typical humidity while patterning was 50 ± 5%.

Copper Grid Patterning. Patterns were generated by first exposing one side of the grid to steam for 15 s, followed by placing the grid against the substrate and sandwiching the two between two electrodes. A -17 V bias was applied to the substrate while grounding the grid for 45 s.

Post-patterning Modification

Immediately after patterning, samples were briefly rinsed with toluene to remove any free lactone, and then dried with a stream of nitrogen. The sample was then placed in the corresponding deposition solution below.

C_{60}. Samples were placed in a solution of 1 mg/mL C_{60} in toluene at 50° C. After 8 hours, the surface was sonicated in toluene for ca. 30 sec, blown dry with a stream of nitrogen, and returned to the AFM for imaging.

*Pentathiophene butyric acid chloride (**5**).* Samples were placed in a 0.25 mg/mL solution in dry CH_2Cl_2 under inert atmosphere at room temperature. After 8 hours, the surface was sonicated in clean CH_2Cl_2 for ca. 30 sec, rinsed with toluene, blown dry with a stream of nitrogen, and returned to the AFM for imaging.

*Carboxyl-terminated generation-3 benzyl ether dendron (**6**).* Samples were placed in a solution of 1 mg/mL **6** in 95:5 toluene:isopropanol at room temperature. After 8 hours, the surface was sonicated in toluene for ca. 30 sec, blown dry with a stream of nitrogen, and returned to the AFM for imaging.

*Pentathiophene dimethylchlorosilane (**7**).* Samples were placed in a solution of 0.25 mg/mL **7** in dry toluene under inert atmosphere at room temperature. After 8 hours the surface was sonicated in clean toluene for ca. 30 sec, rinsed with toluene, blown dry with a stream of nitrogen, and returned to the AFM for imaging.

Synthesis of Benzoquinone Monolayer Precursor 1.

Scheme 1 describes the synthetic procedure for making the electroactive benzoquinone monolayer precursor used for all patterning reactions. A 2,3,5-trimethylhydroquinone was treated with dimethylacrylic acid under Friedel-Crafts conditions for yield the corresponding lactone. This was oxidized to the quinone acid using N-bromosuccinimide, activated with N-hydroxysuccinimide, and finally coupled with 3-aminopropyltriethoxysilane to yield **1**.

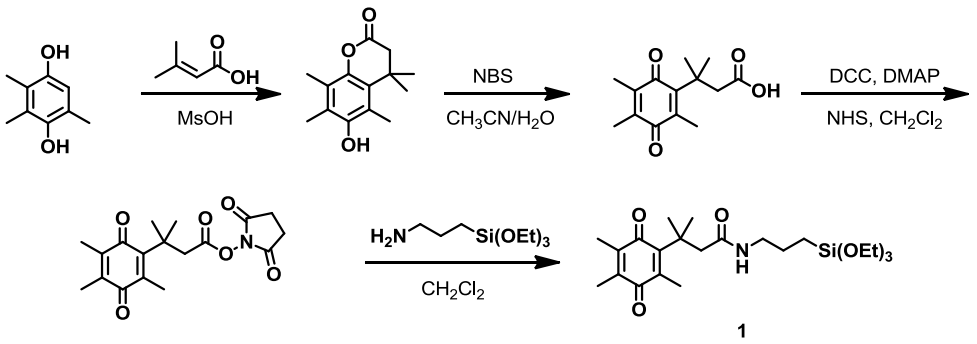

Scheme 1.1. Synthesis of Benzoquinone Monolayer Precursor **1**.

N-(3-Triethoxysilanyl)-3-methyl-3-(2,4,5-trimethyl-3,6-dioxocyclohexa-1,4-dienyl) Butanamide (**1**). To a solution of 3-methyl-3-(2,4,5-trimethyl-3,6-dioxocyclohexa-1,4-dienyl)butanoic acid, N-hydroxysuccinimidyl ester[26] (200 mg, 0.576 mmol) in CH_2Cl_2 (20 mL) was added 3-aminopropyltriethoxysilane (0.285 mg, 1.29 mmol) dropwise, with the resulting reaction mixture stirred overnight at room temperature under inert atmosphere. Solvent was evaporated and the mixture was purified by silica gel chromatography using a 1:1 ethyl acetate:CH_2Cl_2 eluent. Solvent was evaporated to yield 195.3 mg (75%) of a yellow solid. MP: 69.5-70.6° C. ^{1}H NMR (400 MHz, $CDCl_3$) δ 0.579 (t, 2H, J = 8.0 Hz), 1.22 (t, 9H, J = 6.8 Hz), 1.42 (s, 6H), 1.52 (pent, 2H, J = 7.6 Hz), 1.95 (s, 3H), 1.98 (s, 3H), 2.12 (s, 3H), 2.79 (s, 2H), 3.16 (q, 2H, J = 6.5 Hz), 3.82 (q, 6H, J = 7), 5.66 (br s, 1H). ^{13}C NMR (100 MHz, $CDCl_3$) δ 7.67, 12.1, 12.7, 14.0, 18.3, 22.8, 28.8, 38.2, 41.6, 49.3, 58.4, 137.3, 137.7, 143.7, 153.6, 171.6, 187.6, 191.2. IR 3300, 3021, 1640, 1594 cm-1. Calcd: $[M]^+$ ($C_{23}H_{39}NO_6Si$) m/z = 453.64. Found FAB-HRMS $[M]^+$ m/z = 453.2547. Anal. Calcd. for $C_{23}H_{39}NO_6Si$: C, 60.89; H, 8.67; N, 3.09. Found: C, 61.18; H, 8.76; N, 3.18.

Synthesis of pentathiophene butyric acid chloride 5.

The target pentathiophene acid chloride was prepared (Scheme 1.2) from the corresponding benzyl ester. Saponification of the ester with potassium hydroxide yielded the potassium carboxylate salt, which was dried and directly converted to the acid chloride with thionyl chloride to avoid acidic reaction conditions.

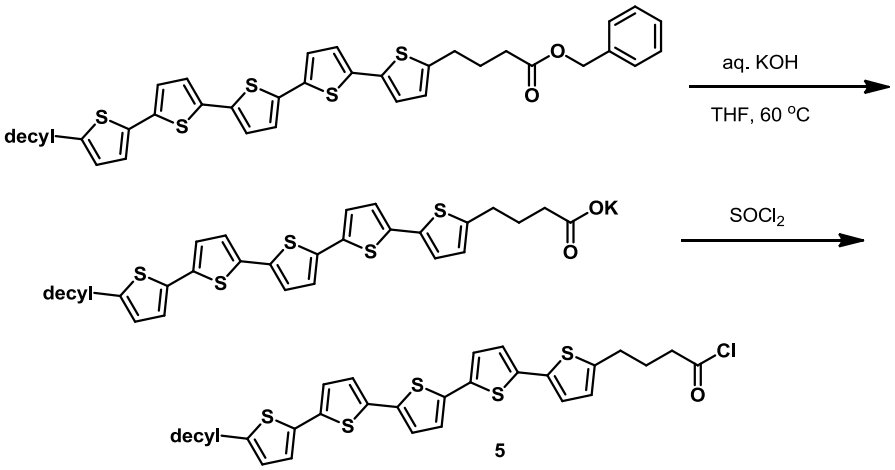

Scheme 1.2. Synthesis of pentathiophene butyric acid chloride **5.**

4-(5’’’’-Decyl-[2,2’;5’,2’’;5’’,2’’’;5’’’,2’’’’] quinquethiophen-5-yl)-butyric acid benzyl ester was prepared according to a previously published procedure.[27]

4-(5’’’’-Decyl-[2,2’;5’,2’’;5’’,2’’’;5’’’,2’’’’] quinquethiophen-5-yl)-butanoyl chloride (5). A flask was charged with 0.57 g (0.78 mmol) 1, 100 mL THF, and 10 mL 5% aq. KOH and was equipped with a reflux condenser. The mixture was heated to 70 °C with stirring overnight during which time the product precipitates out. The mixture was cooled to room temperature and the precipitate was filtered and washed with water, ethanol, and diethyl ether. The filtered solids were air-dried and then placed in a vacuum desiccator over CaCl2 overnight to yield 0.48 g of the orange carboxylate salt. Freshly distilled thionyl chloride was then added to a flask containing the carboxylate salt and a deep red solution formed immediately. The thionyl chloride was removed via distillation and the red residue was dried in vacuo to yield the product, which was used without further purification.

References

(1) Bratton, D.; Yang, D.; Dai, J.; Ober, C.K.. *Polym. Adv. Tech*. **2006**, *17*, 94-103.

(2) Mendes, P.; Yeung, C.; Preece, J. *Nanoscale Res. Lett.* **2007,** *2*, 373-384.

(3) Taylor, P. G.; Lee, J.; Zakhidov, A. A.; Chatzichristidi, M.; Fong, H. H.; DeFranco, J. A.; Malliaras, G. G.; Ober, C. K. *Adv. Mater.* **2009**, *21*, 2314-2317.

(4) Slocik, J. M.; Beckel, E. R.; Jiang, H.; Enlow, J. O.; Zabinski, J. S.; Bunning, T. J.; Naik, R. R. *Adv. Mater*. **2006**, *18*, 2095-2100.

(5) Xu, H.; Hong, R.; Lu, T.; Uzun, O.; Rotello, V. M. *J. Am. Chem. Soc.* **2006,** *128*, 3162-3163.

(6) Im, S. G.; Bong, K. W.; Kim, B.; Baxamusa, S. H.; Hammond, P. T.; Doyle, P. S.; Gleason, K. K. *J. Am. Chem. Soc*. **2008**, *130*, 14424-14425.

(7) Paxton, W. F.; Spruell, J. M.; Stoddart, J. F. *J. Am. Chem. Soc*. **2009,** *131*, 6692-6694.

(8) Backer, S. A.; Suez, I.; Fresco, Z. M.; Rolandi, M.; Fréchet, J. M. *Langmuir* **2007**, *23*, 2297-2299.

(9) Fresco, Z. M.; Suez, I.; Backer, S. A.; Fréchet, J. M. J. *J. Am. Chem. Soc*. **2004**, *126*, 8374-8375.

(10) Piner, R. D.; Zhu, J.; Xu, F.; Hong, S. H.; Mirkin, C. A. *Science* **1999**, *283*, 661-663.

(11) Maoz, R.; Frydman, E.; Cohen, S. R.; Sagiv, J. *Adv. Mater*. **2000**, *12*, 725-731.

(12) Xie, X. N.; Chung, H. J.; Tong, D. M.; Sow, C. H.; Wee, A. T. *J. App. Phys*. **2007**, *102*, 084313-084316.

(13) Yang, M.; Wouters, D.; Giesbers, M.; Schubert, U. S.; Zuilhof, H. *ACS nano*, **2009**, *3*, 2887-2900.

(14) Braunschweig, A. B.; Senesi, A. J.; Mirkin, C. A. *J. Am. Chem. Soc*. **2009**, *131*, 922-923.

(15) Li, Y.; Maynor, B. W.; Liu, J. *J. Am. Chem. Soc*. **2001**, *123*, 2105-2106.

(16) Hodneland, C. D.; Mrksich, M. *J. Am. Chem. Soc.* **2000**, *122*, 4235-4236.

(17) Rohde, R.; Agnew, H.; Yeo, W.; Bailey, R.; Heath, J. *J. Am. Chem. Soc*. **2006**, *128*, 9518-9525.

(18) Wang, B.; Liu, S.; Borchardt, R. T. *J. Org. Chem.* **1995**, *60*, 539-543.

(19) Hoeppener, S.; Maoz, R.; Sagiv, J. *Nano Lett.* **2003**, *3*, 761-767.

(20) Fresco, Z. M.; Fréchet, J. M. *J. Am. Chem. Soc*. **2005**, *127*, 8302-8303.

(21) Wouters, D.; Willems, R.; Hoeppener, S.; Flipse, C. F.; Schubert, U. S. *Adv. Func. Mater*. **2005**, *15*, 938-944.

(22) Jonkheijm, P.; Hoeben, F. J.; Kleppinger, R.; van Herrikhuyzen, J.; Schenning, A. P.; Meijer, E. W. *J. Am. Chem. Soc*. **2003**, *125*, 15941-15949.

(23) Yamamoto, Y.; Zhang, G.; Jin, W.; Fukushima, T.; Ishii, N.; Saeki, A.; Seki, S.; Tagawa, S.; Minari, T.; Tsukagoshi, K.; Aida, T. *Proc. Natl. Acad. Sci*. **2009**, *106*, 21051-21056.

(24) Fresco, Z. M.; Suez, I.; Backer, S. A.; Fréchet, J. M. J. *J. Am. Chem. Soc*. **2004**, *126*, 8374-8375.

(25) Smits, E. C. P.; Mathijssen, S. G. J.; van Hal, P. A.; Setayesh, S.; Geuns, T. C. T.; Mutsaers, K. A. H. A.; Cantatore, E.; Wondergem, H. J.; Werzer, O.; Resel, R.; Kemerink, M.; Kirchmeyer, S.; Muzafarov, A. M.; Ponomarenko, S. A.; de Boer, B.; Blom, P. W. M.; de Leeuw, D. M. *Nature*, **2008**, *455*, 956-959.

(26) Rohde, R.; Agnew, H.; Yeo, W.; Bailey, R.; Heath, J. *J. Am. Chem. Soc.* **2006**, *128*, 9518-9525.

(27) Chen, J.; Murphy, A. R.; Esteve, J.; Ogletree, D. F.; Salmeron, M.; Fréchet, J. M. J. *Langmuir*, **2004**, *20*, 7703-7710.

Chapter 2
Thermally Activated, Single Component Epoxy Systems

Abstract

A single component epoxy system in which the resin and hardener components found in many two-component epoxies are combined onto the same molecule is described. The single molecule precursor to the epoxy resin contains both multiple epoxide moieties and a diamine held latent by thermally degradable carbamate linkages. These bis-carbamate "single molecule epoxies" have an essentially infinite shelf life and access a significant range in curing temperatures related to the structure of the carbamate linkages used.

Introduction

Epoxies are an important class of thermosetting polymers with diverse applications including adhesives, structural materials, paints, coatings, concrete, printed circuit boards, microelectronic encapsulation, the aerospace industry, and other consumer applications. In addition, recent interest has surfaced for using epoxies as self healing materials,[1] chemical resists,[2] and composites with nanotubes.[3] The widespread utility of epoxy formulations can be explained by a combination of their exceptional processability prior to curing and their excellent post-cure adhesion, mechanical strength and chemical resistance after curing. Additionally, the high-density three-dimensional network of epoxies makes them extremely robust materials, making them the thermoset of choice for many long-term applications.

The most common epoxy formulation consists of a multivalent epoxide ("resin") and multivalent amine ("hardener") to form a polymeric network of essentially infinite molecular weight. This reaction traditionally requires the two components to be stored separately and mixed immediately prior to use. Attempts to increase the amine latency traditionally take advantage of solubility or phase differences between the epoxy and the amine.[4-9] While these can still be packaged and marketed as single component systems, they have limitations most particularly with respect to shelf life. Additionally, amines can be made more latent through chemical modification, for example as their ketimine derivatives.[10-12] This strategy is indeed effective in increasing latency, but it requires rigorous processing to ensure that all components are water free due to the well known lability of ketimines.

In the design of latent amine epoxies, we wanted to take advantage of the ability to block an amine with a thermally removable group. While the use of blocking agents is a strategy that has seen some recent and limited use in amine epoxies,[13,14] it has historically been much more prevalent in polyurethane chemistry.[15-19] Although blocking groups are effective in rendering a functional group unreactive until an appropriate stimulus is applied, most blocking agents once removed do not participate in the polyurethane cure. Typically the blocking agents remain as unreactive by-product diluents, which can leach out over time and possibly present environmental or health problems. An alternative strategy is to use the blocking agent as the connecting linchpin between the hardener and resin. With this design, the atom economy of the curing reaction is increased and the production of toxic byproducts eliminated. Herein we describe such a strategy by using the susceptibility of the carbamate functional group to decompose under a thermal stimulus, and demonstrate its applicability toward the synthesis and characterization of "single component epoxies".

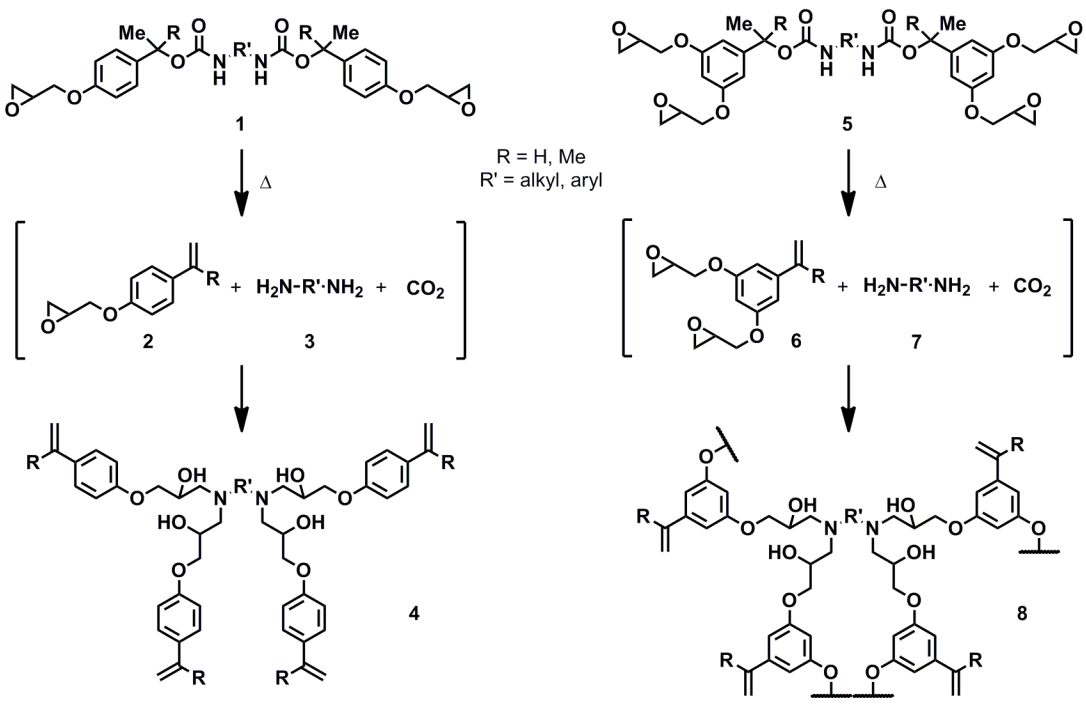

Scheme 2.1. Overview of thermal deprotection and curing of model compound **1** and epoxy precursor **5** to give oligomer **4** and crosslinked epoxy **8**.

Results and Discussion

The synthetic design of these single component amine epoxy precursors are inspired by previous work with a carbamate deprotection mechanism using ultraviolet light as the trigger.[20-25] Rather than using this motif as a UV-curable system, which operates at an inefficient wavelength for large-scale use (280 nm) and has a poor quantum yield (with many deleterious side reactions), we decided to take advantage of the thermal instability of the carbamate functional group.[19] The overall process of thermal deprotection and curing of our "single component epoxies" is summarized in Scheme 2.1. In contrast to phenyl carbamate, the functionality commonly used in a blocked isocyanate, which thermally decomposes into an isocyanate and a phenol, the carbamate moieties of our epoxy precursors (e.g. **1** and **5**) are designed to undergo the entropically favorable thermal decomposition to yield carbon dioxide, an eliminated alkene (**2** and **6**), and a primary diamine (**3** and **7**). Because the eliminated alkene contains at least one epoxide moiety, it can react with the newly formed primary amine, thus realizing the key step in the formation of an epoxy thermoset. In practice, the epoxy precursor should contain at least two latent amines and four epoxy moieties (such as **5**) in order to produce a crosslinked epoxy thermoset. Epoxy precursors that have a low epoxy/amine ratio and cannot crosslink (such as **1**) were still used as model compounds to illustrate the structure/function relationship between molecular design and deprotection temperature.

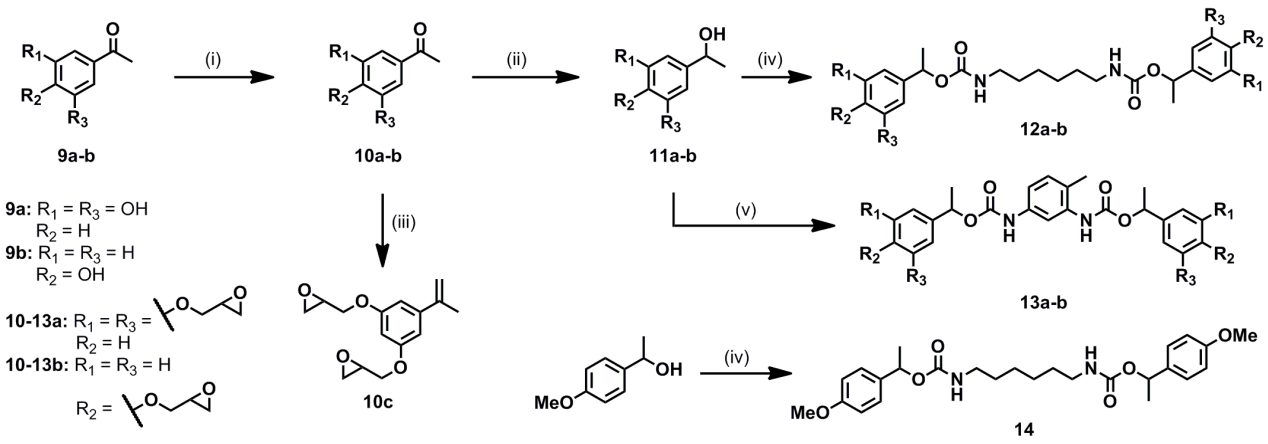

Scheme 2.2. Synthesis of secondary benzylic epoxy precursors **12** and **13** and non-curing control precursor **14**. Reagents and conditions: (i) epibromohydrin, Cs_2CO_3, DMF; (ii) $NaBH_4$, MeOH/THF; (iii) CH_3PH_3PBr, n-BuLi, THF; (iv) 1,6-diisocyanatohexane, toluene; (v) 2,4-tolylene diisocyanate, toluene.

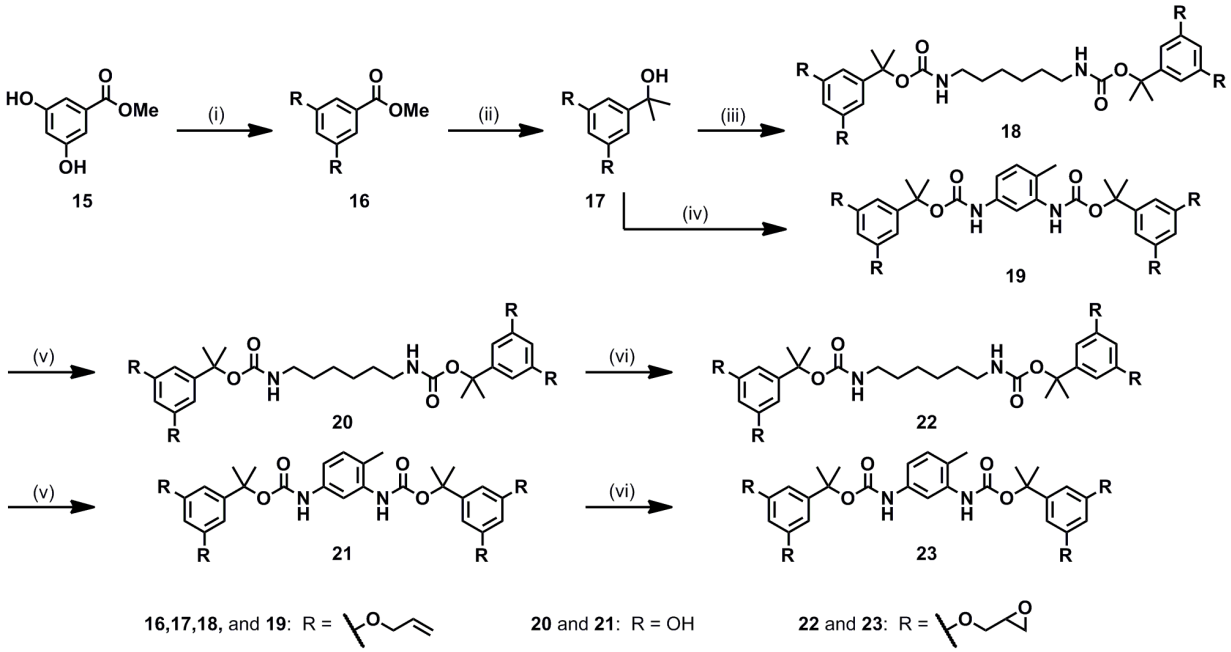

Scheme 2.3. Synthesis of tertiary benzylic epoxy precursors **22** and **23**. Reagents and conditions: (i) allyl bromide, K_2CO_3, DMF; (ii) methylmagnesium bromide, THF; (iii) 1,6-diisocyanatohexane, cat. methyllithium, THF; (iv) 2,4-tolylene diisocyanate, cat. methyllithium, THF; (v) $Pd(PPH_3)_4$, $NaBH_4$, MeOH/THF; (vi) epibromohydrin, Cs_2CO_3, DMF

The synthetic route to access these epoxy precursors depends upon the degree of substitution of the benzylic carbon. Scheme 2.2 outlines the preparation of bis-carbamate epoxy precursors **13** and **15**, which are derived from a secondary benzylic alcohol in a facile three-step process. For example, **13a** is prepared from 3,5-dihydroxyacetophenone **9a** by alkylation with epibromohydrin in the presence of cesium carbonate to afford **10a** followed by reduction with sodium borohydride and bis-carbamation with a diisocyanate to yield the desired secondary bis-carbamate.

In the case of tertiary bis-carbamates **22** and **23**, the synthetic sequence starting from methyl 3,5-dihydroxybenzoate is somewhat lengthier requiring five steps due to the need for a

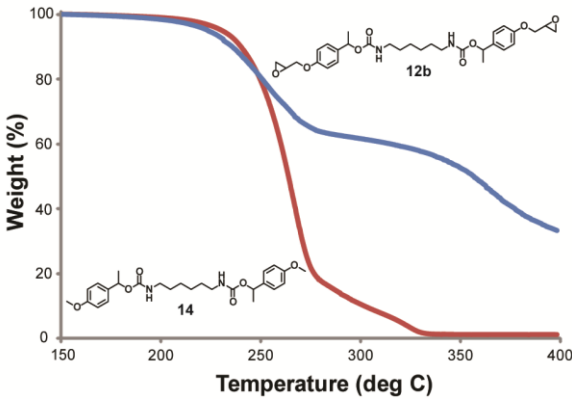

Figure 2.1. Comparison of TGA traces for monomer **12b** (blue) and control **14** (red). Reprinted with permission from Unruh et al. *Macromolecules* **2011**, *44*, 6318. Copyright 2011 American Chemical Society.

protection-deprotection sequence (Scheme 2.3). The starting material **15** was first bis-allylated to afford **16,** which was then treated with two equivalents of methylmagnesium bromide to afford the tertiary benzylic alcohol **17**. Allyl protection of the phenols of **15** was crucial to enable the selective methyllithium-catalyzed bis-carbamation of the tertiary alcohol to produce alkyl bis-carbamate **18** and aryl bis-carbamate **19**. The allyl groups were then removed via palladium-catalyzed sodium borohydride reduction to give the hydroxylated bis-carbamates **20** and **21**. Finally, four epoxide groups were installed using epibromohydrin and cesium carbonate to afford the desired epoxies **22** and **23**. Direct epoxidation of the allyl groups using conventional reagents (mCPBA or DMDO) were unsuccessful. Although the two synthetic pathways differ in length and ease of preparation, the overall synthetic scheme has flexibility with respect to the substitution of the benzylic carbon, the substitution around the phenyl ring, and the nature of the diisocyanate. This flexibility allowed access to a small library of epoxy precursors with a significant range of deprotection and curing temperatures.

When heated past the deprotection temperature of the carbamate moiety, the epoxy precursors display a decomposition with two inflection points. TGA monitoring confirmed the first inflection, corresponding to the weight change expected from the loss of 2 CO_2 molecules from the epoxy material, as well as some evaporation of the diamine and glycidyl ether formed post-deprotection. Following initial weight loss, the weight of the sample subjected to TGA analysis only decreases slowly, likely as a result of evaporation, until the second inflection point occurs at an elevated temperature (>350 °C). Only bis-carbamates that include epoxy groups displayed this relative stability after loss of CO_2, as seen by TGA comparison between epoxy **12b** and **14** (Figure 1). The control epoxy **14** was designed to release CO_2 at a similar temperature as epoxy **12b**, but without the ability to cure. IR monitoring of the deprotection of epoxy precursor **13b** diluted in a matrix of poly(methacrylonitrile) heated to 160°C (Figure 2.2) shows that the carbamate NH peak at 3329 cm^{-1} is replaced by a broader peak centered at 3386 cm^{-1}, primarily is due to the amine of the deprotected monomer. Although this precursor is diluted in a polymer matrix, it is possible that background curing may give rise to hydroxyls in this region of the spectrum. In addition, the IR spectra showed a relative increase in transmission at 1717 cm^{-1} corresponding to the loss of the carbamate carbonyl as it is converted to CO_2, compared to the nitrile stretch of the polymer matrix which changes minimally during the heating period.

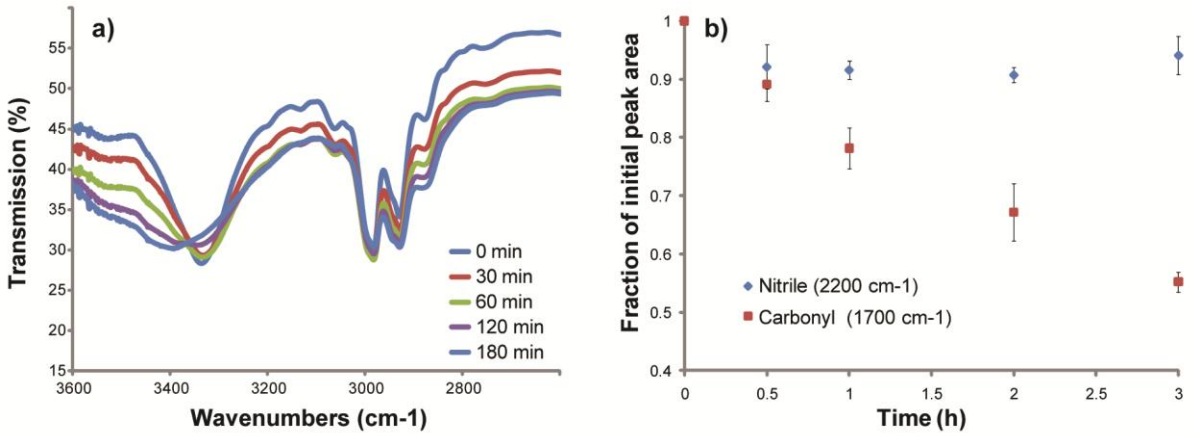

Figure 2.2. a) Selected IR spectra of films, and b) relative peak ratios of carbonyl and nitrile stretches of precursor **13b** (as a 200 mM solution in a mixture of 11% poly(methacrylonitrile) in nitromethane) as a function of curing times at 160 °C. Reprinted with permission from Unruh et al. *Macromolecules* **2011**, *44*, 6318. Copyright 2011 American Chemical Society.

The curing of epoxies is also known to produce a large DSC exotherm, specifically due to epoxide ring opening by the amine. As shown by Figure 2.3, the cure exotherm only appears once the temperature of CO_2 release is reached. A subsequent DSC scan shows no further exotherm as the cure is complete. As shown in Table 1 for a variety of precursors, cure always follows deprotection, the onsets of which may differ by as little as 4 to as much as 16 °C. Interestingly, while the T_g values of the cured thermosets match well with those obtained from cured amine epoxies and depend upon the aliphatic or aromatic nature of the amine curing agent,[26] the measured enthalpy of cure is less than that typical of amine epoxies, generally regarded to be on the order of 100 kJ/equivalent of epoxide.[27]

When compared to the first entry in Table 2.1, a control system consisting of the byproducts of thermal carbamate deprotection, the lower energies of the bis-carbamate monomers are likely due to small amounts of evaporation of one or both byproducts during the release of CO_2. Because the carbamate deprotection follows Arrhenius kinetics, a statistical portion of the monomer will deprotect and thus cure at temperatures below the measured TGA onset. Isothermal DSC curing studies with precursors **13b** and **23**, the two lowest-curing monomers, reflect this behavior where both molecules can cure completely at 160 °C in ca. 90 and 50 minutes (Figure 2.4), despite having very similar deprotection onsets (170 and 176 °C, respectively).

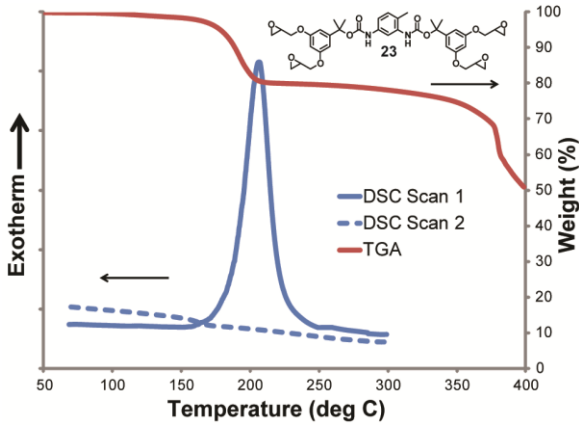

Figure 2.3. Combined DSC and TGA traces for monomer **23**. Reprinted with permission from Unruh et al. *Macromolecules* **2011**, *44*, 6318. Copyright 2011 American Chemical Society.

Table 2.1. Deprotection and curing characteristics for epoxy monomers and model compounds. TGA and DSC data were obtained at a heating rate of 10 °C/min.

Compound	TGA deprotection onset (°C)	DSC exotherm onset (°C)	Maximum of DSC exotherm peak (°C)	Enthalpy of cure (kJ/eq. epoxide)	T_g (∞) (°C)
10c + 1,6-diaminohexane	-	58	74	105	112
12a	252	271	304	74	123
12b	222	239	265	87	-
13a	227	247	291	78	156
13b	176	192	222	89	-
22	211	220	236	85	114
23	170	174	205	93	163

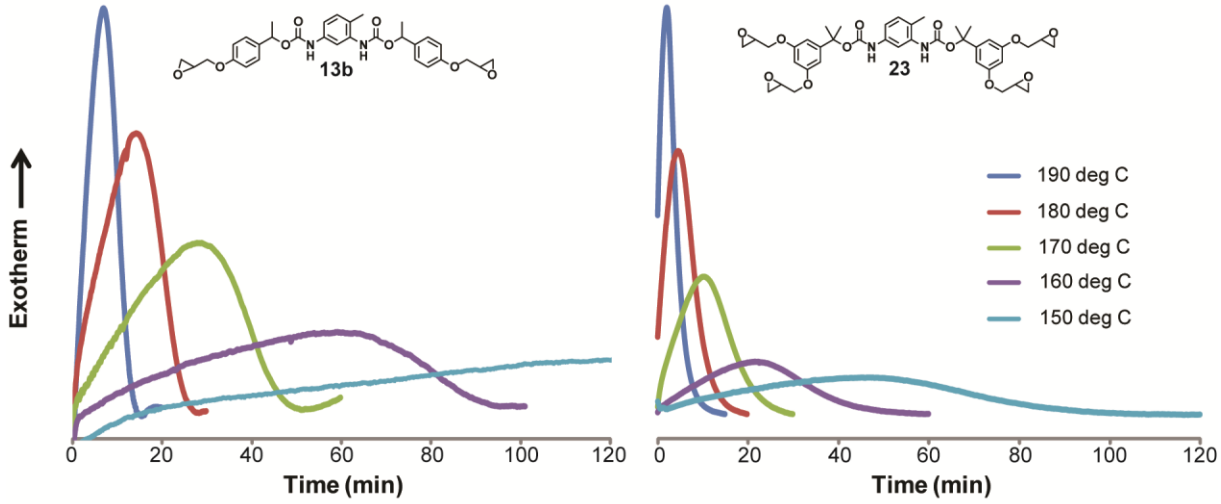

Figure 2.4. DSC isothermal comparison of monomers **13b** and **23**. Reprinted with permission from Unruh et al. *Macromolecules* **2011**, *44*, 6318. Copyright 2011 American Chemical Society.

Examination of the deprotection parameters for the various structures studied suggests the following: (i) 1,4--substitution leads to a lower deprotection temperature than 1,3,5-substitution, (ii) increasing the substitution of the benzylic carbon results in a lower deprotection temperature, and (iii) aryl bis-carbamates deprotect at lower temperatures than alkyl bis-carbamates. These patterns reflect an increase in the ability to stabilize a partial positive charge arising in the benzylic carbon in the transition state and the well-known fact[15] that aryl carbamates are less thermally stable than their alkyl counterparts, presumably due to the electron-withdrawing effect of the aryl group.

As a result of curing, the gaseous carbon dioxide produced by the decomposition of the carbamate moieties remains trapped within the film forming spherical bubbles, shown by Figure 2.5. As expected, the size of these bubbles varies according to the curing temperature, with smaller bubbles formed within the film cured at a lower temperature, and dramatically larger bubbles formed in a film cured at a higher temperature. The size of the bubbles likely varies due to a variety of factors, most notably the impact of temperature on the rates of carbamate decomposition and curing. As the curing temperature increases, CO_2 is generated more quickly

and is trapped to a larger extent within the rapidly curing film, resulting in larger bubbles. Lower curing temperatures both generate CO_2 more slowly and allow a greater amount of the generated gases to diffuse or escape from the film before it is fully cured.

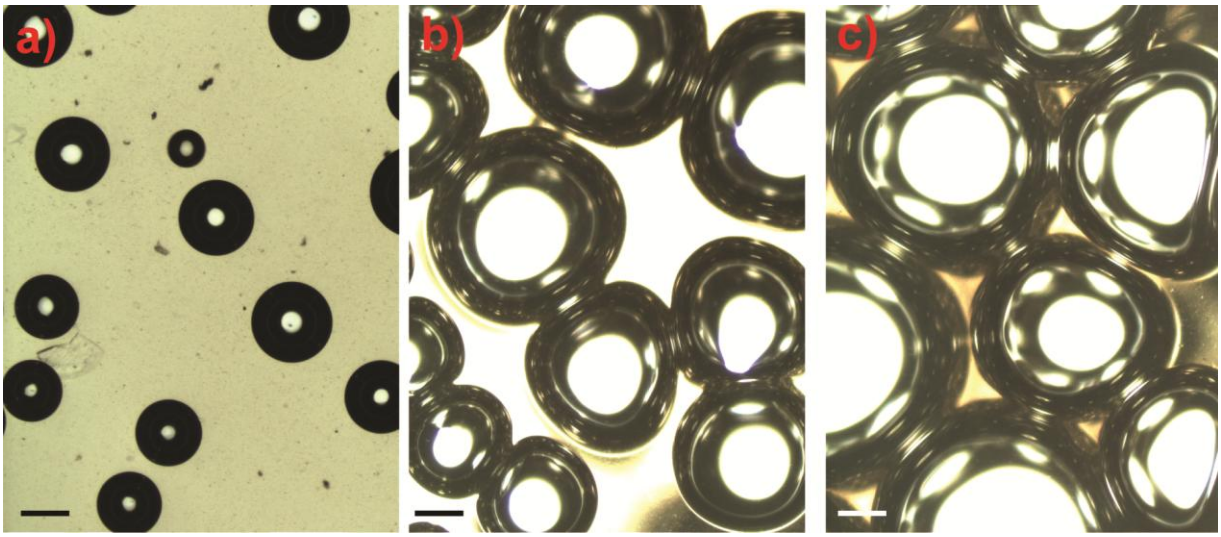

Figure 2.5. Comparison of CO_2 bubbles produced in cured resins of epoxy **23**, cured fully at different temperatures: a) 160 °C for 1 h; b) 180 °C for 30 min; c) 200 °C for 15 min. Scale bar is 200 µm. Reprinted with permission from Unruh et al. *Macromolecules* **2011**, *44*, 6318. Copyright 2011 American Chemical Society.

Conclusions

We have developed a novel design strategy towards single component latent amine epoxies, in which we combine the latent amine and the epoxide onto the same molecule. The thermal trigger used in this epoxy design is analogous to that used for blocked isocyanates in polyurethane coatings. Utilizing a small library of epoxy precursors, we have shown that the cure temperatures can be adjusted through small structural changes to yield a range of self-curing epoxy-urethane monomers which cure in relatively short periods at elevated temperatures to give thermosets that may be useful as foam dielectrics, adhesives, sealants, and coatings.

Experimental

Materials. All reagents were obtained from commercial sources and used without further purification unless otherwise noted. All solvents used were reagent grade (99.9%) unless otherwise noted. Tetrahydrofuran, toluene and dichloromethane were purified under argon by passing through two columns of neutral alumina on a commercial apparatus. Water was purified using a Barnstead NANOpure Diamond purification system. Compounds containing stereocenters were isolated as mixtures of stereoisomers.

Characterization. Elemental analysis was performed by the UC Berkeley analytical facilities. ^{1}H and ^{13}C NMR measurements were conducted on a Bruker AVB-400 nuclear magnetic resonance spectrometer. Differential scanning calorimetry (DSC) measurements were performed with a TA Instruments Q200 differential scanning calorimeter with standard aluminum pans. Monomers were used neat in all DSC experiments, with the exception of entry 1 of Table 1, where equimolar amounts of 1,6-diaminohexane and compound **10c** were mixed together prior to pan weighing. Ramped DSC scans were performed at a rate of 10 °C/min, and reported cure enthalpy values are an average of two measurements. Isothermal DSC analyses were performed by rapidly ramping the sample to the desired cure temperature before the starting

time. Thermogrametric analyses (TGA) were performed with a TA Instruments G5000 thermogravimetric analyzer, and were performed at a rate of 10 °C/min. Infrared spectra were taken with a Thermo Scientific Nicolet 6700 Fourier transform infrared spectrometer. Films were prepared by gently heating and stirring a mixture of the epoxy precursor in an 11 wt% poly(methacrylonitrile) solution in nitromethane until homogeneous, and then spin-coating onto NaCl disks at 1500 rpm for 60 s, drying at 90 °C for 15 min and placement in a vacuum dessicator until use. Relative peak ratios calculated using FTIR are an average of three films. Optical microscopy was performed with a Fisher Scientific Micromaster Inverted Digital Microscope on samples with uniform (10 mm) thickness. Samples were cured at temperatures for time limits that were determined by isothermal DSC measurements with CO_2 evolution permitted.

Preparation of 3,5-Diglycidoxyacetophenone (10a). To a solution of 3,5-dihydroxyacetophenone **9a** (1.01 g, 6.65 mmol) in DMF (20 mL) was added epibromohydrin (2.20 mL, 26.6 mmol) followed by cesium carbonate (4.77 g, 14.6 mmol). This reaction was stirred overnight, after which 100 mL anhydrous ether was added to the reaction mixture. The organic layer was washed with 0.1 M NaOH, water, brine, and dried over anhydrous $MgSO_4$. Solvent was evaporated to yield 975 mg (53%) of a light yellow solid. ^{1}H NMR ($CDCl_3$, 400 MHz) δ 2.57 (s, 3H), 2.77-2.78 (dd, 2H), 2.92-2.94 (t, 2H), 3.36-3.39 (m, 2H), 3.93-3.97 (dd, 2H), 4.29-4.33 (dd, 2H), 6.72-6.73 (t, 1H), 7.13-7.14 (d, 2H); ^{13}C NMR ($CDCl_3$, 100 MHz) δ 26.7, 44.5, 49.9, 69.0, 69.1, 106.5, 107.2, 139.0, 159.6, 197.4. IR ($CHCl_3$, cm^{-1}) 3051, 2970, 2923, 1684, 1595, 1444, 1363, 1298, 1177, 1156, 1063, 910. Anal. Calcd for $C_{14}H_{16}O_5$: C, 63.6; H, 6.1. Found: C, 63.48, H, 5.99.

Preparation of 4-Glycidoxyacetophenone (10b). To a solution of 4-hydroxyacetophenone **9b** (3.67 g, 27.0 mmol) in dry DMF (50 mL) was added cesium carbonate (13.17 g, 40.4 mmol) and epibromohydrin (3.33 mL, 40.4 mmol). This reaction was stirred overnight, after which 250 mL water was added. The organics were extracted with ether, washed with 0.1 M NaOH and brine, dried over anhydrous magnesium sulfate, and solvents were removed in vacuo to yield 3.14 g (62%) of a clear oil. ^{1}H NMR ($CDCl_3$, 400 MHz) δ 2.56 (s, 3H), 2.77-2.79 (dd, 1H), 2.92-2.94 (dd, 1H), 3.36-3.39 (m, 1H), 3.97-4.02 (dd, 1H), 4.30-4.34 (dd, 1H), 6.95-6.97 (d, 2H), 7.92-7.95 (d, 2H). ^{13}C NMR ($CDCl_3$, 100 MHz) δ 26.4, 44.6, 49.9, 68.9, 114.3, 130.2, 130.6, 162.3, 196.7. IR ($CHCl_3$, cm^{-1}) 3061, 3003, 2930, 1684, 1676, 1598, 1510, 1420, 1360, 1271, 1243, 1176, 1026, 959, 915. Anal. Calcd for $C_{11}H_{12}O_3$: C, 68.7; H, 6.3. Found: C, 68.43; H, 6.12.

Preparation of 2-(3,5-Diglycidoxyphenyl)propene (10c). A methyltriphenylphosphine bromide (1.66 g, 4.66 mmol) in dry THF (25 mL) was cooled to -78 °C, and n-butyllithium (2.5 M in hexanes, 4.66 mmol) was added dropwise. After 10 minutes, a solution of acetophenone **10a** (1.23 g, 4.66 mmol) in dry THF was added dropwise, and the solution was allowed to stir at room temperature for 12 h. The mixture was then filtered through a plug of Celite, concentrated in vacuo, and purified via silica gel chromatography (1:10 – 1:4 ethyl acetate in hexanes). Solvents were removed to yield 285 mg (23%) of a white solid. ^{1}H NMR ($CDCl_3$, 400 MHz) δ 2.11 (s, 3H), 2.75-2.77 (dd, 2H), 2.90-2.92 (t, 2H), 3.34-3.36 (m, 2H), 3.93-3.97 (dd, 2H), 4.21-4.24 (dd, 2H), 5.08 (s, 1H), 5.34 (s, 1H), 6.44-6.45 (t, 1H), 6.65-6.66 (d, 2H); ^{13}C NMR ($CDCl_3$, 100 MHz) δ 22.1, 45.0, 50.4, 69.1, 100.9, 105.5, 113.3, 143.3, 143.9, 159.7. IR ($CHCl_3$, cm^{-1}) 3084, 2926, 1770, 1593, 1435, 1346, 1253, 1176, 1131, 1063, 909. Anal. Calcd for $C_{15}H_{18}O_4$: C, 68.7, H, 6.9. Found: C, 68.75, H, 7.01.

Preparation of 1-(3,5-Diglycidoxyphenyl)ethanol (**11a)**. A solution of acetophenone **10a** (6.96 g, 26.3 mmol) in THF (50 mL) and methanol (100 mL) was cooled to 0 °C, and then sodium

borohydride (1.99 g, 52.7 mmol) was added. The reaction was allowed to stir at room temperature for 2 h, at which point starting material was completely consumed by thin layer chromatography (1:1 ethyl acetate:hexanes) and the reaction was quenched with aqueous 1 M NaHSO4. The mixture was concentrated and extracted with diethyl ether. The organic portion was washed with brine, dried over magnesium sulfate, and solvent was removed to afford 6.28 g (89%) of a light yellow oil. ^{1}H NMR ($CDCl_3$, 400 MHz) δ 1.48-1.50 (d, 3H), 2.32 (br s, 1H), 2.78-2.80 (t, 2H), 2.93-2.95 (t, 2H), 3.36-3.39 (m, 2H), 3.74-3.83 (dd, 2H), 4.17-4.21 (dd, 2H), 4.83-4.88 (q, 1H), 6.44 (s, 1H), 6.60 (s, 2H). ^{13}C NMR ($CDCl_3$, 100 MHz) δ 25.2, 44.7, 50.1, 68.8, 70.3, 100.6, 104.5, 148.8, 159.7. IR (neat, cm^{-1}) 3422, 2973, 2928, 2876, 1601, 1449, 1346, 1294, 1176, 1131, 1055, 909. Anal. Calcd for $C_{14}H_{18}O_5$: C, 63.2; H, 6.8. Found: C, 62.89; H, 7.07.

Preparation of 1-(4-Glycidoxyphenyl)ethanol (**11b)**. A solution of the acetophenone **10b** (3.10 g, 16.1 mmol) methanol (50 mL) was cooled to 0 °C, and then sodium borohydride (1.20 g, 32.3 mmol) was added. The reaction was allowed to stir at room temperature for 2 h, at which point starting material was completely consumed by thin layer chromatography (1:1 ethyl acetate:hexanes) and the reaction was quenched with aqueous 1 M NaHSO4. The mixture was concentrated and extracted with diethyl ether. The organic portion was washed with brine, dried over magnesium sulfate, and solvent was removed to afford 3.02 g (96%) of a clear oil. ^{1}H NMR ($CDCl_3$, 400 MHz) δ 1.51-1.52 (d, 3H), 1.76 (br s, 1H), 2.79-2.81 (dd, 1H), 2.93-2.96 (dd, 1H), 3.37-3.41 (m, 1H), 3.98-4.02 (dd, 1H), 4.24-4.28 (dd, 1H), 4.87-4.92 (q, 1H), 6.92-6.96 (d, 2H), 7.32-7.34 (d, 2H); ^{13}C NMR ($CDCl_3$, 100 MHz) δ 25.1, 44.8, 50.2, 68.8, 70.0, 114.6, 126.7, 138.6, 157.9. IR (neat, cm^{-1}) 3404, 2971, 2925, 1610, 1513, 1453, 1241, 1178, 1088, 1035, 902. Anal. Calcd for $C_{11}H_{14}O_3$: C, 68.0; H, 7.26. Found: C, 67.75; H, 7.28.

Preparation of N,N'-Bis[[1-(3,5-diglycidoxyphenyl)ethoxy]carbonyl]hexane-1,6-diamine (12a). The alcohol **11a** (2.0 g, 7.68 mmol) and 1,6-diisocyanatohexane (968 mg, 5.76 mmol) were added to 3 mL of toluene in a microwave reaction vial. The reaction was heated to 120 °C for 5 hours in microwave, at which time no starting material was observed via thin layer chromatography (2:1 ethyl acetate:hexanes). The entire reaction contents were purified with silica gel chromatography (1:1 to 3:1 ethyl acetate:hexanes). Solvent was removed in vacuo to yield 954 mg (35%) of a clear oil. ^{1}H NMR ($CDCl_3$, 400 MHz) δ 1.28 (br s, 4H), 1.45-1.47 (d, 10 H), 2.72-2.74 (dd, 4H), 2.87-2.89 (t, 3.85), 3.11-3.12 (br d, 4H), 3.31-3.33 (dd, 4H), 3.87-3.91 (dd, 4H), 4.18-4.20 (d, 4H), 4.83 (br s, 2H), 5.64-5.68 (q, 2H), 6.39 (s, 2H), 6.50-6.51 (d, 4H); ^{13}C NMR ($CDCl_3$, 100 MHz) δ 22.7, 26.3, 30.0, 40.9, 44.8, 50.2, 69.0, 72.4, 100.7, 105.3, 145.2, 156.0, 159.8. IR (neat, cm^{-1}) 3341, 2979, 2931, 2861, 1707, 1599, 1529, 1450, 1355, 1262, 1178, 1050, 910. Anal. Calcd for $C_{36}H_{48}N_2O_{12}$: C, 61.7; H, 6.9; N, 4.0. Found: 61.84; H, 6.79; N, 4.10.

Preparation of N,N'-Bis[[1-(4-glycidoxyphenyl)ethoxy]carbonyl]hexane-1,6-diamine (12b). The alcohol **11b** (1 g, 5.15 mmol) and 1,6-diisocyanatohexane (519 mg, 3.09 mmol) were added to 3 mL toluene. This mixture was heated to 90 °C and stirred overnight. The reaction was purified via silica gel chromatography (1:1 ethyl acetate:hexane) to yield 871 mg (61 %) of a white solid. ^{1}H NMR ($CDCl_3$, 400 MHz,) δ 1.28 (br s, 4H), 1.45 (br s, 4H), 1.49-1.51 (d, 6H), 2.74-2.75 (dd, 2H), 2.89-2.91 (t, 2H), 3.09 – 3.15 (m, 4H), 3.32-3.36 (m, 2H), 3.92-3.95 (dd, 2H), 4.19-4.22 (dd, 2H), 4.69 (s, 2H), 5.71-5.76 (q, 2H), 6.87-6.89 (d, 4H), 7.25-7.29 (d, 4H); ^{13}C NMR ($CDCl_3$, 100 MHz) δ 22.3, 26.4, 30.0, 40.9, 44.9, 50.3, 68.9, 72.3, 114.7, 127.7, 135.1, 156.2, 158.2. IR ($CHCl_3$, cm^{-1}) 3340, 2931, 1701, 1612, 1514, 1242, 1179, 1063, 1034, 912. Anal. Calcd for $C_{30}H_{40}N_2O_8$: C, 64.7; H, 7.2; N, 5.0. Found: C, 64.74; H, 7.24; N, 5.28.

Preparation of N,N'-Bis[[1-(3,5-diglycidoxyphenyl)ethoxy]carbonyl]toluene-2,4-diamine (13a). The alcohol **11a** (1.05 g, 3.94 mmol) and 2,4-tolylenediisocyanate (343 mg, 1.97 mmol) were added to dry toluene (3 mL) and heated to 90 °C overnight. The entire contents were purified via silica gel chromatography (1:1 to 3:1 ethyl acetate:hexanes). Solvent was removed in vacuo to yield 510 mg (36%) of a colorless solid. ^{1}H NMR ($CDCl_3$, 400 MHz) δ 1.52-1.56 (dd, 6H), 2.18 (s, 3H), 2.74-2.75 (m, 4H), 2.89-2.91 (m, 4H), 3.32-3.36 (m, 4H), 3.89-3.93 (m, 4H), 4.19-4.23 (m, 4H), 5.74-5.80 (m, 2H), 6.40-6.43 (m, 2H), 6.51 (br s, 1H), 6.55-6.56 (m, 4H), 6.81 (br s, 1H), 7.03-7.05 (d, 1H), 7.18-7.20 (d, 1H), 7.77 (s, 1H); ^{13}C NMR ($CDCl_3$, 100 MHz) δ 17.1, 22.4, 22.6, 25.3, 44.8, 50.2, 68.9, 70.4, 101.0, 104.6, 105.2, 105.3, 105.4, 105.5, 130.9, 159.8. IR ($CHCl_3$, cm^{-1}) 2917, 1721, 1598, 1530, 1446, 1224, 1177, 1046, 904. Anal. Calcd for $C_{37}H_{42}N_2O_{12}$: C, 62.9; H, 6.0; N, 4.0. Found: C, 62.62; H, 6.12; N, 3.60.

Preparation of N,N'-Bis[[1-(4-glycidoxyphenyl)ethoxy]carbonyl]toluene-2,4-diamine (13b). The alcohol **11b** (1 g, 5.15 mmol) and 2,4-tolylenediisocyanate (538 mg, 3.09 mmol) were added to 3 mL toluene. This mixture was heated to 90 °C and stirred overnight. The reaction was purified via silica gel chromatography (1:1 ethyl acetate:hexane) to yield 341 mg (24 %) of a white solid.^{1}H NMR ($CDCl_3$, 400 MHz,) δ 1.55-1.60 (m, 6H), 2.16 (s, 3H), 2.74-2.76 (dd, 2H), 2.89-2.92 (m, 2H), 3.34-3.36 (m, 2H), 3.94-3.98 (dd, 2H), 4.19-4.24 (m, 2H), 5.82-5.88 (d, 2H), 6.39 (s, 1H), 6.58 (s, 1H), 6.88-6.92 (m, 4H), 7.02-7.04 (d, 1H), 7.18 (br s, 1H), 7.30-7.34 (t, 4H), 7.77 (s, 1H); ^{13}C NMR ($CDCl_3$, 100 MHz) δ 17.2, 22.1, 22.3, 44.9, 50.3, 69.0, 73.3, 109.4, 114.9, 127.8, 127.9, 130.9, 134.6, 136.9, 153.2, 158.5, 164.2. IR ($CHCl_3$, cm^{-1}) 3320, 2980, 2922, 1718, 1611, 1514, 1227, 1179, 1063, 1035, 913. Anal. Calcd for $C_{31}H_{34}N_2O_8$: C, 66.2; H, 6.1; N, 5.0. Found: C, 65.82; H, 5.96; N, 5.21.

Preparation of N,N'-Bis[[1-(4-methoxyphenyl)ethoxy]carbonyl]hexane-1,6-diamine (14). To a solution of 1-(4-Methoxyphenyl)ethanol (1.04 g, 6.82 mmol) in dry toluene (3 mL) was added 1,6-diisocyanatohexane (690 mg, 4.11 mmol). This reaction was heated at 90 °C for 10 h, and then purified via silica gel chromatography (1:2 to 2:1 ethyl acetate:hexanes) to yield 986 mg (61%) of a white solid. ^{1}H NMR ($CDCl_3$, 400 MHz) δ 1.26-1.29 (m, 4H), 1.42-1.46 (m, 4H), 1.50-1.52 (d, 6H), 3.10-3.15 (m, 4H), 3.79 (s, 6H), 4.70 (br s, 2H), 5.74-5.75 (q, 2H), 6.86-6.88 (d, 4H), 7.27-7.29 (d, 4H); ^{13}C NMR ($CDCl_3$, 100 MHz) δ 22.3, 26.4, 30.0, 55.4, 72.4, 113.9, 127.6, 134.5, 156.2, 159.3. IR ($CHCl_3$, cm^{-1}) 3552, 2933, 1700, 1614, 1516, 1247, 1178, 1065, 1035. Anal. Calcd for $C_{26}H_{36}O_6$: C, 66.1; H, 7.7; N, 5.9. Found: C, 66.36; H, 7.74; N, 6.07.

Preparation of methyl 3,5-diallyloxybenzoate (16). To a solution of methyl 3,5-dihydroxybenzoate **15** (5 g, 29.7 mmol) in dry DMF (50 mL) was added potassium carbonate (12.3 g, 89.1 mmol) and allyl bromide (4.66 mL, 74.3 mmol). This reaction was stirred overnight, after which 250 mL diethyl ether was added, and the organic layer was washed with 0.1 M NaOH, brine, and dried over magnesium sulfate. Solvent was removed in vacuo and recrystallized in ethyl acetate and hexanes to yield 6.7 g (91%) of a white solid. ^{1}H NMR ($CDCl_3$, 400 MHz) δ 3.90 (s, 3H), 4.54-4.55 (d, 4H), 5.28-5.31 (d, 2H), 5.40-5.44 (d, 2H), 6.01-6.05 (m, 2H), 6.69 (s, 1H), 7.20 (s, 2H); ^{13}C NMR ($CDCl_3$, 100 MHz) δ 52.3, 69.0, 107.1, 108.1, 117.9, 131.9, 132.8, 159.6, 166.8. IR ($CHCl_3$, cm^{-1}) 2973, 1723, 1597, 1446, 1323, 1301, 1235, 1168, 1053, 930. Anal. Calcd for $C_{14}H_{16}O_4$: C, 67.7; H, 6.5. Found: C, 67.74; H, 6.53.

Preparation of 1-(3,5-diallyloxyphenyl)-1-methylethanol (17). To a solution of the preceding methyl ester **16** (6.4 g, 25.9 mmol) in dry THF (100 mL) was added a 3 M solution of methylmagnesium bromide in ether (19 mL, 57 mmol). This reaction was stirred overnight and quenched with saturated aqueous ammonium chloride. The mixture was concentrated and extracted with diethyl ether. The organic layers were combined, washed with brine, and dried

over magnesium sulfate. Solvent was removed in vacuo, and was purified via silica gel chromatography, eluting with 1:3 ethyl acetate:hexanes to yield 4.7 g (73%) of a clear oil. ^{1}H NMR ($CDCl_3$, 400 MHz) δ 1.53 (s, 6H), 2.18 (s, 1H), 4.49-4.51 (dt, 4H), 5.25-5.29 (dq, 2H), 5.38-5.43 (dq, 2H), 5.99-6.09 (m, 2H), 6.37-6.38 (t, 1H), 6.65-6.66 (d, 2H); ^{13}C NMR ($CDCl_3$, 100 MHz) δ 31.7, 68.9, 72.6, 99.8, 104.0, 117.8, 133.3, 152.0, 159.6. IR (neat, cm^{-1}) 3415, 2977, 1595, 1438, 1423, 1362, 1293, 1166, 1053, 927. Anal. Calcd for $C_{15}H_{20}O_3$: C, 72.6; H, 8.1. Found: C, 72.22; H, 8.10.

Preparation of N,N'-Bis[[1-(3,5-diallyloxyphenyl)-1-methylethoxy]carbonyl]hexane-1,6-diamine (18). The alcohol **17** (9.67 g, 39.0 mmol) was added to 30 mL dry tetrahydrofuran. A solution of 1.6 M methyllithium in ether (2.44 mL, 3.90 mmol) was added dropwise, and the resulting solution was heated to reflux for 1 h. The reaction was cooled to room temperature, and a solution of 1,6-diisocyanatohexane (3.91 g, 23.3 mmol) in 20 mL tetrahydrofuran was added dropwise via addition funnel. The reaction was heated back to reflux overnight, after which it was cooled to room temperature and concentrated. The residue was dissolved in ethyl acetate, washed with water, dried, and purified via silica gel chromatography (1:2 ethyl acetate:hexane) to yield 3.86 g (30%) of a clear oil that solidified over time. ^{1}H NMR ($CDCl_3$, 400 MHz) δ 1.28 (br s, 4H), 1.43 (br s, 4H), 1.71 (s, 12H), 3.05-3.07 (d, 4H), 4.48-4.50 (dt, 8H), 4.76-4.77 (d, 2H), 5.25-5.29 (dq, 4H), 5.37-5.43 (dq, 4H), 5.99-6.09 (m, 4H), 6.36-6.37 (t, 2H), 6.53-6.54 (d, 4H); ^{13}C NMR ($CDCl_3$, 100 MHz) δ 26.3, 29.1, 30.0, 40.4, 68.9, 80.4, 99.6, 104.0, 117.8, 133.4, 149.4, 149.4, 155.2, 159.6. IR ($CHCl_3$, cm^{-1}) 3348, 2980, 2932, 2860, 1701, 1596, 1521, 1448, 1363, 1260, 1149, 1053, 928. Anal. Calcd for $C_{38}H_{52}N_2O_8$: C, 68.6; H, 7.9; N, 4.2. Found: C, 68.49, H, 7.96; N, 4.54.

Preparation of N,N'-Bis[[1-(3,5-diallyloxyphenyl)-1-methylethoxy]carbonyl]toluene-2,4-diamine (19). Methyllithium (756 µL, 1.6 M) was added to a solution of the alcohol **17** (3 g, 12.1 mmol) in dry tetrahydrofuran (20 mL). This was heated to reflux for 1 h, then allowed to cool to room temperature before cooling on an ice bath. A solution of tolylene 2,4-diisocyanate (1.26 g, 7.26 mmol) in dry tetrahydrofuran (10 mL) was added dropwise to the reaction mixture. After addition was complete, the mixture was heated to reflux overnight. The mixture was concentrated, and the resulting residue was extracted with ethyl acetate, washed, dried, evaporated, and purified via silica gel chromatography (1:2 to 1:1 ethyl acetate:hexane) to yield 1.523 (38%) of a clear oil that had traces of starting material. ^{1}H NMR ($CDCl_3$, 400 MHz) δ 1.74 (s, 6H), 1.78 (s, 6H), 2.18 (s, 3H), 4.47-4.54 (m, 8H), 5.23-5.29 (m, 4H), 5.36-5.43 (m, 4H), 6.00-6.05 (m, 4H), 6.36-6.37 (t, 1H), 6.38 (t, 1H), 6.44 (br s, 1H), 6.54-6.57 (dd, 4H), 6.66-6.67 (d, 2H), 7.00-7.02 (d, 1H), 7.59 (br s, 1H); ^{13}C NMR ($CDCl_3$, 100 MHz) δ 17.1, 28.9, 31.7, 53.5, 68.9, 72.7, 81.7, 99.7, 99.8, 103.9, 104.0, 117.7, 117.8, 130.7, 133.3, 136.3, 136.9, 148.6, 148.7, 151.9, 159.6, 159.7. IR ($CHCl_3$, cm^{-1}) 2982, 1712, 1597, 1528, 1449, 1166, 1142, 1054, 927. Anal. Calcd for $C_{38}H_{52}N_2O_8$: C, 69.8; H, 6.9; N, 4.2. Found: C, 70.3, H, 7.5; N, 2.9.

Preparation of N,N'-Bis[[1-(3,5-dihydroxyphenyl)-1-methylethoxy]carbonyl]hexane-1,6-diamine (20). The bis-carbamate **18** (1.36 g, 2.04 mmol) was dissolved in methanol (12 mL) and tetrahydrofuran (22 mL). Tetrakis(triphenylphosphine)palladium (231 mg, 0.20 mmol) was added, and the solution was cooled in an ice bath before adding sodium borohydride (771 mg, 20.4 mmol). The mixture was stirred for 4 h before thin layer chromatography (2:1 ethyl acetate:hexane) showed reaction completion. The mixture was quenched with sodium bisulfate and concentrated. The residue was extracted with ethyl acetate, and the combined extracts were washed, dried, and evaporated, purified via silica gel chromatography (1:1 to 5:1 ethyl acetate:hexane), and finally triturated with CH_2Cl_2, ethyl acetate, and hexanes to give 978 mg

(95%) of a light tan solid. ^{1}H NMR (DMSO-d6, 400 MHz) δ 1.19 (br s, 4H), 1.33 (br s, 4H), 1.57 (s, 12 H), 2.84-2.85 (q, 4H), 6.05-6.06 (t, 2H), 6.17 (d, 4H), 6.95-6.98 (t, 2H), 9.08 (s, 4H); ^{13}C NMR (DMSO-d6, 100 MHz) δ 14.6, 26.5, 29.6, 29.9, 79.3, 101.1, 103.1, 149.8, 155.3, 158.4. IR (KBr, cm^{-1}) 3343, 2976, 2928, 1684, 1597, 1516, 1441, 1332, 1266, 1139, 996, 959. Anal. Calcd for $C_{26}H_{36}N_2O_8$: C, 61.9; H, 7.2; N, 5.6. Found: C, 61.87; H, 7.29; N, 5.55.

Preparation of N,N'-Bis[[1-(3,5-hydroxyphenyl)-1-methylethoxy]carbonyl]toluene-2,4-diamine (21). The bis-carbamate **19** (1.5 g, 2.2 mmol) was added to tetrahydrofuran (25 mL) and methanol (20 mL)**.** Tetrakis(triphenylphosphine)palladium (2.07 g, 0.179 mmol) was added, and the solution was cooled to 0° C before adding sodium borohydride (500 mg, 13.2 mmol). This mixture was stirred for 2 h, when it was quenched with saturated aqueous ammonium chloride, concentrated, and extracted with ethyl acetate. The combined extracts were washed, dried, evaporated, and purified via silica gel chromatography (1:1 to 5:1 ethyl acetate:hexanes) to yield a dark oil that was triturated with ethyl acetate, CH_2Cl_2, and hexanes to yield 900 mg (78%) of an off-white solid. ^{1}H NMR (DMSO-d6, 400 MHz) δ 1.64 (s, 12H), 2.09 (s, 3H), 6.06-6.07 (q, 2H), 6.22-6.24 (dd, 4H), 6.97-6.99 (d, 1H), 7.07-7.10 (d, 1H), 7.40 (s, 1H), 8.63 (br s, 1H), 9.12 (s, 2H), 9.13 (s, 2H), 9.44 (br s, 1H); ^{13}C NMR (DMSO-d6, 100 MHz) δ 17.2, 20.8, 29.1, 31.2, 70.5, 79.9, 100.1, 100.8, 100.9, 102.5, 102.6, 103.0, 114.6, 125.3, 130.0, 136.6, 137.4, 148.7, 148.9, 152.0, 152.7, 152.9, 157.8, 158.0, 158.1. IR (KBr, cm^{-1}) 3295, 2967, 1683, 1587, 1432, 1227, 1125, 1037, 993, 958. Anal. Calcd for $C_{27}H_{30}N_2O_8$: C, 63.5; H, 5.9; N, 5.4. Found: C, 63.29; H, 6.12; N, 5.29.

Preparation of N,N'-Bis[[1-(3,5-diglycidoxyphenyl)-1-methylethoxy]carbonyl]hexane-1,6-diamine (22). N,N'-dimethylformamide (10 mL) was added to the tetrahydroxybis-carbamate **20** (900 mg, 1.80 mmol) and cesium carbonate (2.85 g, 7.39 mmol). Epibromohydrin (4.93 g, 36 mmol) was then added, and the mixture was stirred overnight. The mixture was diluted with water and extracted with diethyl ether. The combined extracts were washed with 0.1 M aqueous NaOH, dried, evaporated, and purified via silica gel chromatography, eluting with 2:1 CH_2Cl_2:ethyl acetate, to yield 600 mg (45%) of a light yellow oil. ^{1}H NMR ($CDCl_3$, 400 MHz) δ 1.27 (br s, 4H), 1.43 (br s, 4H), 1.70 (s, 12H), 2.72-2.74 (dd, 4H), 2.88-2.90 (t, 4H), 3.05-3.06 (br d, 4H), 3.31-3.34 (m, 4H), 3.89-3.93 (dd, 4H), 4.16-4.19 (dd, 4H), 4.80 (br s, 2H), 6.37 (s, 2H), 6.55-6.56 (d, 4H); ^{13}C NMR ($CDCl_3$, 100 MHz) δ 26.2, 29.0, 30.0, 40.4, 44.8, 50.1, 68.8, 80.2, 99.4, 104.2, 149.6, 155.2, 159.4. IR ($CHCl_3$, cm^{-1}) 3362, 2980, 2931, 1711, 1597, 1521, 1448, 1257, 1176, 1153, 1058, 912. Anal. Calcd for $C_{38}H_{52}N_2O_{12}$: C, 62.6; H, 7.2; N, 3.8. Found: C, 62.74; H, 7.43; N, 3.67.

Preparation of N,N'-Bis[[1-(3,5-diglycidoxyphenyl)-1-methylethoxy]carbonyl]toluene-2,4-diamine (23). Dry N,N'-dimethylformamide (2 mL) was added to the tetrahydroxy bis-carbamate **21** (750 mg, 1.46 mmol) and cesium carbonate (2.26 g, 5.86 mmol) under nitrogen atmosphere. Epibromohydrin (2.9 mL, 35.2 mmol) was added via syringe, and the mixture was stirred for 48 h. The mixture was then diluted with water and extracted with diethyl ether. The combined extracts were washed with water, dried, evaporated, and purified via silica gel chromatography (1:20 to 1:5 ethyl acetate:dichloromethane) to yield 575 mg (53%) of a white solid. ^{1}H NMR ($CDCl_3$, 400 MHz) δ 1.74-1.78 (d, 12H), 2.19 (s, 3H), 2.73-2.74 (m, 4H), 2.87-2.89 (m, 4H), 3.31-3.33 (m, 4H), 3.91-3.93 (m, 4H), 4.15-4.21 (m, 4H), 6.36-6.40 (dt, 2H), 6.46 (br s, 1H), 6.56-6.60 (dd, 4H), 6.65 (br s, 1H), 7.00-7.02 (d, 2H), 7.22 (br s, 1H), 7.59 (s, 1H); ^{13}C NMR ($CDCl_3$, 100 MHz) δ 17.9, 29.0, 44.9, 50.3, 68.9, 69.0, 99.8, 99.9, 104.3, 104.4, 130.9, 136.4, 137.0, 149.1, 149.0, 149.1, 159.6, 159.7. IR ($CHCl_3$, cm^{-1}) 3340, 2983, 2928, 1729, 1598,

1530, 1448, 1232, 1176, 1138, 1051, 910. Anal. Calcd for $C_{39}H_{46}N_2O_{12}$: C, 63.7; H, 6.3; N, 3.8. Found: C, 63.45; H, 6.51; N, 3.92.

References

1) Meng, L. M.; Yuan, Y. C.; Rong, M. Z.; Zhang, M. Q. *J. Mater. Chem*. **2010**, *20*, 6030-6038.
2) Wu, C.; Hsu, S. L. *J. Micromech. Microeng*. **2010**, *20*, 015006.
3) Zhao, Y.; Barrera, E. V. *Adv. Func. Mater*. **2010**, ASAP
4) Gilbert, M. D.; Schneider, N. S.; MacKnight, W. J. *Macromolecules* **1991**, *24*, 360-369.
5) Güthner, T.; Hammer, B. *J. Appl. Polym. Sci*. **1993**, *50*, 1453-1459.
6) Fedtke, M.; Domaratius, F.; Walter, K.; Pfitzmann, A. *Polym. Bull*. **1993**, *31*, 429-435.
7) Hidekazu, I.; Masahiko, O.; Hideo, Y. European Patent 0193068, September 3, 1986.
8) Great Britain Patent 1,121,196, July 24, 1968.
9) Dooley, J. U.S. Patent 5,077,376, May 21, 1990.
10) Kayser, R. H.; Pollack, R. M. *J. Am. Chem. Soc*. **1977**, *99*, 3379-3387.
11) Suzuki, K.; Matsu-Ura, N.; Horii, H.; Sugita, Y.; Sanda, F.; Endo, T. *J. Appl. Polym. Sci*. **2002**, *83*, 1744-1749.
12) Suzuki, K.; Matsu-ura, N.; Horii, H.; Sugita, Y.; Sanda, F.; Endo, T. *J. Appl. Polym. Sci*. **2003**, *88*, 878-882.
13) Schile, R.D. U.S. Patent Application 20080227950, September 18, 2008.
14) Larsen, D.W. U.S. Patent 4,111,917, Sep. 5, 1978.
15) Wicks Jr., Z. W. *Prog. Org. Coat*. **1975**, *3*, 73-99.
16) Wicks Jr., Z. W. *Prog. Org. Coat*. **1981**, *9*, 3-28.
17) Wicks, D. *Prog. Org. Coat*. **1999**, *36*, 148-172.
18) Wicks, D. *Prog. Org. Coat*. **2001**, *41*, 1-83.
19) Spindler, R.; Fréchet, J.M.J. *Macromolecules* **1993**, *26*, 4809-4813.
20) Cameron, J. F.; Fréchet, J. M. J. *J. Org. Chem.* **1990**, *55*, 5919-5922.
21) Birr, C.; Lochinger, W.; Stahnke, G.; Lang, P. *Liebigs. Ann. Chem*. **1972**, *763*, 162-172.
22) Cameron, J.; Fréchet, J.M.J. *J. Photochem. Photobiol. A*. **1991**, *59*, 105-113.
23) Cameron, J.F,; Willson, C.G.; Fréchet, J.M.J., *J. Chem. Soc. Perkin Trans. I*, **1997**, 2429-42.
24) Cameron, J.F.; Willson, C.G.; Fréchet, J.M.J. *J. Am. Chem. Soc.* **1996,** *118*, 12925-12937.
25) Cameron, J.F.; Willson, C.G.; Fréchet, J.M.J. *J. Chem. Soc., Chem. Commun*. **1995**, 923-924.
26) Petrie, E. M. *Epoxy Adhesive Formulations*; McGraw-Hill: Blacklick, OH, USA, 2005, p 68.
27) Klute, C.H.; Viehmann, W. *J. Appl. Polym. Sci.* **1961**, *5*, 86-95.

Chapter 3
High Aspect Ratio Nanowires from Diketopyrrolopyrrole-Containing Small Molecules for Organic Electronics Applications

Abstract

One-dimensional nanocrystals (e.g. nanowires) made from organic small molecules have attracted increasing interest for the facile fabrication of organic electronic devices. These nanoparticles could provide the ability to control thin film morphology while retaining the solution processability advantages of existing fabrication methodologies. Using a promising small molecule shown to have good performance on organic photovoltaics, we show how small structural variations within the molecule vary the solid state packing and charge transport properties. In addition, these nanowires are compared to thin films of the same molecule both with respect to degree of crystallinity as well as hole mobility in organic field effect transistors. Optically active small molecule nanowires such as these may be attractive for the introduction of solution-processable, highly ordered nanoscale crystalline domains in the fabrication and optimization of organic electronic devices.

Introduction

Compared to inorganic and metallic semiconductors, organic semiconductors presently attract much attention in the scientific and industrial communities because of their potential as cost-effective and scalable alternatives in applications such as light-emitting devices, field effect transistors, and photovoltaics.[1-6] While solution processability, large scale synthesis, and electronic and molecular tunability are desirable attributes of organic semiconductors,[7, 8] the performance of these devices is highly sensitive to the morphology the molecules achieve in the solid state. In particular, thin film molecular packing strongly influences band gap and charge carrier mobility, both critical attributes in organic semiconductor devices.[9-11] Although ideally a thin film would consist of a uniform and ordered semiconductor packing, most organic semiconductors form polycrystalline thin films where grain boundaries inhibit charge transport and miniscule differences in device fabrication can have dramatic affects on their resulting properties.[12, 13]

An alternative to polycrystalline thin film devices is through the formation of single crystalline organic semiconductors, which contain minimal amounts of grain boundaries and molecular disorder and thus perform better than their thin film counterparts.[14-18] Forming single crystals from organic semiconductors can be a time consuming and inconsistent process, with the resulting crystals too brittle to be used in applications other than fundamental studies of charge transport. Nanoscale crystalline organic semiconductors, however, lack this brittleness and have the ability to be deposited on flexible substrates.[19-21] Because many one-dimensional (1D) nanocrystals self-assemble along the π-π stacking direction, the intermolecular interactions intrinsic to forming 1D nanocrystals also favor the same molecular packing that produces high charge carrier mobility.[22-24] Moreover, suspensions of nanocrystals can be handled with many of the same solution deposition techniques used to generate thin film devices.[25] Thus, devices fabricated with 1D nanocrystals (e.g. nanowires) have the possibility to combine the high performance of single crystal devices with the ease of processability of polycrystalline thin films.

Organic photovoltaics (OPVs), which require nanoscale segregation between donor and acceptor materials while preserving distinct pathways to transport charge, provide in theory an

ideal application for a solution processable 1D nanostructure, provided that a such a nanostructure is on the order of the exciton diffusion length intrinsic to the material used to make the nanostructures. Although bulk heterojunction OPVs are now reaching efficiencies as high as 7.7%,[26] nanowire/fullerene bulk heterojunction OPVs have thus far been made from self-assembled polymers.[27-29] Despite these promising results, there is a lack of reports on nanowires made from monodisperse, high purity small molecules for use in OPVs. Recently, a class of molecules have been synthesized by the Fréchet group that are designed to self-assemble within the active layer of OPVs to generate highly ordered domains, resulting in high-efficiency OPVs.[30] These molecules contain an alkylated diketopyrrolopyrrole (DPP) moiety in the core flanked by electron-rich end groups which direct intermolecular self-assembly. Herein we synthesize nanowires of one of the molecules in this study, a DPP bis-triphenylamine (DPP-TPA), and compare its crystallinity and electronic properties to that of thin films of the same molecule. In addition, we synthesize two structural analogues of DPP-TPA and compare their solid state crystallinity and ability to conduct charge.

Results and Discussion

The synthetic design of these DPP-TPA molecules is inspired by previous work on diketopyrrolopyrrole-containing small molecules with similar donor-acceptor-donor architectures in organic photovoltaics.[30] DPP-TPA can be synthesized in a straightforward four-linear-step sequence,[31] starting with the formation, alkylation, and bromination of the DPP core (Scheme 3.1). Triphenylamine can then be attached on either end through Suzuki cross-coupling. Two different DPP-TPA derivatives were synthesized, one with a linear decyl alkyl chain and the other with a branched (2-ethyl)hexyl chain. While both provided ample solubility in nonpolar organic solvents, it was expected that the two alkyl chains would affect formation of crystalline domains, either through changing the crystal geometry or altering crystallization kinetics.

Scheme 3.1. Synthesis of alkylated DPP-TPA small molecules **5a** and **5b.**

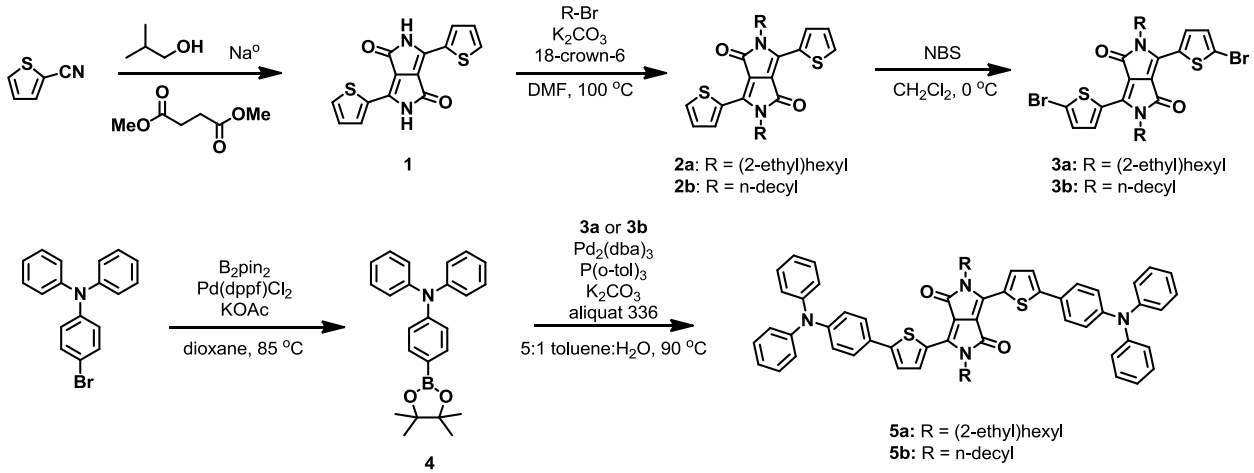

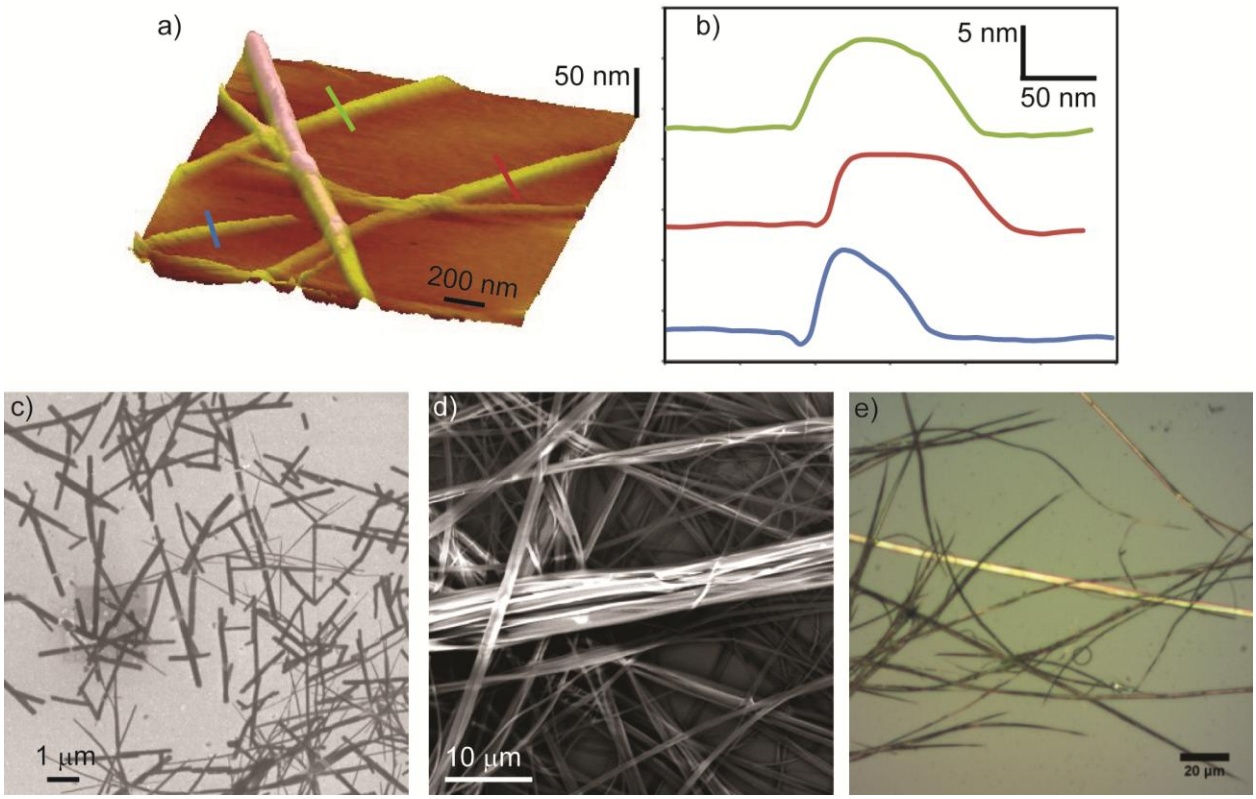

Figure 3.1. a) AFM image of **5b** on Si/SiO_2, cast immediately after nanowire formation. b) Line scans of wires in image (a). c) and d) SEM images of **5b**, c) cast immediately after formation on Si/SiO_2; d) cast after 48 h on Si/SiO_2. e) Optical microscope image of **5b**, cast after 48 h on glass.

Nanowires were formed through typical solution-phase methods, where molecules with predominant π-π stacking over side-chain van der Waals interactions rapidly self-assemble into crystalline domains. Specifically, a solution of the molecule in chloroform, a "good" solvent, is rapidly dispersed into methanol or ethanol, both "bad" solvents. Interestingly, while all the molecules used in the initial organic photovoltaic study[30] formed nanocrystalline domains when precipitated, the DPP-TPA molecules displayed a proclivity to self-assemble into 1D nanowires with a high aspect ratio. Immediately after initiation of precipitation, ordered nanostructures are formed which have a length of microns, widths ranging from 70-100 nm, and heights on the order of 7-10 nm, as measured by AFM (Figure 3.1a and b). Surfactants were not used in order to minimize barriers to charge conduction in the final particle film. While the initial wires are relatively monodisperse in terms of size as seen in Figure 3.1c, as the wires sit in suspension they increase in size and tend to aggregate, resulting in bundles and clusters of micron-scale wires, seen under SEM in Figure 3.1d and optically in Figure 3.1e. Because these bundles inevitably contain grain boundaries

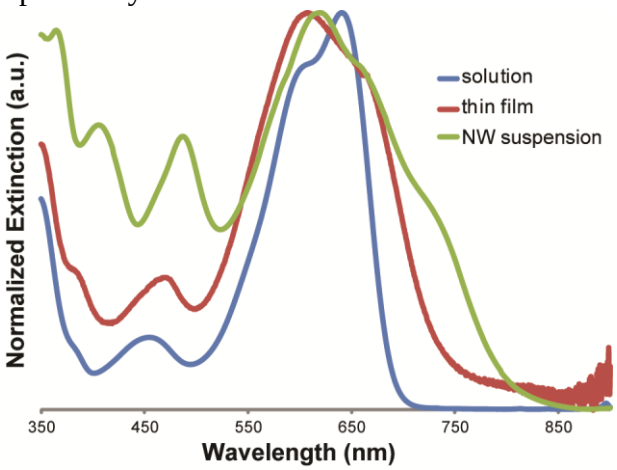

Figure 3.2. UV-vis spectra comparing the optical features of **5b** in $CHCl_3$ solution, spin cast from $CHCl_3$ onto quartz as a thin film, and as a nanowire dispersion in ethanol.

and trap sites, we found that casting the nanowires immediately after formation led to the most consistent device results.

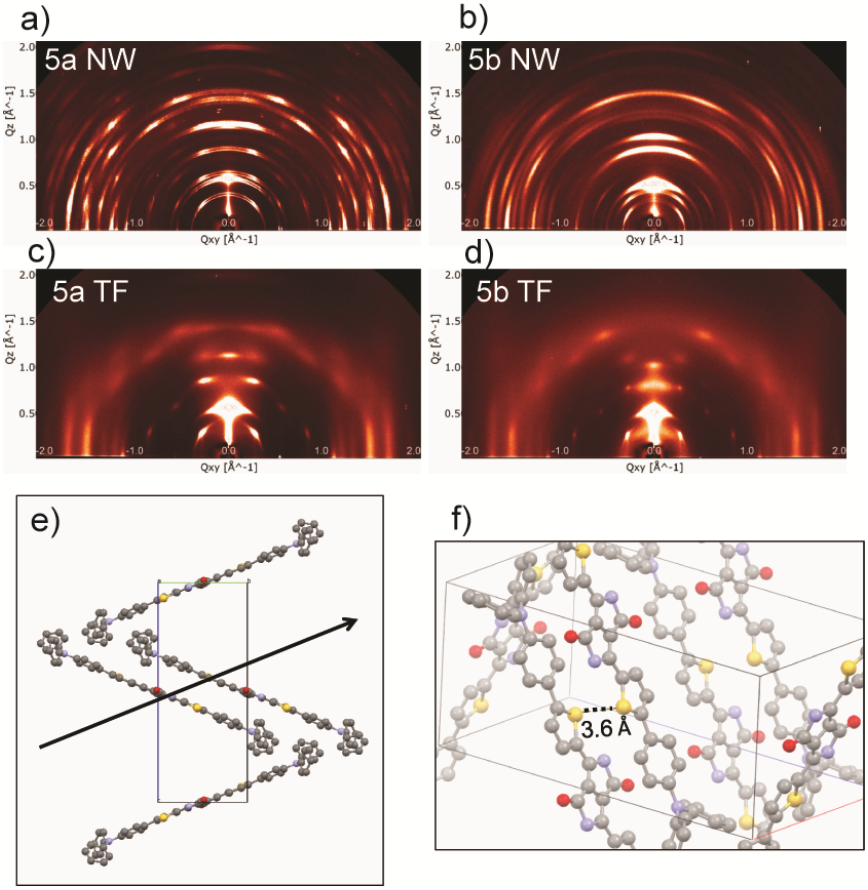

Figure 3.3. 2D GIXS scans of (a) **5a** nanowires, (b) **5b** nanowires, (c) **5a** thin film, (d) **5b** thin film. (e) and (f) Single crystal X-ray structure of **5a**, (e) viewed down the *a*-axis with the black arrow indicating probable electron transport direction; (f) angle view showing overlap. Alkyl chains are omitted for clarity. The thiophene-thiophene interplanar distance is ~3.6 Å, indicating π-π overlap between adjacent molecules.

To elucidate the differences in molecular packing between the DPP-TPA small molecules in thin film and nanowire states as well as to gain further insight into how the condensation of small molecules into nanoparticles influences their ability to form crystalline domains, the nanowires were investigated by both UV-vis spectroscopy and GIXS. In particular, UV-vis spectroscopy has been shown to be quite successful in characterizing the degree of order within colloidal nanocrystalline domains.[32] Spectra of both the thin film and nanowire dispersion of **5b** were compared to a sample of the same molecule fully solvated in chloroform (Figure 3.2). In solution, **5b** exhibits a maximum absorption at 637 nm, exhibiting a typical intramolecular charge transfer between diketopyrrolopyrrole and triphenylamine. When cast as a thin film the maximum absorption is blue-shifted slightly, which is attributed to either an overall lack of crystalline regions within the thin film or a higher prevalence of crystal defects within the thin film, both likely caused by the head-to-head coupling of the side chains in the small molecule giving rise to H-aggregates. However, the onset of absorption is also red-shifted relative to the solution phase due to increased order through solid-state π-π stacking. The presence of both a blue-shifted absorption maximum and a red-shifted absorption onset indicates that there are both regions of order due to intermolecular π-π stacking as well as significant portions of the thin film

with amorphous features or order due to side-chain interactions. When the nanowires are suspended in ethanol, the maximum absorption red-shifts relative to the thin film, the absorption onset red-shifts even further, and a new absorption feature appears at 702 nm. When compared to the thin film, the colloidal spectrum exhibits a clear enhancement of order through π-π stacking relative to order provided through van der Waals interactions within the side chains.

As a means to further investigate the differences in crystallinity between not only DPP-TPA nanowires and their thin films but also DPP-TPA nanowires with different alkyl side chains, 2D GIXS spectra were taken of **5a** and **5b** both as spin-cast thin films, but also as thin films of nanowires drop-cast from their ethanol suspensions (Figure 3.3 a-d). The scattering pattern clearly show sharply-defined peaks and rings for both **5a** and **5b** nanowires, suggesting a higher degree of crystallinity than the thin films, which appear more amorphous with less sharply defined peaks and rings. Two interesting observations can be made when comparing the nanowire scattering patterns between **5a** and **5b**. First, because the patterns for both appear as mainly concentric arcs instead of peaks, the crystalline features are not orienting themselves in relation to the substrate, indicating that the crystallinity of the film was established prior to deposition. Second, **5a** and **5b** have drastically different scattering patterns and appear to consist of multiple unit cells, thus showing different packing geometries despite differing only by their side chains. Because these nanowire films were made soon after formation thereby kinetically trapping the crystals, the differences seen in the nanowire GIXS signifies the influence of the side chain in directing the arrangement of the DPP-TPA small molecules into forming crystalline domains. Likely due to the increased planarity of the DPP-thiophene core relative to the triphenylamine moiety, a single crystal X-ray analysis of **5a** shows a close face-to-face packing within individual DPP-TPA molecules, with substantial overlap between the DPP-thiophene cores (Figure 3.3 e and f). The interplanar distance between the sulfurs of two thiophene units are 3.6 Å, indicating strong face-to-face π-π stacking between molecules and suggesting charge transport both along the DPP-thiophene core as well as from molecule to molecule.

Table 3.1. OFET conditions and device data for DPP-TPA thin films.

	Substrate	**Conditions**	**Hole mobility (cm^2/Vs)**	**V_{th} (V)**	**On/Off ratio**
5a	UV/O_3–treated SiO_2	As cast	1.5×10^{-4}	-20	10^3
		110 °C – 10 min	3.65×10^{-4}	-7	10^4
	OTS-treated SiO_2	As cast	2.09×10^{-4}	-10	10^3
		110 °C – 10 min	1.8×10^{-3}	-16	10^4
5b	Bare SiO_2	As cast	3.63×10^{-4}	-19	10^5
		110 °C – 10 min	1.31×10^{-3}	-19	10^4
	UV/O_3–treated SiO_2	As cast	7.14×10^{-4}	1.2	10^5
		110 °C – 10 min	1.44×10^{-3}	8	10^2
	HMDS-treated SiO_2	As cast	2.29×10^{-4}	3	10^4
		110 °C – 10 min	6.70×10^{-4}	4	10^3
	OTS-treated SiO_2	As cast	1.04×10^{-4}	0	10^3
		110 °C – 10 min	1.43×10^{-3}	-7	10^4

To evaluate the performance of DPP-TPA nanowires for electronic device applications, bottom contact OFETs were fabricated and compared to thin film DPP-TPA OFETs. The thin film OFETs were fabricated by spin-coating a solution of the small molecule fully dissolved in chloroform. The charge carrier mobility in solution-processed OFETs is very dependent upon solid-state packing, orientation, and elimination of amorphous regions and grain boundaries. The surface treatments, annealing conditions, and device data for the thin film OFETs are summarized in Table 3.1. Although modifying the surface through the use of UV/ozone

treatment or self-assembled monolayers has been shown to affect both the mobility and threshold voltage (V_{th}) of OFETs,[33-35] films of **5b** exhibited decreased V_{th} values compared to the untreated SiO_2 surface but gave similar hole mobilities all on the order of 10^{-4} $cm^2V^{-1}s^{-1}$, and the UV/ozone treated surface gave the best mobility for the as-cast film. In contrast, thin films of **5a** on treated surfaces had similar mobilities but higher turn-on voltages, with the best-performing devices fabricated on OTS-treated surfaces. Thermal annealing in all cases increased mobility, in the cases of the bare SiO_2 (for **5b**) and the OTS-treated SiO_2 (for both **5a** and **5b**) surfaces by nearly a full order of magnitude.

While the thin film OFETs can fabricated by traditional solution processing and readily tested through existing instrumentation, the novelty of fabricating and testing nanowire OFETs led us to attempt a variety of different fabrication approaches. In addition, making an accurate measurement of the mobility of a nanocrystalline domain of a semiconductor is an inherently difficult process, so each fabrication approach brings with it different pros and cons. The first approach we tried was inspired by the fully-coated film produced by solution-processed OFETs, where a nanowire suspension in ethanol is repeatedly spin-coated onto the surface. In theory, this approach leads to a buildup of nanowires on the surface over time, a fully (or close to it) covered surface, and a totally (or mostly) filled transistor channel. The viability of consecutive spin-coating is shown in Figure 3.4, where a suspension of nanowires of **5b** in ethanol is repeatedly spin-coated onto quartz at a low spin rate, (300 rpm). Although there is clear buildup of nanowires on the quartz surface as measured both optically and by UV-vis spectroscopy, the low concentration of nanowire in the ethanol suspension requires a substantial number of iterative depositions before appreciable buildup is achieved. In addition, the rightmost film in Figure 3.4a shows that even after 50 depositions, the surface is not homogeneously covered in nanowires.

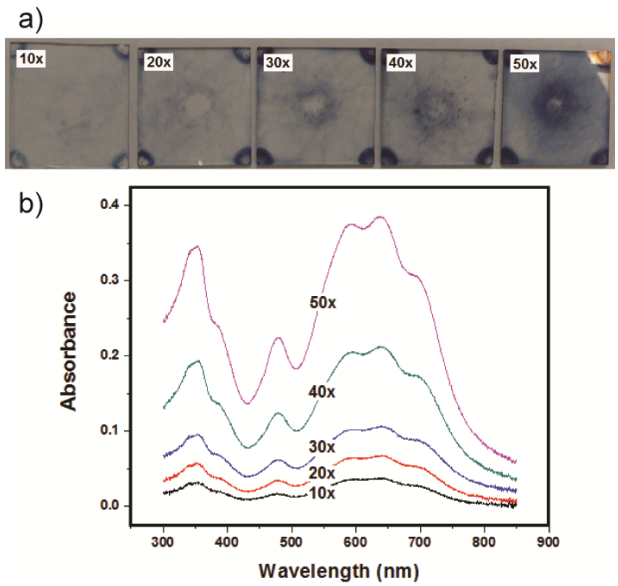

Figure 3.4. a) Optical microscope images of a quartz film with corresponding number of nanowire depositions. Each deposition was spin-cast at 300 rpm for 30 s from ethanol nanowire suspension. b) UV-vis spectra from corresponding films in (a).

OFETs were formed using this process where a surface was subjected to 35 consecutive depositions of nanowires from ethanol suspension, and a typical image of the FET channel as well as representative output and transfer curves are shown in Figure 3.5. Mobilities, summarized in Table 3.2, are on par with those measured in thin film DPP-TPA OFETs, with the highest a device of **5b** nanowires with a UV/ozone treated surface and is annealed for a short time at elevated temperature. There are some interesting differences between the device performances depending upon the molecule used. **5a** nanowire devices have slightly higher mobilities than their thin film devices, but annealing decreases both mobility and on/off ratio. Interestingly, in the case of a **5b** device with an OTS-treated surface, annealing substantially increases mobility and decreases the threshold voltage. Although annealing should not change the crystalline packing of the molecules within a nanowire, it is probable that a brief period of

elevated temperature removes traces of solvent left behind from deposition and promotes a more intimate contact with the surface of the dielectric, thus lowering interfacial trap states. The extent to which annealing can generate a more intimate contact then depends upon the dimensions of the nanowire, where smaller nanowires experience a larger change due to interface than larger nanowires. **5b** nanowires form faster and are able to be deposited immediately after initiation of precipitation, they are smaller in size and thus see a larger effect from annealing, whereas the devices made from **5a** nanowires sat for nearly 1 h before starting consecutive depositions, giving larger nanowires that experienced a smaller annealing effect. As nanowire formation kinetics differ between **5a** and **5b**, it is likely that careful control over how long the **5a** suspension sits before starting deposition (not immediately after initiation but less than an hour) could yield nanowires of comparable size to the **5b** nanowires.

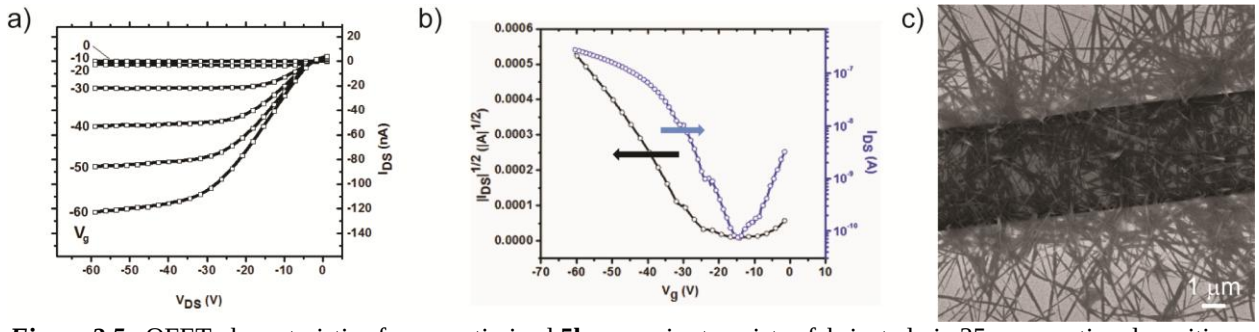

Figure 3.5. OFET characteristics for an optimized **5b** nanowire transistor fabricated via 35 consecutive depositions from ethanol suspension. a) Output characteristics; b) Transfer characteristics; c) Representative SEM image of FET channel.

The mobilities obtained from the nanowires demonstrate that the electronic character of the semiconducting small molecule is not degraded during nanowire formation or device fabrication, an astonishing feat when considering that 35 consecutive spins were required to fabricate the device. There are two key limitations with this measurement that lead us to believe that this is not the true mobility of the crystalline nanowire, however. First, the heterogeneous geometries of the nanowires as deposited leads to a multitude of spatial scenarios where the nanowires may be in contact with any combination of either or both electrodes, the dielectric, or other nanowires. This nonuniformity lead to barriers to charge injection and extraction, manifested through a high contact resistance. Second, we assumed that roughly 75% of the channel was filled with nanowires, which simplified the dimensional calculations required to calculate mobility but whose accuracy is nearly impossible to verify. As a result we concluded that while this OFET was an important step in ascertaining a meaningful nanowire measurement, an OFET consisting of a single nanowire would overcome both limitations as described above.

Table 3.2. OFET conditions and device data for nanowires of **5a** and **5b** fabricated by 35 consecutive depositions from ethanol suspension.

	Substrate	Conditions	Hole mobility (cm^2/Vs)	V_{th} (V)	On/Off ratio
5a	UV/O_3–treated SiO_2	As cast	3.8×10^{-4}	-12	10^4
		110 °C – 10 min	6.58×10^{-5}	-9	10^3
	OTS-treated SiO_2	As cast	6.18×10^{-4}	-14	10^3
		110 °C – 10 min	No signal	-	-
5b	UV/O_3–treated SiO_2	As cast	1.4×10^{-3}	-24	10^5
		110 °C – 10 min	2.04×10^{-3}	-23	10^4
	OTS-treated SiO_2	As cast	2.76×10^{-4}	-28	10^4
		110 °C – 10 min	9.01×10^{-4}	-12	10^4

The next step was to attempt to fabricate and measure a single wire OFET. When handled with minimal agitation, the nanowires in the suspension eventually grow to reach microns in length, large enough to be handled with a micromanipulator. The ability to select a single microwire and place it across both electrodes circumvents the random geometries that spin-coating from suspension that led to prior difficulties in producing a successful OFET. With this in mind, microwire OFETs using wires grown from suspension of **5a** for ~2 weeks was placed on devices using a micromanipulator. Whereas the FETs were measured under inert conditions, the micromanipulations were performed at atmosphere. Figure 3.6a shows an optical microscope image of a device with 2 µm channel lengths. Unfortunately the signal is noisy and no drain current saturation is observed in either device (Figure 3.6b), and increasing the channel length of 20 µm led to similar results. Because this effect happens in both cases, short channel effects where charge transport through the bulk dominates the measured current are almost certainly being experienced.[36] In addition, the noisy output curves also indicate high contact resistance, which is surprising considering the micromanipulation was hypothesized to generate intimate contact to the source and drain electrodes. Finally, an SEM imaging the device from Figure 3.6a from a 45 degree angle (Figure 3.6c) shows a clear air gap between the bridging microwire and the dielectric. As the air gap changes both the dimensions and the permittivity of the dielectric, this non-ideal device architecture is also contributing to noise and increased bulk transport.

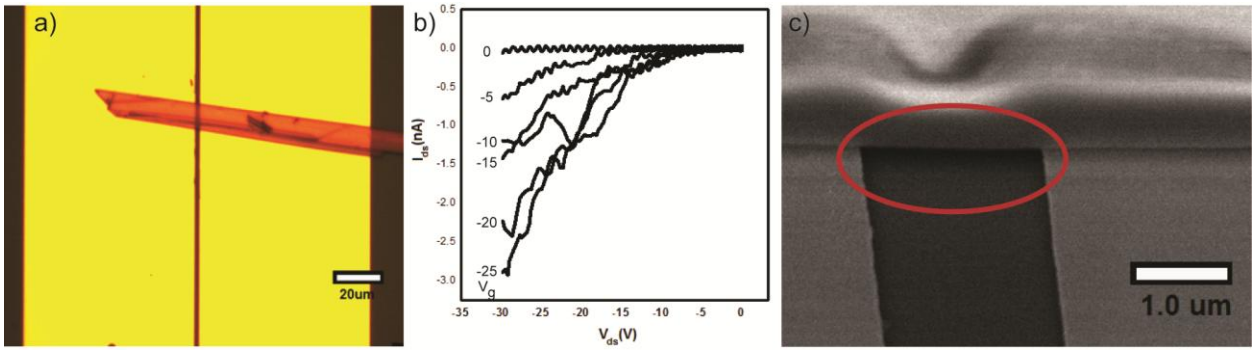

Figure 3.6. (a) Optical images of FET microwire devices of **5a**, with 2 µm channel lengths. (b) Output characteristics of (a). (e) SEM image of device (a), taken at a 45° angle showing air gap that exists between the microwire and the dielectric. Red oval added to clarify region of interest.

Based upon the limitations of fabricating OFETs via micromanipulation, we next attempted spin-coating a dilute suspension of microwires, a process less delicate than micromanipulation. We hypothesized that this process should allow the wires to better adhere to the surface, limit contact resistance, and give a more ideal device architecture. An OFET was fabricated in this manner, where a two day-old suspension of **5a** in ethanol was spin-coated onto a device with a bare SiO_2 surface. The device, whose performance and a representative image is shown in Figure 3.7, had a measured mobility in air of $\mu_h = 7.4 \times 10^{-3}$ $cm^2V^{-1}s^{-1}$. This is the highest value obtained for a crystalline DPP-TPA crystal, and is over an order of magnitude higher than the optimized **5a** thin film device mobilities. While this device performance is encouraging, questions remain concerning the crystallinity of this microwire, as Figure 3.7c clearly shows the wire bending upon itself and crossing the channel twice. Since these nanowires tend to aggregate over time to form micron-scale bundles and clusters (vide supra), this device may contain grain boundaries, defects, and trap sites, all of which hinder device mobility.

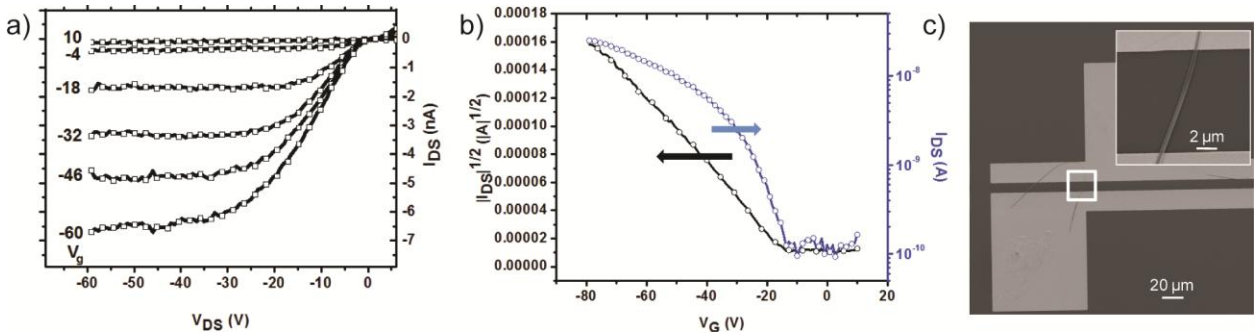

Figure 3.7. OFET characteristics for **5a** microwire transistor fabricated via single deposition from ethanol suspension allowed to grow for 48 h. a) Output characteristics; b) Transfer characteristics; c) Representative SEM image of FET channel. Inset in (c) corresponds to region in white box.

Because of the aforementioned problems with both consecutive deposition and microwire approaches with fabricating and testing these OFETs, it was decided that a single nanowire FET with the nanowires cast from suspension immediately after formation will have the lowest number of grain boundaries and defects, will have smaller dimensions to limit bulk transport, and should thus give the truest mobility value. OFETs fabricated in this manner have typically obtained currents below the detection limit of the instrument likely due to high contact resistance. Although decreasing the channel length in theory should increase the current signal, channels under 5 µm in length typically run in to the same short channel effects experienced with the microwire OFETs. As such, to date we have yet to successfully fabricate and measure a single nanowire device in this manner.

Conclusions and Outlook

The goal of this project was to find a way to establish long-range crystalline order, an important characteristic associated with increased charge transport, in organic electronic devices using a small molecule that has been shown to be successful in OPVs. Traditional methods of forming order, typically thermal annealing post-deposition, while often effective do not completely eliminate grain boundary formation in devices. As an alternative to thermal annealing post-deposition, we envisioned forming pre-organized nanocrystalline domains, which could then be deposited in a controlled fashion to generate high performance devices. In this chapter, we have accumulated a large body of evidence to support our ability to generate nanoscale domains that are indeed more ordered than the same small molecule in a thin film, and we have shown that the electronic character of the nanowires is sustained through nanowire formation and processing. Multiple questions remain, most prominently whether or not it is possible to obtain the "true" mobility of these nanowires; the ramifications of altering the molecular skeleton of the nanowires on the device performance; and if these nanowires can be used successfully in OPVs.

Ideally, a desirable alternative to thermal annealing will satisfy at least one of the following scenarios: (1) it can generate comparable performance but must have better processability; or (2) it can have similar processability but must perform better. While OFETs made from these crystalline domains have been shown to have similar or slightly better hole mobilities than their thin film counterparts, they are not yet able to be processed as easily or as rapidly as thin films and thus the first scenario does not look attainable. We hypothesize that devices made from nanowires, if they are indeed single crystals, should have mobilities an order of magnitude higher than thin film devices, and while we have succeeded with **5a**, short channel effects and high contact resistance have hindered our ability to accurately measure **5b** nanowires.

A successful measurement of these nanowires, it follows, must be done on a channel length long enough to limit these short channel effects. In addition, a more intimate nanowire-electrode contact must be formed to decrease noise and limit contact resistance, either through brief thermal annealing (which we demonstrated did enhance signal to noise ratio in isolated cases); modifying the gold surface to improve the physical connection between electrode and semiconductor channels;[37] by using a four point probe; or fabricating a device with top-contact geometry.

Although there are many literature examples of conjugated small molecules that have been shown to form nanowires, our approach is unique in that we use a visible-light absorbing small molecule that has been shown to generate power in OPVs. Thus, the ultimate proof of concept experiment with this material is to fabricate a working OPV device using these nanowires and a suitable acceptor. The fact that these nanowires are unstable in solvents conventionally used for nanowire/fullerene OPVs (such as chloroform, toluene, and chlorobenzene) presents significant processing difficulties. The use of an alcohol-soluble fullerene derivative or some other alcohol-soluble acceptor material may provide a means to circumvent these limitations.

Experimental

Materials. All reagents were obtained from commercial sources and used without further purification unless otherwise noted. Unless otherwise noted, all reactions were carried out under nitrogen with standard Schlenk techniques, and all glassware used in palladium-catalyzed reactions were oven-dried prior to use. All solvents used were reagent grade (99.9%) unless otherwise noted. Toluene, water, and dioxane used in palladium-catalyzed coupling reactions were degassed using three freeze-pump-thaw cycles before use. Flash chromatography was performed using Silicycle SilicaFlash® P60 (particle size 40-63 μm, 230-400 mesh) silica gel. Compounds containing stereocenters were obtained as a mixture of stereoisomers.

Characterization. Elemental analysis was performed by the UC Berkeley analytical facilities. ^{1}H and ^{13}C NMR measurements were conducted on a Bruker AVB-400 nuclear magnetic resonance spectrometer. UV-vis-NIR spectra were taken using a Shimadzu 3600 spectrophotometer. Crystals suitable for x-ray were prepared by vapor diffusion of ethanol into toluene. Atomic force microscopy was performed using a Digital Instruments (Veeco) Multimode AFM with a Nanoscope V controller and RTESP tips. Scanning electron microscopy was performed on a JEOL field emission scanning electron microscope. Grazing incidence X-ray scattering (GIXS) spectra were obtained at the Stanford Synchrotron Radiation Lightsource on beamline 11-3. The sample was irradiated at a fixed incident angle (angle = 0.10°), and the GIXS patterns were recorded with a 2D detector (MAR345 image plate). The X-ray energy was 12.72 keV (λ = 0.975 Å). Samples were prepared by drop-casting multiple layers of the as-synthesized nanowires or spin-casting a solution of the nanowire precursor onto silicon (100) substrates coated with native oxide.

Small molecule X-ray diffraction was performed at the Lawrence Berkeley National Laboratory Advanced Light Source on Beamline 11.3.1. Crystals suitable for X-ray analysis were grown by vapor diffusion of ethanol into toluene. Crystals were removed from the sample tube, placed in Paratone oil on a microscope slide, and examined using a microscope in crossed polarizers. Good examples were picked up on a Mitegen Kaptan loop on a magnetic base and mounted in the 100(2) K nitrogen cold stream provided by an Oxford Cryostream low temperature apparatus on the goniometer head of a Bruker AXS D85 diffractometer equipped with an ApexII CCD detector. The crystal was centered and initial diffraction data were

collected using synchrotron radiation monochromated with silicon (111) to $\lambda = 0.77490$ Å, to determine the orientation matrix, unit cell, and the crystal quantity. A full sphere of data was collected using 0.3° ω scans at 3 different ϕ settings. The data were integrated with SAINT to provide indices and intensities for the reflections. A multi-scan absorption correction was applied using the program SADABS 2008/1. The structure was solved by direct methods (SHELKS) and refined by full-matrix least-squares on F^2 (SHELXL-97).

OFET device preparation and testing.

Bottom contact field effect transistors (FETs) were fabricated using conventional photolithographic methods on silicon wafers with a 300 nm thermally grown silicon dioxide gate dielectric (Addison Engineering). Prior to deposition of the organic film, the FET substrates were cleaned by sonicating sequentially in a surfactant solution (Hellmanex II, 1% in H_2O), DI water, acetone, and isopropyl alcohol for 20 minutes each. Organic field effect transistors were fabricated on substrates with four different gate dielectric surface conditions; namely untreated bare SiO_2, UV/O_3 oxidized SiO_2, 1,1,1,3,3,3-hexamethyldisilazane (HMDS) treated SiO_2, and n-octadecyltrichlorosilane (OTS) functionalized SiO_2. Bare SiO_2 substrates were used 'as is' immediately following the sonication cleaning procedure. Oxidized SiO_2 dielectrics were produced by exposing to UV/O_3 for 30 minutes using a UVOCS, Inc. ultraviolet-ozone cleaning system (model T10X10). HMDS treated surfaces were fabricated by first exposing the substrate to 30 minutes of UV/O_3 treatment followed by exposure to HMDS vapor at 80°C under static vacuum (~ 1mbar). For OTS surfaces, 30 minutes UV/O_3 was followed by soaking in a 40 mM solution of n-octadecyltrichlorosilane in hexanes for 2 hours. OTS functionalized substrates were removed from the OTS solution and sonicated in toluene for 30 seconds to remove physisorbed molecules, rinsed with isopropyl alcohol, and dried with a light N_2 stream. Films were spuncoat at 1500 RPM for 1 second (Specialty Coating Systems, model P6700) from 3mg/ml solutions in chloroform or chlorobenzene under N_2 atmosphere inside a glovebox. The films were allowed to dry for a minimum of 30 minutes prior to electrical analysis using an HP 4155C semiconductor parameter analyzer. Electrical characterization was performed under N_2 inside a glovebox.

General method for solution-phase nanowire synthesis.

In a typical experiment, 10 mg of a given DPP-TPA was dissolved in 1 mL of chloroform (CHCl3, anhydrous, 99%) and stirred overnight at room temperature. After complete dissolution, aliquots of this solution were diluted with CHCl3 to produce 1 and 0.1 mg/mL concentrations; both concentrations were then used for synthesis. At the same time, ethanol (EtOH, 200 proof, molecular biology grade) was bubbled with nitrogen for 30 min and immediately transferred to a glovebox. Next, 100 μL of the DPP-TPA solution was loaded into a syringe and subsequently introduced dropwise (rate ~10 μL/s) into 3 mL of the stirring (550 rpm) EtOH. Particle formation was carried out in a nitrogen glovebox. Typically, this suspension was then allowed to sit for ~1 h before being deposited onto the surface for analysis (in the case of **5a**) or immediately deposited (in the case of **5b)** However, because the nanowire suspension contains no surfactants or stabilizing ligands to inhibit particle aggregation, the nanowires will keep growing and eventually aggregate over an appreciable time scale.

Preparation of alkylated DPP precursors.

3,6-Di(thiophen-2-yl)pyrrolo[3,4-c]pyrrole-1,4(2H,5H)-dione (1). A 500 mL 3-necked flask connected to a reflux condenser was charged with *tert*-amyl alcohol (250 mL). Sodium metal (2.56 g, 108 mmol) immersed in mineral oil was thoroughly washed with hexanes and cut into

small pieces. Sodium metal pieces were slowly added to the reaction mixture over a 1.5 h period. After addition was complete, the temperature was slowly increased to 120 °C, during which the metal pieces began to bubble and the reaction mixture turned light yellow. After all sodium metal pieces were dissolved, 2-thiophenecarbonitrile (11.9 g, 108 mmol) was added to the solution followed by the dropwise addition over 1 h of dimethyl succinate (5.29 g, 36.2 mmol), during which the solution turned dark red. The reaction contents were stirred at 120 °C for 2 h, and then precipitated into acidic MeOH (400 mL MeOH and 20 mL conc. HCl). Filtration of the suspension through a Buchner funnel yielded a maroon solid (9.10 g), which was used in subsequent reactions without further purification.

2,5-Bis(2-ethylhexyl)-3,6-di(thiophen-2-yl)pyrrolo[3,4-c]pyrrole-1,4(2H,5H)-dione (2a): To a nitrogen-purged solution of **1** (2.04 g, 6.79 mmol), potassium carbonate (2.82 g, 20.4 mmol), and 18-crown-6 (54 mg, 0.204 mmol) in DMF (70 mL) was added (2-ethylhexyl)bromide (3.94 g, 20.4 mmol). The mixture was heated to 100 ^{o}C for 48 h, after which the reaction was cooled to room temperature and precipitated into water. The solids were washed with water and methanol, dissolved in chloroform, concentrated, and purified via silica gel chromatography with chloroform as eluent to yield 677 mg (19%) of a purple solid. ^{1}H NMR (400 MHz, $CDCl_3$): δ 8.89 (d, 2H), 7.61 (d, 2H), 7.25 (m, 2H), 4.01 (m, 4H), 1.85 (m, 2H), 1.29 (m, 16H), 0.85 (m, 12H). ^{13}C (100 MHz, $CDCl_3$): δ 161.8, 140.5, 135.4, 130.6, 130.0, 128.5, 108.0, 45.9, 39.2, 30.3, 28.4, 23.6, 23.2, 14.1, 10.6. HRMS (EI, *m/z*) Calcd. for $C_{30}H_{40}N_2O_2S_2$ $[M]^+$: 524.2531; found: 524.2535. Anal. Calcd. for $C_{30}H_{40}N_2O_2S_2$: C, 68.66; H, 7.68; N, 5.34; found: C, 68.73; H, 7.90; N, 5.34.

2,5-Bis(decyl)-3,6-di(thiophen-2-yl)pyrrolo[3,4-c]pyrrole-1,4(2H,5H)-dione (2b): To a nitrogen-purged solution of **1** (2.01 g, 6.69 mmol), potassium carbonate (2.77 g, 20.1 mmol), and 18-crown-6 (53 mg, 0.201 mmol) in DMF (70 mL) was added decyl bromide (4.44 g, 20.1 mmol). The mixture was heated to 100 ^{o}C for 48 h, after which the reaction was cooled to room temperature and precipitated into water. The solids were washed with water and methanol, dissolved in chloroform, concentrated, and precipitated into methanol to yield 1.44 g (37%) of a purple solid. ^{1}H NMR (400 MHz, $CDCl_3$): δ 8.93 (d, 2H), 7.64 (d, 2H), 7.29 (t, 2H), 4.07 (t, 4H), 1.74 (m, 4H), 1.41-1.25 (m, 28H), 0.87 (t, 6H). ^{13}C (100 MHz, $CDCl_3$): δ 161.3, 135.2, 130.7, 128.6, 42.2, 31.9, 29.9, 29.5, 29.3, 29.2, 25.8, 22.7, 14.1. HRMS (ESI, *m/z*) Calcd. for $C_{34}H_{49}N_2O_2S_2$ $[M+H]^+$: 581.3230; found: 581.3228. Anal. Calcd. for $C_{34}H_{48}N_2O_2S_2$: C, 70.30; H, 8.33; N, 4.82; found: C, 70.57; H, 8.48; N, 4.85.

3,6-Bis(5-bromothiophen-2-yl)-2,5-bis(2-ethylhexyl)pyrrolo[3,4-c]pyrrole-1,4(2H,5H)-dione (3a). A solution of **2a** (834 mg, 1.59 mmol) in chloroform (50 mL) was cooled to 0 ^{o}C, and n-bromosuccinimide (707 mg, 3.97 mmol) was added portionwise. The reaction was stirred at room temperature for 1 h, at which point it was concentrated and purified with silica gel chromatography (2:3 hexanes in chloroform) to yield 939 mg (86%) of a purple solid. ^{1}H NMR (400 MHz, $CDCl_3$): δ 8.65 (d, 2H), 7.22 (d, 2H), 3.98-3.87 (m, 4H), 1.83 (m, 2H), 1.33-1.25 (m, 16 H), 0.91-0.85 (dt, 12 H). ^{13}C (100 MHz, $CDCl_3$): 161.4, 139.4, 135.4, 131.5, 131.1, 119.0, 107.9, 46.0, 39.1, 30.2, 28.3, 23.5, 23.0, 14.0, 10.5. HRMS (ESI, *m/z*) Calcd. for $C_{30}H_{39}Br_2N_2O_2S_2$ $[M+H]^+$: 681.0814; found: 681.0816. Anal. Calcd. for $C_{30}H_{38}Br_2N_2O_2S_2$: C, 52.79; H, 5.61; N, 4.10; found: C, 52.79; H, 5.81; N, 4.09.

3,6-Bis(5-bromothiophen-2-yl)-2,5-bis(decyl)pyrrolo[3,4-c]pyrrole-1,4(2H,5H)-dione (3b). A solution of **2b** (1.45 g, 2.50 mmol) in chloroform (75 mL) was cooled to 0 ^{o}C, and n-bromosuccinimide (933 mg, 5.24 mmol) was added portionwise. The reaction was stirred at room temperature for 1 h, at which point it was concentrated and purified with silica gel

chromatography (2:3 hexanes in chloroform) to yield 1.52 g (82%) of a purple solid. ^{1}H NMR (400 MHz, $CDCl_3$): δ 8.69 (d, 2H), 7.24 (d, 2H), 3.98 (t, 4H), 1.71 (m, 4H), 1.41-1.26 (m, 28H), 0.87 (t, 6H). ^{13}C NMR omitted due to lack of solubility. HRMS (ESI, *m/z*) Calcd. for $C_{34}H_{47}Br_2N_2O_2S_2$ $[M+H]^+$: 737.1440; found: 737.1447. Anal. Calcd. for $C_{34}H_{46}Br_2N_2O_2S_2$: C, 55.28; H, 6.28; N, 3.79; found: C, 55.21; H, 6.36; N, 3.77.

N,N-Diphenyl-4-(4,4,5,5-tetramethyl-1,3,2-dioxaborolan-2-yl)aniline (4). A 3-neck 250 mL round bottom flask was charged with a stir bar, 4-bromotriphenylamine (4.00 g, 12.4 mmol), bis(pinacolato)diboron (3.29 g, 13.0 mmol), anhydrous KOAc (3.31 g, 33.6 mmol), dichloro[1,1'-bis(diphenylphosphino)-ferrocene]palladium(II) dichloromethane adduct ($Pd(dppf)Cl_2 \cdot CH_2Cl_2$) (271 mg, 0.332 mmol) and degassed dioxane (120 mL). After the reaction mixture was heated at 85 °C for 16 h, it was extracted with diethyl ether and washed with distilled water. The organic extract was dried over $MgSO_4$, and solvent was removal under reduced pressure yielded a brown viscous oil. Purification with flash chromatography (25 % hexanes in CH_2Cl_2) yielded 4.30 g of tacky off-white solid (95 %). ^{1}H NMR (400 MHz, $CDCl_3$): δ 7.67 (d, 2H), 7.26 (t, 4H), 7.11 (d, 4H), 7.04 (m, 4H), 1.34 (s, 12H). ^{13}C (100 MHz, $CDCl_3$): δ 150.7, 147.5, 136.0, 129.43, 125.1, 123.5, 121.9, 83.7, 25.0. HRMS (EI, *m/z*) Calcd. for $C_{24}H_{26}BNO_2$ $[M]^+$: 371.2057; found: 371.2068. Anal. Calcd. for $C_{24}H_{26}BNO_2$: C, 77.64; H, 7.06; N, 3.77; found: C, 77.61; H, 7.04; N, 3.93.

3,6-Bis(5-(4-(diphenylamino)phenyl)thiophen-2-yl)-2,5-bis(2-ethylhexyl)pyrrolo[3,4-c]pyrrole-1,4(2H,5H)-dione (5a). A 25 mL Schlenk tube charged with **3a** (139 mg, 0.204 mmol), **4** (159 mg, 0.428 mmol), bis(dibenzylideneacetone)palladium (3.74 mg, 2 mol %), tri-*o*-tolylphosphine (4.96 mg, 8 mol %), anhydrous K_2CO_3 (221 mg, 1.06 mmol), 1 drop of aliquat 336, was evacuated and backfilled with nitrogen 3 times, and then toluene (4 mL) and water (0.8 mL) were added. The reaction mixture was heated at 90 °C for 16 h before being precipitated into 250 mL of MeOH. The precipitates were filtered through a 20 μm nylon membrane, dissolved in chloroform, and concentrated. Purification by silica gel chromatography (35% to 20% hexanes in chloroform) yielded 123 mg (56%) of the desired product as a metallic purple solid. ^{1}H NMR (400 MHz, $CDCl_3$): δ 8.99 (d, 2H), 7.51 (d, 2H), 7.37 (d, 2H), 7.31-6.99 (m, 16H), 4.08-4.06 (m, 4H), 1.95 (m, 2H), 1.41-1.26 (m, 16H), 0.93-0.84 (dt, 12H). HRMS (FAB, *m/z*) Calcd. for $C_{66}H_{66}N_4O_2S_2$ $[M]^+$: 1010.4622; found: 1010.4638. Anal. Calcd. for $C_{66}H_{66}N_4O_2S_2$: C, 78.38; H, 6.58; N, 5.54; found: C, 78.10; H, 6.78; N, 5.32.

3,6-Bis(5-(4-(diphenylamino)phenyl)thiophen-2-yl)-2,5-bis(decyl)pyrrolo[3,4-c]pyrrole-1,4(2H,5H)-dione (5b). Reaction conditions and workup were the same as for **5a,** except **3b** (101 mg, 0.137 mmol), **4** (107 mg, 0.287 mmol), bis(dibenzylideneacetone)palladium (2.51 mg, 2 mol %), tri-*o*-tolylphosphine (3.35 mg, 8 mol %), anhydrous K_2CO_3 (146 mg, 1.06 mmol), 1 drop of aliquat 336, toluene (2.75 mL) and water (0.5 mL) were used. Purification by silica gel chromatography (45% to 20% hexanes in chloroform) yielded 123 mg (84%) of the desired product as a metallic blue solid. ^{1}H NMR (400 MHz, $CDCl_3$): δ 9.00 (d, 2H), 7.55 (d, 4H), 7.38 (d, 2H), 7.32-7.06 (m, 16H), 4.11 (t, 4H), 1.78 (m, 4H), 1.44-1.23 (m, 28H), 0.85 (t, 6H). HRMS (FAB, *m/z*) Calcd. for $C_{70}H_{74}N_4O_2S_2$ $[M]^+$: 1066.5248; found: 1066.5260. Anal. Calcd. for $C_{70}H_{74}N_4O_2S_2$: C, 78.76; H, 6.99; N, 5.25; found: C, 78.58; H, 7.15; N, 5.11.

References

(1) Arias, A. C. MacKenzie, J. D. McCulloch, I. Rivnay, J.; Salleo, A. *Chem. Rev*. **2010**, *110*, 3-24.
(2) Horowitz, G. *Adv. Mater*. **1998**, *10*, 365-377.
(3) Mitschke, U.; Bäuerle, P. *J.Mater. Chem*. **2000**, *10*, 1471-1507.
(4) Muccini, M. *Nat. Mater*. **2006**, *5*, 605-613.
(5) Murphy, A. R.; Fréchet, J. M. J. *Chem. Rev*. **2007**, *107*, 1066-1096.
(6) Thompson, B. C.; Fréchet, J. M. J. *Angew. Chem*. **2008**, *47*, 58-77.
(7) Afzali, A. Dimitrakopoulos, C. D.; Breen, T. L. *J. Am. Chem. Soc*. **2002**, *124*, 8812-8813.
(8) Anthony, J. E. Brooks, J. S. Eaton, D. L.; Parkin, S. R. *J. Am. Chem. Soc*. **2001**, *123*, 9482-9483.
(9) Joseph Kline, R. McGehee, M. D.; Toney, M. F. *Nat. Mater*. **2006**, *5*, 222-228.
(10) DeLongchamp, D. M. Kline, R. J. Lin, E. K. Fischer, D. A. Richter, L. J. Lucas, L. A. Heeney, M. McCulloch, I.; Northrup, J. E. *Adv. Mater*. **2007**, *19*, 833-837.
(11) DeLongchamp, D. M. Sambasivan, S. Fischer, D. A. Lin, E. K. Chang, P. Murphy, A. R. Fréchet, J. M. J.; Subramanian, V. *Adv. Mater*. **2005**, *17*, 2340-2344.
(12) Fichou, D. *J. Mat. Chem*. **2000**, *10*, 571-588.
(13) Nelson, S. F. Lin, Y.-Y. Gundlach, D. J.; Jackson, T. N. *Appl. Phys. Lett*. **1998**, *72*, 1854-1856.
(14) Karl, N. *Synthetic Met*. **2003**, *133-134*, 649-657.
(15) Briseno, A. L. Mannsfeld, S. C. B. Ling, M. M. Liu, S. Tseng, R. J. Reese, C. Roberts, M. E. Yang, Y. Wudl, F.; Bao, Z. *Nature* **2006**, *444*, 913-7.
(16) Boer, R. W. I. de; Gershenson, M. E. Morpurgo, A. F.; Podzorov, V. *Phys. Status Solidi A*. **2004**, *201*, 1302-1331.
(17) Gershenson, M. E.; Podzorov, V. *Rev. Mod. Phys*. **2006**, *78*, 973-989.
(18) Sundar, V. C. Zaumseil, J. Podzorov, V. Menard, E. Willett, R. L. Someya, T. Gershenson, M. E.; Rogers, J. A. *Science* **2004**, *303*, 1644-1646.
(19) Briseno, A. L. Tseng, R. J. Ling, M.-M. Falcao, E. H. L. Yang, Y. Wudl, F.; Bao, Z. *Adv. Mater*. **2006**, *18*, 2320-2324.
(20) Tang, Q. Li, H. He, M. Hu, W. Liu, C. Chen, K. Wang, C. Liu, Y.; Zhu, D. *Adv. Mater*. **2006**, *18*, 65-68.
(21) Tang, Q. Li, H. Song, Y. Xu, W. Hu, W. Jiang, L. Liu, Y. Wang, X.; Zhu, D. *Adv. Mater*. **2006**, *18*, 3010-3014.
(22) Curtis, M. D. Cao, J.; Kampf, J. W. *J. Am. Chem. Soc*. **2004**, *126*, 4318-28.
(23) Datar, A. Balakrishnan, K. Yang, X. Zuo, X. Huang, J. Oitker, R. Yen, M. Zhao, J. Tiede, D. M.; Zang, L. *J. Phys. Chem B*. **2006**, *110*, 12327-12332.
(24) Balakrishnan, K. Datar, A. Oitker, R. Chen, H. Zuo, J.; Zang, L. *J. Am. Chem. Soc*. **2005**, *127*, 10496-7.
(25) Briseno, A. L. Mannsfeld, S. C. B. Lu, X. Xiong, Y. Jenekhe, S. A. Bao, Z.; Xia, Y. *Nano Lett*. **2007**, *7*, 668-675.
(26) Chen, H.-Y. Hou, J. Zhang, S. Liang, Y. Yang, G. Yang, Y. Yu, L. Wu, Y.; Li, G. *Nat. Photonics*. **2009**, *3*, 649-653.
(27) Chen, H.-C. Wu, I.-C. Hung, J.-H. Chen, F.-J. Chen, I.-W. P. Peng, Y.-K. Lin, C.-S. Chen, C.-H. Sheng, Y.-J. Tsao, H.-K.; Chou, P.-T. *Small*. **2011**, *7*, 1098-1107.
(28) Kim, J. S. Lee, J. H. Park, J. H. Shim, C. Sim, M.; Cho, K. *Adv. Func. Mater*. **2010**, *21*, 480-486.
(29) Xin, H. Reid, O. G. Ren, G. Kim, F. S. Ginger, D. S.; Jenekhe, S. A. *ACS nano*. **2010**, *4*, 1861-72.
(30) Lee, O. P. Yiu, A. T. Beaujuge, P. M. Woo, C. H. Holcombe, T. W. Millstone, J. E. Douglas, J. D. Chen, M. S.; Frechet, J. M. J. Submitted to *Adv. Mater*.
(31) Tamayo, A. B. Tantiwiwat, M. Walker, B.; Nguyen, T.-Q. *J. Phys. Chem. C*. **2008**, *112*, 15543-15552.
(32) Burda, C. Chen, X. Narayanan, R.; El-Sayed, M. A. *Chem. Rev*. **2005**, *105*, 1025-1102.
(33) Gundlach, D. J. Nichols, J. A. Zhou, L.; Jackson, T. N. *Appl. Phys. Lett*. **2002**, *80*, 2925-2927.
(34) Lin, Y.-Y. Gundlach, D. J. Nelson, S. F.; Jackson, T. N. *IEEE Electr. Device L*. **1997**, *18*, 606-608.
(35) Kobayashi, S. Nishikawa, T. Takenobu, T. Mori, S. Shimoda, T. Mitani, T. Shimotani, H. Yoshimoto, N. Ogawa, S.; Iwasa, Y. *Nat. Mater*. **2004**, *3*, 317-322.
(36) Hirose, T. Nagase, T. Kobayashi, T. Ueda, R. Otomo, A.; Naito, H. *Appl. Phys. Lett*. **2010**, *97*, 083301-083303.
(37) Sun, J. Devine, R. Dhar, B. M. Jung, B. J. See, K. C.; Katz, H. E. *ACS Appl. Mater*. **2009**, *1*, 1763-1769.

Chapter 4
Thienooxypyrrolines as Acceptor Building Blocks in Organic Electronics

Abstract

The donor-acceptor approach has been a successful design rationale in the development of new materials for high performing organic electronics. Inspired by the desirable characteristics of diketopyrrolopyrrole and isoindigo moieties, a synthetic pathway to access thienooxypyrrolines (TOP) is described and evaluated as a new acceptor building block for donor-acceptor small molecules and polymers. Preliminary OPV and OFET studies are conducted with a small library of TOP-containing small molecules and polymers. In addition, future targets for TOP-containing small molecules and polymers are suggested based upon the OPV and OFET results.

Introduction

As global energy consumption and concern about our environmental impact both increase, the development of clean, renewable sources of energy has become paramount. With the potential to supply the world's energy needs from just a fraction of daily sunlight, solar power is a particularly promising technology. Because they are lightweight, flexible, inexpensive, and solution processable, organic semiconductors are an emerging cost-effective and scalable approach for the production of transistor and photovoltaic devices.[1-3] In contrast to conventional inorganic solar cells, however, organic photovoltaics (OPVs) suffer from decreased efficiencies, currently at a maximum of 7.7% PCE.[4]

In organic photovoltaics, current research focuses primarily on the design and synthesis of semiconducting materials capable of both light absorption and charge transport. Specifically, the best-performing photovoltaic donor materials show a band gap narrow enough to harvest a large number of solar photons (between 1.2 to 1.9 eV), with optimal HOMO/LUMO levels to ensure a driving force for charge separation and to maximize open circuit voltage (V_{oc}) when matched with a suitable acceptor.[5-10] In addition, the most successful materials have sufficient miscibility to achieve the optimal nanostructure within the active layer of a bulk heterojunction (BHJ).[11-14] Design of new donor photovoltaic materials thus should not only address the electronic criteria outlined above but should also provide pathways for derivatization, usually through the installation of alkyl solubilizing groups, to achieve sufficient solubility while minimizing insulating bulk.

A common approach toward designing low band gap materials is to combine electron-rich (donor) and electron-poor (acceptor) building blocks, forming internal donor-acceptor structures. This allows a modular approach towards the development of new materials, as the optoelectronic, photophysical, and film-forming properties of the materials can be fine-tuned by choosing appropriate donor and acceptor units. This donor-acceptor approach has been utilized in both polymer-based OPVs,[4,15-19] where high molecular weight materials ensure interconnectivity throughout the active layer to maximize charge extraction, as well as small molecule-based OPVs,[20,21] whose monodispersity affords more straightforward synthesis, purification,

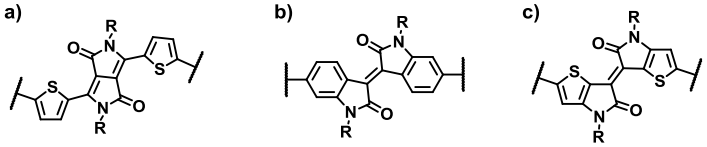

Scheme 4.1. Comparison of three acceptor building blocks. a) diketopyrrolopyrrole; b) isoindigo; c) thienooxyprroline.

and characterization at the cost of decreased active layer interconnectivity and lower device efficiencies.

One such acceptor building block that is emerging as a promising candidate in OPVs is diketopyrrolopyrrole (DPP). When blended with PCBM derivatives in the active layer, both DPP-based small molecules[22-24] and polymers[6,25-31] have exhibited excellent PV properties., with maximum PCEs of 4.4% and 4.7%, respectively. Very recently, another acceptor building block based on isoindigo has been introduced, which also has been shown to be promising in both OPVs and organic field-effect transistors (OFETs).[32-37] Isoindigo is a structural isomer of the pigment indigo and is a common intermediate in drug development. As seen in Scheme 1, both DPP and isoindigo are centrosymmetric and contain ketopyrrole units in their core. These ketopyrroles strongly contribute towards its electron-withdrawing character. In addition, both DPP and isoindigo allow for alkylation via the pyrrole nitrogen, providing a pathway to optimize nanomorphology. Despite isoindigo's promising photovoltaic properties, however, device efficiencies are typically lower than those found for DPP, with 3.0% and 1.7% obtained for polymer[37] and small molecule[33] OPVs, respectively. A possible explanation for these results is a lack of planarity between the 6-membered ring on isoindigo and 5- and 6-membered rings of co-monomers. Repulsion between hydrogens on adjacent rings causes out-of-plane twisting, resulting in a disruption of conjugation and decreased interchain electron transport. This lack of planarity is not a problem found in DPP-based materials, which are flanked by 5-membered thiophene rings. Inspired by both DPP and isoindigo-based material approaches, we designed a new building block, the thienooxypyrroline (Scheme 1c), which contains both the centrosymmetric dihydroketopyrrole found in isoindigo with the 5-membered terminal rings found in DPP. Herein we describe the synthesis of the thienooxypyrroline building block and illustrate its incorporation into small molecules and polymers for OPV and OFET applications. Although this work as of writing the thesis is incomplete, the preliminary optoelectronic properties of the resulting materials as well as initial device results should warrant future consideration of thienooxypyrroline as a promising building block in high-performance organic electronic materials.

Results and Discussion

Although the thienooxypyrroline monomer design is inspired by previous work using isoindigo as a motif, the pathway to accessing thienooxypyrrolines (Scheme 4.2) differs substantially. For example, while isoindigos can be accessed using aniline as a starting point, the lack of stability of 3-aminothiophene forced us to form 3-alkylaminothiophenes, interestingly stable and storable for long periods at 0 ^{o}C, via Ullman coupling from 3-bromothiophene using N,N-dimethylaminoethanol as both a solvent and ligand for the copper catalyst.[38] The 3-alkylaminothiophene **1** readily undergoes cyclization in the presence of oxalyl chloride to yield alkylated 2,3-dioxothieno[3,2-b]pyrrole **2**. While attempts to deoxygenate **2** through traditional Wolff-Kishner routes to give alkylated 2*H*-3-oxothieno[3,2-b]pyrrolines (**4**) proved fruitless, an alternate route through first treating **1** with chloroacetyl chloride to form the [N-alkyl-N-(3-thienyl)aminocarbonylmethyl]chloride **3** followed by palladium-catalyzed C-H functionalization[39] to close the ring and give **4**. Although attempts to reductively dimerize **2** or oxidatively dimerize **4** to give **5** were unsuccessful, an equimolar ratio of **2** and **4** in refluxing acetic acid readily condensed to give **5**, which was brominated to give the final monomer **6.**
Small molecules **7** and **8** were synthesized from Suzuki cross-coupling reactions from the boronic pinacol ester-derived pyrene and benzofuran, respectively. Polymers **PTOPT** and **PTOPBDT** were synthesized using Stille polycondensation with bis(trimethylstannyl)

functionalized thiophene and benzodithiophene, respectively. All small molecules and polymers showed appreciable solubility in chloroform, toluene, and chlorobenzene.

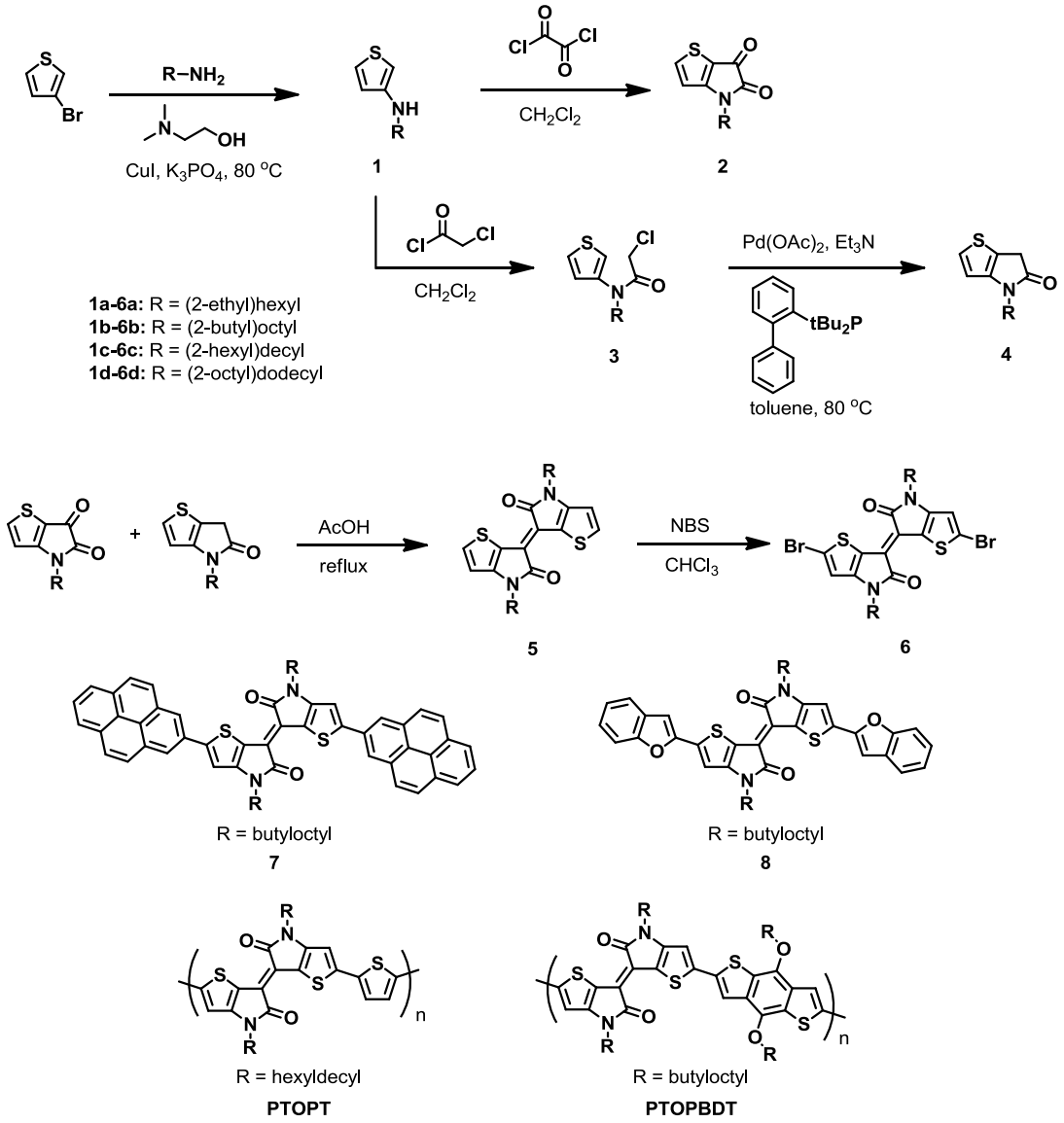

Scheme 4.2. Synthesis of thienooxypyrroline monomers, and structures of thienooxypyrroline-containing small molecules **7** and **8** and polymers **PTOPT** and **PTOPBDT**.

The UV-vis absorption spectra of the small molecules and polymers are shown in Figure 4.1. A solution of small molecule **7** in chloroform displays strong absorption bands in the visible region, at 629 and 670 nm, corresponding to the intramolecular charge transfer between pyrene and thienooxypyrroline. Small molecule **8** in chloroform solution displays a slightly redshifted absorption profile (absorbing at 644 and 692 nm) relative to **7**, which could be due to a difference in strength of the two electron-donating groups. In addition, the pyrene of **7** lies out of plane relative to the thienooxypyrroline units because of the ortho-hydrogens on the benzene rings and thus could also contribute to the observed hypsochromic onset. In thin films, both small molecules broaden and redshift, indicating aggregation or increased order through π-π stacking in the solid state. Small molecule **7** in particular displays a prominent peak at 746 nm due to the strong propensity for pyrene to self-assemble. The optical band gaps of the small

molecules (Table 4.1), measured from the onsets of absorption, are 1.44 and 1.43, respectively. These are some of the lowest optical band gaps measured for donor-acceptor small molecules, well below those measured for DPP-based and isoindigo-based small molecules. Cyclic voltammetry (CV) was used on thin films of each small molecule in a 0.1 M solution of tetrabutylammonium hexafluorophosphate in acetonitrile. Their HOMO and LUMO energy levels (Table 1) offset those of PCBM (-6.0 and -4.2 eV, respectively) to ensure a driving force for charge separation. The combined desirable properties of a good absorption profile, a low band gap, and offsetting energy levels with PCBM all suggest that these small molecules should be promising candidates for bulk heterojunction OPVs.

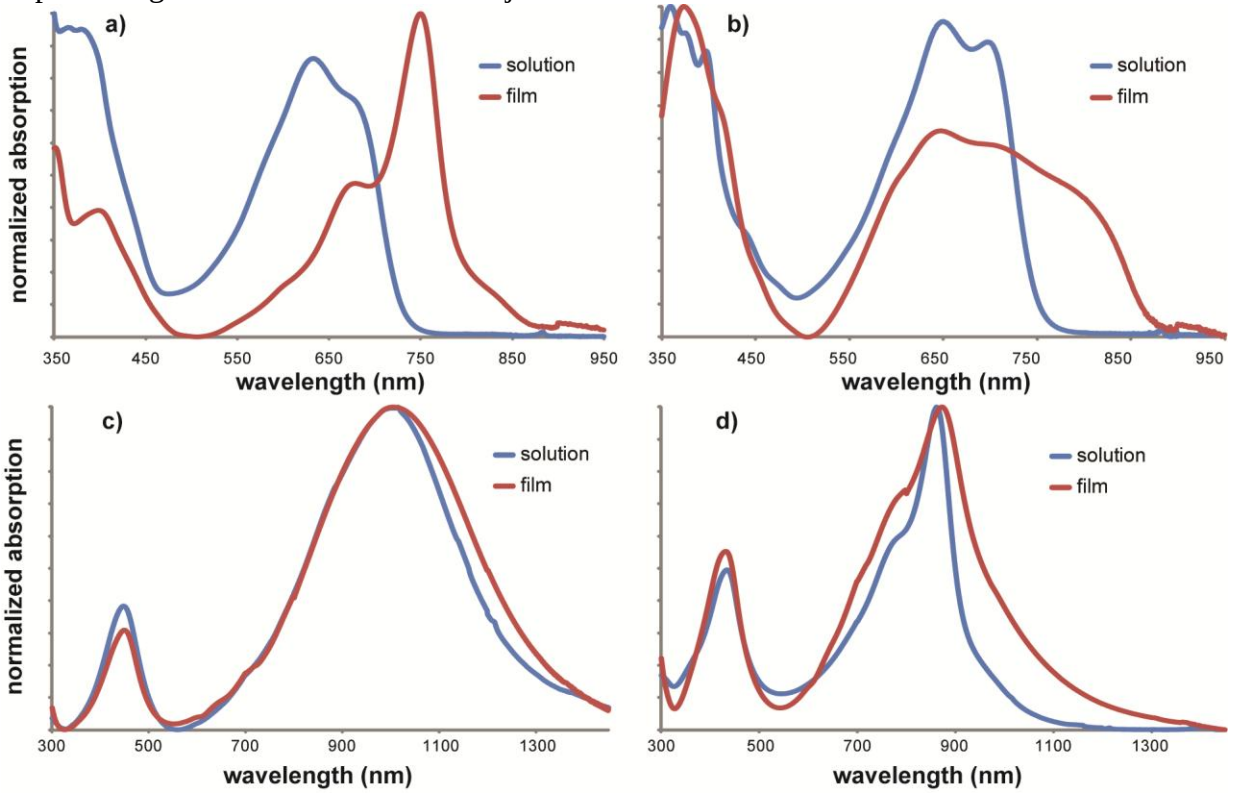

Figure 4.1. UV-vis absorption spectra of small molecules a) **7** and b) **8**, and polymers c) **PTOPT** and d) **PTOPBDT** in $CHCl_3$ solution and in the solid state.

Table 4.1. Synthetic, optical, and electrochemical properties of the synthesized conjugated small molecules and polymers.

	Mn (Da)[a]	**PDI**[a]	**E_g^{opt} (eV)**[b]	**E_{on}^{ox} (V)/ HOMO (eV)**[c]	**E_{on}^{red} (V)/ LUMO (eV)**[c]	**E_g^{CV} (eV)**[c]
7	-	-	1.44	0.75/-5.41	-0.80/-3.86	1.55
8	-	-	1.43	0.83/-5.49	-0.83/-3.83	1.66
PTOPT	7000	1.3	0.93	0.48/-5.14	-0.76/-3.90	1.24
PTOPBDT	25000	2.1	1.08	0.85/-5.51	-0.71/-3.95	1.56

[a] Determined by SEC in chloroform against polystyrene standards. [b] Recorded from thin films spin-cast from chloroform solution onto quartz. [c] Recorded from thin films drop-cast from chloroform solution onto platinum wire electrodes.

In contrast to the small molecules which absorb largely in the visible region, the polymers **PTOPT** and **PTOPBDT** in both solution and film absorb largely in the near infrared due to the increase in effective conjugation length manifested through the high degree of

planarity of the corresponding donor-acceptor pairs. This results in a dramatically lower optical band gap, measured as 1.08 eV for **PTOPBDT** and 0.93 for **PTOPT**. While the HOMO/LUMO levels of the polymers still offset those of PCBM, the fact that these polymers absorb largely outside of the visible portion of the spectrum makes them less ideal for organic photovoltaics. The considerable redshift these polymers exhibit suggests substantial charge delocalization along the polymer chain, perhaps to the benefit of charge mobility in OFETs.

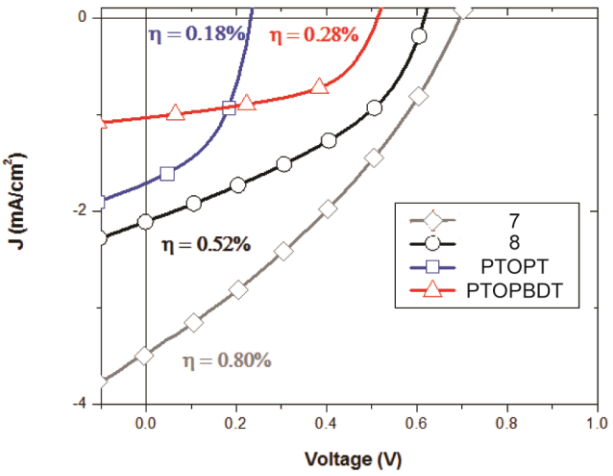

Figure 4.2. J-V curves of optimized solar cells based upon $PC_{71}BM$ blends.

OPVs were fabricated from the thienooxypyrroline small molecules and polymers in the configuration glass/ITO/PEDOT:PSS/donor material:$PC_{71}BM$/Al. $PC_{71}BM$ was preferentially chosen as the electron acceptor over $PC_{61}BM$ for two reasons. First, $PC_{71}BM$ absorbs light in the visible region considerably better than $PC_{61}BM$.[40] Second, while $PC_{71}BM$ has similar electronic properties as $PC_{61}BM$, it also has a slightly lower LUMO level than $PC_{61}BM$, thus offering a larger driving force for charge transfer in OPVs. Typical variables such as weight ratio of material to $PC_{71}BM$ and solvent or additive/solvent combination used to deposit the blend were optimized to maximize efficiency, and the optimized PV parameters are shown in Table 4.2 and plotted in Figure 4.2. Because the V_{oc} measured in the OPV is fundamentally linked to the band gap of the donor material through the empirical formula $eV_{oc} = E_g - 0.6$ eV, a tradeoff exists between a low-lying HOMO to maximize V_{oc} and a low band gap to harvest more solar photons and enhance short-circuit current density, J_{sc}. Thus, it is encouraging that **7** and **8** have higher V_{oc} values (0.70 and 0.62 V, respectively) than the polymers, which have been shown to have significantly lower band gaps. Largely owing to large V_{oc} and J_{sc} values, OPVs fabricated with **7** had the best performance out of this series of materials, with 0.80% power conversion efficiency despite having a miniscule fill factor (0.33). This suggests that the fabricated films lack the desired morphology to achieve high performance, and further morphological optimization or use of a different solubilizing group on the thienooxypyrroline may lead to better devices. Largely due to the polymers' low band gap and their inability to absorb a significant portion of the visible light spectrum, **PTOPT** and **PTOPBDT** not surprisingly have lower V_{oc} values (0.23 and 0.51 V, respectively) and lower efficiencies (0.18 and 0.28%, respectively) than the small molecules.

Table 4.2. PV parameters of optimized solar cells fabricated using thienooxypyrroline-containing small molecules and polymers.

	Blend ratio[a]	Solvent	V_{oc} (V)	J_{sc} (mA/cm^2)	FF	η (%)
7	2:1	Chlorobenzene	0.70	3.49	0.33	0.80
8	1:2	Chlorobenzene	0.62	2.11	0.40	0.52
PTOPT	1:2	Chloroform[b]	0.23	1.72	0.46	0.18
PTOPBDT	1:2	Chlorobenzene	0.51	1.03	0.53	0.28

[a] Weight ratio of material:$PC_{71}BM$. [b] 2 wt % chloronaphthalene in chloroform.

Bottom-gate/top-contact OFETs were fabricated by spin-coating solutions of the material (3 mg/mL in $CHCl_3$ or chlorobenzene) onto a variety of substrates designed to optimize the semiconductor-dielectric interface. Because small molecules **7** and **8** do not form as high quality

films than the polymers, they were only able to form films on the hydrophobic surfaces (HMDS and OTS) when cast from chloroform, and not the higher-boiling solvent chlorobenzene. Nevertheless, all devices exhibited typical p-channel transistor behavior (Table 4.3), but the calculated mobilities depended strongly on the material used. The hole mobility of a pristine film of **7** was on the order of 10^{-3} $cm^2V^{-1}s^{-1}$ for untreated surfaces and 10^{-2} $cm^2V^{-1}s^{-1}$ for HMDS and OTS-treated surfaces, but was as high as 0.106 $cm^2V^{-1}s^{-1}$ for a device on a UV/ozone-treated surface, as seen in Figure 4.3a. Interestingly, devices annealed at 110 °C on that same surface saw a decrease in mobility by two orders of magnitude. Although surface morphological analysis with AFM may shed some light as to the nature of this mobility decrease, it is possible that thermal annealing disrupts some of the stacking of pyrene moieties that have been shown to prominently exist in the thin film UV/vis spectra for **7**. Pristine films of **8**, on the other hand, all gave lower mobilities than **7**, each on the order of 10^{-3} $cm^2V^{-1}s^{-1}$ with a maximum of 8 x 10^{-3} $cm^2V^{-1}s^{-1}$ on the HMDS-treated film (Figure 4.3b). While the pristine films of **PTOPBDT** had hole mobilities on the order of 10^{-5} $cm^2V^{-1}s^{-1}$, films of **PTOPT** had encouragingly high mobilities three orders of magnitude higher, with a maximum mobility of 5.7 x 10^{-2} $cm^2V^{-1}s^{-1}$ on the HMDS-treated surface (Figure 4.3c). This mobility is three times higher than a structurally analogous isoindigo-thiophene copolymer[34] suggests that the increased planarity of thienooxypyrroline leads to better molecular packing and higher OFET performance. It is also important to note that because the **PTOPT** OFET does not saturate as seen in Figure 4.3c, the mobility calculation is likely an underestimation, and the true device mobility may indeed be higher than reported.

Table 4.3. Device performance characteristics of the OFETs fabricated using thienooxypyrroline-containing small molecules and polymers.

	Substrate	**Solvent**	**Hole mobility (cm^2/Vs)**	**V_{th}(V)**	**On/off ratio**
7	Bare SiO_2	Chloroform	5.45 x 10^{-3}	-40	10^5
		Chlorobenzene	1.01 x 10^{-3}	-10	10^4
	UV/O_3-treated SiO_2	Chloroform	0.106	-4	10^4
			2.23 x 10^{-3}[a]		10^3[a]
		Chlorobenzene	4.18 x 10^{-3}	-12	10^5
	HMDS-treated SiO_2[b]	Chloroform	2.27 x 10^{-2}	-12	10^5
	OTS-treated SiO_2[c]	Chloroform	3.1 x 10^{-2}	-15	10^4
8	Bare SiO_2	Chloroform	1.96 x 10^{-3}	-30	10^5
		Chlorobenzene	1.98 x 10^{-3}	-35	10^4
	UV/O_3-treated SiO_2	Chloroform	2.5 x 10^{-3}	-6	10^4
		Chlorobenzene	1.89 x 10^{-3}	-15	10^4
	HMDS-treated SiO_2[b]	Chloroform	8.0 x 10^{-3}	-13	10^4
	OTS-treated SiO_2[c]	Chloroform	2.43 x 10^{-3}	-13	10^4
PTOPT	Bare SiO_2	Chloroform	1.56 x 10^{-2}	-10	10^2
		Chlorobenzene	1.11 x 10^{-2}	-8	10^2
	UV/O_3-treated SiO_2	Chloroform	2.8 x 10^{-2}	-3	10^3
		Chlorobenzene	1.6 x 10^{-2}	-15	10^2
	HMDS-treated SiO_2[b]	Chloroform	5.7 x 10^{-2}	8	10^3
	OTS-treated SiO_2	Chloroform	5.3 x 10^{-2}	-0.6	10^3
		Chlorobenzene	6.4 x 10^{-2}	-11	10^2
PTOPBDT	Bare SiO_2	Chloroform	6.97 x 10^{-5}	-3	10^4
	UV/O_3-treated SiO_2	Chloroform	5.33 x 10^{-5}	-0.1	10^3
	HMDS-treated SiO_2	Chloroform	1.31 x 10^{-5}	-7.5	10^2
	OTS-treated SiO_2	Chloroform	3.49 x 10^{-5}	-6	10^3

[a] Film was annealed at 110 °C for 10 min. [b, c] No material was deposited on surface after spin-coating.

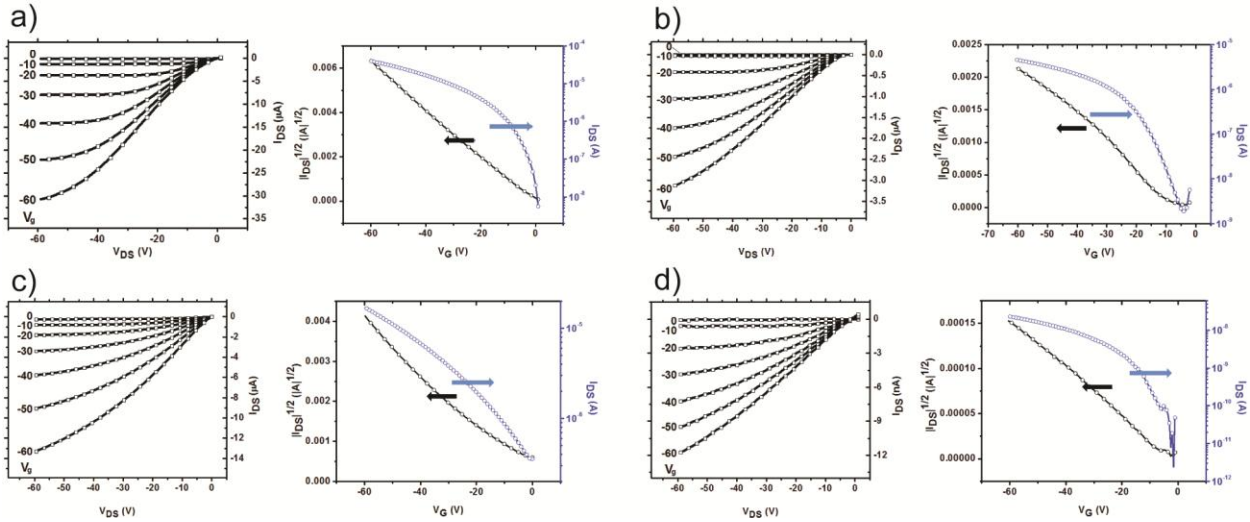

Figure 4.3. Representative OFET output (left) and transfer (right) curves for optimized devices fabricated from a) **7**; b) **8**; c) **PTOPT**; and d) **PTOPBDT**.

Conclusions and Outlook

In this chapter, a synthetic pathway to access thienooxypyrrolines, a new acceptor building block is described for donor-acceptor small molecules and polymers for organic electronics applications. The synthetic design of this molecule was inspired by the electron-withdrawing capability of isoindigo as well as the planarity of diketopyrrolopyrrole. A small library of thienooxypyrroline-containing small molecules and polymers were synthesized as a preliminary probe into organic electronic devices. Indeed, the band gaps in TOP-containing polymers appear that they can be lowered to a point where their usefulness in OPVs becomes limited. Nevertheless, the novelty of the TOP moiety results in a multitude of building block combinations that can be explored, both in small molecules and polymers. In addition, the electrochemical characteristics show promise for these materials as n-type acceptor materials in OPVs. The following are suggested synthetic targets for future small molecules and polymers.

Small molecules. The unprecedentedly low band gap intrinsic to TOP-containing small molecules can be exploited in additional studies. First and foremost, a solubilizing group study on the TOP-pyrene small molecule **7** will be warranted to further optimize the promising results of this molecule in OPVs and OFETs. Additional donor moieties can be screened as well, for example alkylated bithiophenes and terthiophenes, for example those shown in Scheme 4.3a, have shown decent success paired with DPP. In addition, inspired by the nanowires formed by DPP-triphenylamines in Chapter 3, a similar study with TOP-triphenylamines (Scheme 4.3b) would be an interesting comparison.

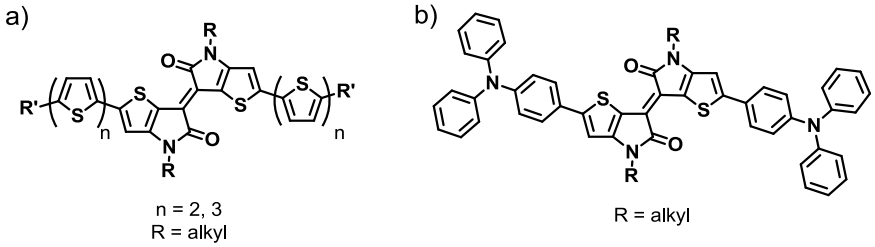

Scheme 4.3. Structures of proposed compounds (a) TOP-oligothiophene and (b) TOP-triphenylamine.

Polymers. The exceedingly low optical band gaps that **PTOPT** and **PTOPBDT** possess limit their usefulness in OPVs, with a possible exception being tandem solar cells where these

polymers would be solely a near-infrared absorbing material. The exceptional hole mobility of PTOPT may be useful for OFETs, however. With ample literature evidence that suggest adding additional thiophene units enhances charge carrier mobility, the next step for this TOP monomer is to attempt polymerization with bithiophene, terthiophene, and thienothiophene (Scheme 4.4a). Whereas TOP polymers, when polymerized with a 5-membered ring (such as thiophene and benzodithiophene) have this tremendously high planarity and low band gap, it has yet to be seen whether 6-membered rings such as carbazoles and fluorenes can disrupt this planarity, resulting in a larger band gap (Scheme 4.4b).

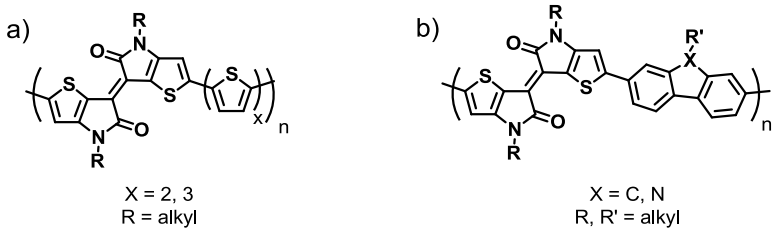

Scheme 4.4. Structures of proposed polymers (a) PTOPBT and PTOPTT and (b) PTOP-carbazole and PTOP-fluorene.

Experimental

Materials. All reagents were obtained from commercial sources and used without further purification unless otherwise noted. Unless otherwise noted, all reactions were carried out under nitrogen with standard Schlenk techniques, and all glassware used in palladium-catalyzed reactions were oven-dried prior to use. All solvents used were reagent grade (99.9%) unless otherwise noted. Toluene used in palladium-catalyzed coupling reactions were degassed using three freeze-pump-thaw cycles before use. Flash chromatography was performed using Silicycle SilicaFlash® P60 (particle size 40-63 μm, 230-400 mesh) silica gel.

Characterization. Elemental analysis was performed by the UC Berkeley analytical facilities. ^{1}H and ^{13}C NMR measurements were conducted on a Bruker AVB-400 nuclear magnetic resonance spectrometer. UV-vis-NIR spectra were taken using a Shimadzu 3600 spectrophotometer. Cyclic voltammetry was performed with a Solartron 1285 potentiostat with CorrWare software. Samples were cast as thin films from chloroform solution onto platinum wire electrodes immersed in dry acetonitrile under inert environment with 0.1 M tetrabutylammonium tetrafluoroborate as a supporting electrolyte. Onsets of reduction and oxidation were standardized to Fc/Fc^{+}, set at 5.12 eV.

OPV device fabrication.

All devices were fabricated on ITO-coated glass substrates (pre-patterned, R = 20 Ω-1, Thin Film Devices, Inc.). The substrates were sonicated for 20 minutes in 2% Helmanex soap water and rinsed extensively with deionized (DI) water. They were then sonicated for 20 minutes in DI water, 20 minutes in acetone, and 20 minutes in isopropyl alcohol, followed by drying under a stream of air. The substrates were then UV-ozone cleaned for 5 minutes. A thin layer (30-40 nm) of PEDOT:PSS (Clevios PH) was spin-coated onto each substrate at 4000 RPM for 40 s, followed by 10 minutes of drying at 140 °C in air. The samples were then transferred to a glovebox under N_2, where the active layers were spin-coated at 2000 RPM for 40 s. The cathode was thermally evaporated under vacuum (~10-7 torr) through a shadow mask that defines an active area of ~0.03 cm2. Some of the samples were then thermally annealed by placing them substrate-side down (active layer facing up) on a hot plate. Current-voltage (J-V) curves were

measured using a Keithley 2400 source-measure unit under AM 1.5 G solar illumination at 100 mW cm-2 (1 sun) using a Thermal-Oriel 150W solar simulator.

OFET device preparation and testing.

Bottom contact field effect transistors (FETs) were fabricated using conventional photolithographic methods on silicon wafers with a 300 nm thermally grown silicon dioxide gate dielectric (Addison Engineering). Prior to deposition of the organic film, the FET substrates were cleaned by sonicating sequentially in a surfactant solution (Hellmanex II, 1% in H_2O), DI water, acetone, and isopropyl alcohol for 20 minutes each. Organic field effect transistors were fabricated on substrates with four different gate dielectric surface conditions; namely untreated bare SiO_2, UV/O_3 oxidized SiO_2, 1,1,1,3,3,3-hexamethyldisilazane (HMDS) treated SiO_2, and n-octadecyltrichlorosilane (OTS) functionalized SiO_2. Bare SiO_2 substrates were used 'as is' immediately following the sonication cleaning procedure. Oxidized SiO_2 dielectrics were produced by exposing to UV/O_3 for 30 minutes using a UVOCS, Inc. ultraviolet-ozone cleaning system (model T10X10). HMDS treated surfaces were fabricated by first exposing the substrate to 30 minutes of UV/O_3 treatment followed by exposure to HMDS vapor at 80°C under static vacuum (~ 1mbar). For OTS surfaces, 30 minutes UV/O_3 was followed by soaking in a 40 mM solution of n-octadecyltrichlorosilane in hexanes for 2 hours. OTS functionalized substrates were removed from the OTS solution and sonicated in toluene for 30 seconds to remove physisorbed molecules, rinsed with isopropyl alcohol, and dried with a light N_2 stream. Films were spuncoat at 1500 RPM for 1 second (Specialty Coating Systems, model P6700) from 3mg/mL solutions in chloroform or chlorobenzene under N_2 atmosphere inside a glovebox. The films were allowed to dry for a minimum of 30 minutes prior to electrical analysis using an HP 4155C semiconductor parameter analyzer. Electrical characterization was performed under N_2 inside a glovebox.

Synthesis of thienooxypyrroline monomers.

Synthesis of 3-(N-alkylamino)thiophenes. To a mixture of 3-bromothiophene (1 equiv), the desired amine (1.5 equiv), tribasic potassium phosphate (2 equiv), and copper (I) iodide (0.1 equiv), N,N-dimethylaminoethanol that had been degassed with nitrogen was added (amount corresponding to millimoles 3-bromothiophene used such that the final concentration was 1 M). This mixture was heated at 80 °C for 48 h, after which it was filtered through a plug of Celite, concentrated, distilled under vacuum to remove remaining solvent and free amine, and purified via silica gel chromatography to give the product, obtained in all cases as a dark brown oil.

3-[N-(2-ethylhexyl)amino]thiophene (1a): Column eluent: 1:1 DCM:hexane; yield: 53%. ^{1}H NMR (400 MHz, $CDCl_3$): δ 7.14 (dd, 1H), 6.61 (dd, 1H), 5.92 (m, 1H), 3.58 (br s, 1H), 2.98 (d, 2H), 1.58-1.50 (m, 1H), 1.48-1.30 (m, 8H), 0.93-0.89 (m, 6H). ^{13}C NMR (100 MHz, $CDCl_3$): δ 149.1, 125.0, 119.9, 94.7, 49.4, 39.2, 31.4, 29.0, 24.5, 23.1, 14.1, 11.0. HRMS (ESI, *m/z*) Calcd. for $C_{12}H_{22}NS$ $[M+H]^+$: 212.1467; found: 212.1467. Anal. Calcd. for $C_{12}H_{21}NS$: C, 68.19; H, 10.01; N, 6.63; found: C, 68.40; H, 10.53; N, 6.78.

3-[N-(2-butyloctyl)amino]thiophene (1b): Column eluent: 1:2 DCM:hexane; yield, 45%. ^{1}H NMR (400 MHz, $CDCl_3$): δ 7.15 (dd, 1H), 6.62 (dd, 1H), 5.92 (m, 1H), 3.58 (br s, 1H), 2.98 (d, 2H), 1.61-1.59 (m, 1H), 1.33-1.28 (m, 16H), 0.92-0.87 (m, 6H). ^{13}C NMR (100 MHz, $CDCl_3$): δ 149.4, 125.3, 120.2, 95.1, 50.1, 38.1, 32.5, 32.2, 32.1, 30.0, 29.3, 27.1, 23.4, 23.0, 14.4. HRMS (ESI, *m/z*) Calcd. for $C_{16}H_{30}NS$ $[M+H]^+$: 268.2093; found: 268.2094. Anal. Calcd. for $C_{16}H_{29}NS$: C, 71.85; H, 10.93; N, 5.24; found: C, 71.64; H, 10.57; N, 5.12.

3-[N-(2-hexyldecyl)amino]thiophene (1c): Column eluent: 1:2 DCM:hexane; yield, 44%. ^{1}H NMR (400 MHz, $CDCl_3$): δ 7.12 (dd, 1H), 6.62 (dd, 1H), 5.92 (m, 1H), 3.58 (br s, 1H), 2.98 (d,

2H), 1.64-1.59 (m, 1H), 1.31-1.28 (m, 24H), 0.89 (t, 6H). ^{13}C NMR (100 MHz, $CDCl_3$): δ 149.2, 125.1, 120.0, 94.9, 50.0, 37.9, 32.3, 32.0, 31.9, 30.2, 29.8, 29.7, 29.4, 26.9, 26.8, 22.8, 14.2. HRMS (ESI, *m/z*) Calcd. for $C_{20}H_{38}NS$ $[M+H]^+$: 324.2719; found: 324.2719. Anal. Calcd. for $C_{20}H_{37}NS$: C, 74.24; H, 11.53; N, 4.33; found: C, 73.98; H, 11.79; N, 4.49.

3-[N-(2-octyldodecyl)amino]thiophene (1d): Column eluent: 1:2 DCM:hexane; yield, 41%. ^{1}H NMR (400 MHz, $CDCl_3$): δ 7.15 (dd, 1H), 6.62 (dd, 1H), 5.92 (m, 1H), 3.73 (br s, 1H), 2.98 (d, 2H), 1.60 (m, 1H), 1.31-1.23 (m, 32H), 0.89 (t, 6H). ^{13}C NMR (100 MHz, $CDCl_3$): δ 149.2, 125.1, 120.0, 94.9, 49.9, 37.8, 32.2, 32.0, 31.9, 30.2, 29.8, 29.7, 29.6, 29.4, 26.9, 26.8, 22.8, 14.2. HRMS (ESI, *m/z*) Calcd. for $C_{24}H_{46}NS$ $[M+H]^+$: 380.3345; found: 380.3345. Anal. Calcd. for $C_{24}H_{45}NS$: C, 75.92; H, 11.95; N, 3.69; found: C, 76.07; H, 12.31; N, 3.69.

Synthesis of alkylated 2,3-dioxothieno[3,2-b]pyrrolines. A solution of oxalyl choride (1.1 equiv) in dry dichloromethane (0.67 M) was cooled to 0 °C, and a solution of the corresponding amine **1** (1 equiv) in dry dichloromethane (0.67 M) was added dropwise via addition funnel. After addition was complete, the reaction was allowed to stir for 30 min at room temperature before dropwise addition of a solution of dry triethylamine in dichloromethane (10 mL, 1:1 v/v). The mixture was allowed to stir at room temperature overnight, after which it was concentrated and purified via silica gel chromatography to yield the product.

2,3-dioxo-4-(2-ethylhexyl)thieno[3,2-b]pyrroline (2a): Column eluent: DCM. Orange solid, yield: 87%. ^{1}H NMR (400 MHz, $CDCl_3$): δ 8.00 (d, 1H), 6.76 (d, 1H), 3.49 (d, 2H), 1.71-1.67 (m, 1H), 1.31-1.19 (m, 8H), 0.86-0.78 (m, 6H). ^{13}C NMR (100 MHz, $CDCl_3$): δ 172.9, 165.5, 161.7, 144.2, 113.3, 110.8, 45.9, 38.1, 30.3, 28.4, 23.7, 22.9, 13.9, 10.4. HRMS (ESI, *m/z*) Calcd. for $C_{14}H_{20}NO_2S$ $[M+H]^+$: 266.1209; found: 266.1210. Anal. Calcd. for $C_{14}H_{19}NO_2S$: C, 63.36; H, 7.22; N, 5.28; found: C, 63.45; H, 7.44; N, 5.27.

2,3-dioxo-4-(2-butyloctyl)thieno[3,2-b]pyrroline (2b): Column eluent: 5:1 hexanes:ethyl acetate. Orange solid, yield: 65%. ^{1}H NMR (400 MHz, $CDCl_3$): δ 7.98 (d, 1H), 6.74 (d, 1H), 3.52 (d, 2H), 1.76-1.75 (m, 1H), 1.28-1.23 (m, 16 H), 0.87-0.83 (m, 6H). ^{13}C NMR (100 MHz, $CDCl_3$): δ 173.2, 165.7, 161.9, 143.9, 113.3, 111.2, 46.6, 37.2, 31.9, 31.6, 31.3, 29.7, 28.7, 26.5, 23.1, 22.8, 14.2, 14.1. HRMS (ESI, *m/z*) Calcd. for $C_{18}H_{28}NO_2S$ $[M+H]^+$: 322.1835; found: 322.1835. Anal. Calcd. for $C_{18}H_{27}NO_2S$: C, 67.25; H, 8.47; N, 4.36; found: C, 67.47; H, 8.80; N, 4.37.

2,3-dioxo-4-(2-hexyldecyl)thieno[3,2-b]pyrroline (2c): Column eluent: 6:1 hexanes:ethyl acetate. Orange solid, yield: 53%. ^{1}H NMR (400 MHz, $CDCl_3$): δ 8.00 (d, 1H), 6.75 (d, 1H), 3.53 (d, 2H), 1.61 (m, 1H), 1.29-1.24 (m, 24 H), 0.88-0.85 (m, 6H). ^{13}C NMR (100 MHz, $CDCl_3$): δ 173.0, 165.5, 161.7, 143.7, 113.1, 111.0, 46.4, 37.0, 31.8, 31.7, 31.4, 29.9, 29.5, 29.4, 29.2, 26.4, 26.3, 22.6, 14.1, 14.0. HRMS (ESI, *m/z*) Calcd. for $C_{22}H_{36}NO_2S$ $[M+H]^+$: 378.2461; found: 378.2464. Anal. Calcd. for $C_{22}H_{35}NO_2S$: C, 69.98; H, 9.34; N, 3.71; found: C, 70.09; H, 9.57; N, 3.74.

2,3-dioxo-4-(2-octyldodecyl)thieno[3,2-b]pyrroline (2d): Column eluent: 7:1 hexanes:ethyl acetate. Orange oil, yield: 65%. ^{1}H NMR (400 MHz, $CDCl_3$): δ 8.00 (d, 1H), 6.76 (d, 1H), 3.54 (d, 2H), 1.77 (br s, 1H), 1.29-1.25 (m, 32 H), 0.90-0.86 (m, 6H). ^{13}C NMR (100 MHz, $CDCl_3$): δ 173.0, 165.5, 161.7, 143.7, 113.1, 111.0, 46.4, 36.9, 31.9, 31.8, 31.3, 29.9, 29.6, 29.5, 29.4, 29.3, 29.2, 26.3, 22.7, 22.6, 14.1. HRMS (ESI, *m/z*) Calcd. for $C_{26}H_{44}NO_2S$ $[M+H]^+$: 434.3087; found: 434.3089. Anal. Calcd. for $C_{26}H_{43}NO_2S$: C, 72.00; H, 9.99; N, 3.23; found: C, 72.20; H, 10.25; N, 3.30.

Synthesis of [N-alkyl-N-(3-thienyl)aminocarbonylmethyl]chlorides. A solution of chloroacetyl chloride (1.1 equiv) in dry dichloromethane (0.33 M) was cooled to 0 °C, and then a

solution of the corresponding amine **1** (1 equiv) in dry dichloromethane (1 M) was added slowly via syringe. The solution was allowed to stir for 30 min at room temperature, after which it was concentrated and purified via silica gel chromatography, eluting with DCM, to give the desired product as a dark red oil.

[N-(2-ethylhexyl)-N-(3-thienyl)aminocarbonylmethyl]chloride (3a): Yield: 74%. ^{1}H NMR (400 MHz, $CDCl_3$): δ 7.39 (dd, 1H), 7.20 (d, 1H), 6.95 (d, 1H), 3.89 (s, 2H), 3.69-3.55 (ddd, 2H), 1.50-1.45 (m, 1H), 1.39-1.16 (m, 8H), 0.88-0.81 (m, 6H). ^{13}C NMR (100 MHz, $CDCl_3$): δ 166.7, 139.8, 126.7, 125.9, 121.8, 52.7, 42.0, 37.3, 30.1, 28.5, 23.4, 23.0, 14.1, 10.4. HRMS (ESI, *m/z*) Calcd. for $C_{14}H_{23}ClNOS$ $[M+H]^+$: 288.1183; found: 288.1180. Anal. Calcd. for $C_{14}H_{22}ClNOS$: C, 58.42; H, 7.70; N, 4.87; found: C, 58.43; H, 8.06; N, 4.89.

[N-(2-butyloctyl)-N-(3-thienyl)aminocarbonylmethyl]chloride (3b): Yield: 70%. ^{1}H NMR (400 MHz, $CDCl_3$): δ 7.38 (dd, 1H), 7.20 (d, 1H), 6.95 (d, 1H), 3.88 (s, 2H), 3.62-3.56 (dd, 2H), 1.53-1.51 (m, 1H), 1.27-1.14 (m, 16H), 0.88-0.84 (m, 6H). ^{13}C NMR (100 MHz, $CDCl_3$): δ 166.7, 139.9, 126.7, 125.9, 121.8, 53.1, 42.0, 36.2, 31.8, 31.2, 30.8, 29.7, 28.5, 26.3, 23.4, 23.1, 22.7, 14.1. HRMS (ESI, *m/z*) Calcd. for $C_{18}H_{31}ClNOS$ $[M+H]^+$: 344.1809; found: 344.1806. Anal. Calcd. for $C_{18}H_{30}ClNOS$: C, 62.85; H, 8.79; N, 4.07; found: C, 63.29; H, 9.04; N, 4.13.

[N-(2-hexyldecyl)-N-(3-thienyl)aminocarbonylmethyl]chloride (3c): Yield: 70%. ^{1}H NMR (400 MHz, $CDCl_3$): δ 7.39 (dd, 1H), 7.19 (d, 1H), 6.96 (d, 1H), 3.88 (s, 2H), 3.61 (d, 2H), 1.52-1.50 (m, 1H), 1.29-1.21 (m, 24H), 0.89-0.84 (m, 6H). ^{13}C NMR (100 MHz, $CDCl_3$): δ 166.9, 140.1, 126.9, 126.1, 122.0, 53.3, 42.2, 36.4, 32.1, 32.0, 31.3, 30.2, 29.9, 29.8, 29.5, 26.5, 26.4, 22.9, 22.8, 14.4, 14.3. HRMS (ESI, *m/z*) Calcd. for $C_{22}H_{39}ClNOS$ $[M+H]^+$: 400.2435; found: 400.2431. Anal. Calcd. for $C_{22}H_{38}ClNOS$: C, 66.05; H, 9.57; N, 3.50; found: C, 66.46; H, 9.96; N, 3.49.

[N-(2-octyldodecyl)-N-(3-thienyl)aminocarbonylmethyl]chloride (3d): Yield: 75%. ^{1}H NMR (400 MHz, $CDCl_3$): δ 7.39 (dd, 1H), 7.19 (d, 1H), 6.95 (d, 1H), 3.88 (s, 2H), 3.61 (d, 2H), 1.52-1.50 (m, 1H), 1.28-1.21 (m, 32H), 0.89-0.85 (m, 6H). ^{13}C NMR (100 MHz, $CDCl_3$): δ 166.7, 139.9, 126.7, 125.9, 121.8, 53.1, 42.0, 36.1, 32.0, 31.9, 31.1, 30.0, 29.7, 29.6, 29.5, 29.4, 29.3, 26.3, 22.7, 14.2. HRMS (ESI, *m/z*) Calcd. for $C_{26}H_{47}ClNOS$ $[M+H]^+$: 456.3061; found: 456.3065. Anal. Calcd. for $C_{26}H_{46}ClNOS$: C, 68.46; H, 10.16; N, 3.07; found: C, 68.64; H, 10.61; N, 3.53.

Synthesis of alkylated 3-oxothieno[3,2-b]pyrrolines. A Schlenk tube was charged with palladium acetate (3 mol %), 2-(di-tert-butylphosphino)biphenyl (Pd:ligand 2:1) and the corresponding substrate **3** (1 equiv). The tube was evacuated and backfilled with nitrogen 3 times, and dry triethylamine (1.5 equiv) and degassed toluene (1 M) were added. The tube was placed in an oil bath preheated to 80 °C for 2 h, after which it was diluted to 10 times its original volume with ethyl acetate, filtered through a plug of Celite, concentrated, and purified by silica gel chromatography to give the product.

3-oxo-4-(2-ethylhexyl)thieno[3,2-b]pyrroline (4a): Column eluent: 3:1 DCM:hexanes. Yield, 92%. ^{1}H NMR (400 MHz, $CDCl_3$): δ 7.23 (d, 1H), 6.73 (d, 1H), 3.59-3.51 (m, 4H), 1.77-1.74 (m, 1H), 1.38-1.24 (m, 8H), 0.91-0.85 (m, 6H). ^{13}C NMR (100 MHz, $CDCl_3$): δ 177.9, 147.6, 126.6, 114.3, 112.1, 46.0, 38.6, 36.5, 30.8, 29.0, 24.2, 23.3, 14.3, 10.9. HRMS (ESI, *m/z*) Calcd. for $C_{14}H_{22}NOS$ $[M+H]^+$: 252.1417; found: 252.1414. Anal. Calcd. for $C_{14}H_{21}NOS$: C, 66.89; H, 8.42; N, 5.57; found: C, 66.56; H, 8.34; N, 5.49.

3-oxo-4-(2-butyloctyl)thieno[3,2-b]pyrroline (4b): Column eluent: 3:1 DCM:hexanes. Yield, 52%. ^{1}H NMR (400 MHz, $CDCl_3$): δ 7.24 (d, 1H), 6.73 (d, 1H), 3.57-3.53 (m, 4H), 1.80 (m, 1H), 1.34-1.24 (m, 16 H), 0.97-0.83 (m, 6H). ^{13}C NMR (100 MHz, $CDCl_3$): δ 177.6, 147.3,

126.3, 114.0, 111.8, 46.2, 36.96, 36.2, 31.8, 31.6, 31.5, 31.2, 29.6, 28.7, 26.4, 23.0, 22.7, 14.1. HRMS (ESI, *m/z*) Calcd. for $C_{18}H_{30}NOS$ $[M+H]^+$: 308.2043; found: 308.2039. Anal. Calcd. for $C_{18}H_{29}NOS$: C, 70.31; H, 9.51; N, 4.56; found: C, 69.56; H, 9.51; N, 4.43.

3-oxo-4-(2-hexyldecyl)thieno[3,2-b]pyrroline (4c): Column eluent: 2:1 DCM:hexanes. Yield: 41%. ^{1}H NMR (400 MHz, $CDCl_3$): δ 7.24 (d, 1H), 6.73 (d, 1H), 3.57-3.53 (m, 4H), 1.80 (m, 1H), 1.33-1.24 (m, 24H), 0.97-0.83 (m, 6H). ^{13}C NMR (100 MHz, $CDCl_3$): δ 177.6, 147.3, 126.3, 113.0, 111.9, 46.2, 37.0, 36.2, 31.9, 31.8, 31.5, 30.0, 29.6, 29.6, 29.3, 26.5, 26.4, 22.7, 22.6, 14.2, 14.1. HRMS (ESI, *m/z*) Calcd. for $C_{22}H_{38}NOS$ $[M+H]^+$: 364.2669; found: 364.2665. Anal. Calcd. for $C_{22}H_{37}NOS$: C, 72.67; H, 10.26; N, 3.85; found: C, 72.66; H, 10.32; N, 3.82.

3-oxo-4-(2-hexyldecyl)thieno[3,2-b]pyrroline (4d): Column eluent: 2:1 DCM:hexanes. Yield: 86%. ^{1}H NMR (400 MHz, $CDCl_3$): δ 7.24 (d, 1H), 6.73 (d, 1H), 3.58 (s, 2H), 3.54 (d, 2H), 1.80 (m, 1H), 1.33-1.24 (m, 32H), 0.97-0.83 (m, 6H). ^{13}C NMR (100 MHz, $CDCl_3$): δ 177.7, 147.3, 126.3, 114.0, 111.9, 46.2, 36.9, 36.3, 32.0, 31.9, 31.5, 30.0, 29.7, 29.6, 29.5, 29.3, 29.3, 26.5, 22.8, 22.7, 14.2. HRMS (ESI, *m/z*) Calcd. for $C_{26}H_{46}NOS$ $[M+H]^+$: 420.3295; found: 420.3299. Anal. Calcd. for $C_{26}H_{45}NOS$: C, 74.40; H, 10.81; N, 3.34; found: C, 74.25; H, 11.15; N, 3.38.

Synthesis of alkylated 2-(3-oxothieno[3,2-b]pyrrolino-2-ylidene)-3-oxothieno[3,2-b]pyrrolines. To an equimolar mixture of **2** and **4** glacial acetic acid was added (0.15 M) and the solution was heated to reflux under nitrogen. After 1 h the reaction was cooled to room temperature, poured onto hexanes, washed with water and brine, dried over magnesium sulfate, concentrated, and purified by silica gel chromatography to give the desired product, obtained as a dark purple solid.

2-(3-oxo-4-(2-ethyhexyl)thieno[3,2-b]pyrrolino-2-ylidene)-3-oxo-(2-ethylhexyl)thieno[3,2-b]pyrroline (5a): Column eluent, 2:1 DCM:hexane. Yield: 58%. ^{1}H NMR (400 MHz, $CDCl_3$): δ 7.52 (d, 2H), 6.80 (d, 2H), 3.71-3.68 (m, 4H), 1.85 (m, 2H), 1.40-1.26 (m, 16H), 0.93-0.86 (m, 12H). ^{13}C NMR (100 MHz, $CDCl_3$): δ 171.3, 151.6, 134.3, 121.1, 114.2, 111.4, 45.8, 38.5, 30.6, 28.7, 24.0, 23.0, 14.1, 10.7. HRMS (ESI, *m/z*) Calcd. for $C_{28}H_{39}N_2O_2S_2$ $[M+1]^+$: 499.2447; found: 499.2446. Anal. Calcd. for $C_{28}H_{39}N_2O_2S_2$: C, 67.43; H, 7.68; N, 5.62; found: C, 67.49; H, 7.70; N, 5.59.

2-(3-oxo-4-(2-butyloctyl)thieno[3,2-b]pyrrolinoo-2-ylidene)-3-oxo-(2-butyloctyl)thieno[3,2-b]pyrroline (5b): Column eluent, 1:1 DCM:hexane. Yield: 51%. ^{1}H NMR (400 MHz, $CDCl_3$): δ 7.52 (d, 2H), 6.80 (d, 2H), 3.71-3.68 (m, 4H), 1.85 (m, 2H), 1.40-1.26 (m, 32H), 0.93-0.86 (m, 12H). ^{13}C NMR (100 MHz, $CDCl_3$): δ 171.3, 151.6, 134.2, 121.1, 114.3, 111.4, 46.1, 37.2, 31.8, 31.6, 31.5, 31.2, 29.6, 28.7, 26.4, 24.0, 23.1, 22.7, 22.6, 14.1, 14.0. HRMS (ESI, *m/z*) Calcd. for $C_{36}H_{55}N_2O_2S_2$ $[M+1]^+$: 611.3699; found: 611.3695. Anal. Calcd. for $C_{36}H_{54}N_2O_2S_2$: C, 70.77; H, 8.91; N, 4.59; found: C, 70.65; H, 8.94; N, 4.57.

2-(3-oxo-4-(2-hexyldecyl)thieno[3,2-b]pyrrolino-2-ylidene)-3-oxo-(2-hexyldecyl)thieno[3,2-b]pyrroline (5c): Column eluent, 1:1 DCM:hexane. Yield: 45%. ^{1}H NMR (400 MHz, $CDCl_3$): δ 7.53 (d, 2H), 6.79 (d, 2H), 3.70-3.68 (m, 4H), 1.98 (m, 2H), 1.37-1.23 (m, 48H), 0.90-0.83 (m, 12H). ^{13}C NMR (100 MHz, $CDCl_3$): δ 171.3, 151.6, 134.3, 121.0, 114.2, 111.4, 46.1, 37.2, 31.9, 31.8, 31.6, 31.5, 30.0, 29.7, 29.7, 29.6, 29.3, 26.4, 22.7, 14.1. HRMS (ESI, *m/z*) Calcd. for $C_{44}H_{71}N_2O_2S_2$ $[M+1]^+$: 723.4952; found: 723.4963. Anal. Calcd. for $C_{44}H_{70}N_2O_2S_2$: C, 73.08; H, 9.76; N, 3.87; found: C, 73.28; H, 10.12; N, 3.90.

2-(3-oxo-4-(2-octyldodecyl)thieno[3,2-b]pyrrolino-2-ylidene)-3-oxo-(2-octyldodecyl)thieno[3,2-b]pyrroline (5d): Column eluent, 1:1 DCM:hexane. Yield, 54%. %. ^{1}H NMR (400 MHz, $CDCl_3$): δ 7.53 (d, 2H), 6.79 (d, 2H), 3.70-3.68 (m, 4H), 1.89 (m, 2H), 1.32-

1.23 (m, 64H), 0.89-0.84 (m, 12H). ^{13}C NMR (100 MHz, $CDCl_3$): δ 171.3, 151.6, 134.3, 121.1, 114.2, 111.4, 46.2, 32.0, 31.9, 31.5, 30.0, 29.7, 29.6, 29.5, 29.4, 29.3, 26.4, 22.8, 22.7, 14.2. HRMS (ESI, *m/z*) Calcd. for $C_{52}H_{87}N_2O_2S_2$ $[M+1]^+$: 835.6222; found: 835.6216. Anal. Calcd. for $C_{52}H_{86}N_2O_2S_2$: C, 74.76; H, 10.38; N, 3.35; found: C, 74.92; H, 10.82; N, 3.42.

Synthesis of alkylated 2-(3-oxo-6-bromothieno[3,2-b]pyrrolino-2-ylidene)-3-oxo-6-bromothieno[3,2-b]pyrrolines. A solution of **5** in chloroform (0.25 M) was purged with nitrogen for 15 min, cooled to 0 °C, and then N-bromosuccinimide (2.05 equiv) was added portionwise. The reaction was allowed to stir for 30 min at room temperature, after which it was concentrated and purified by silica gel chromatography to give the product, obtained as a bluish-purple solid.

2-(3-oxo-4-(2-ethylhexyl)-6-bromothieno[3,2-b]pyrrolino-2-ylidene)-3-oxo-4-(2-ethylhexyl)-6-bromothieno[3,2-b]pyrroline (6a): Column eluent, 1:1 hexane:chloroform. Yield: 76%. ^{1}H NMR (400 MHz, $CDCl_3$): δ 6.81 (s, 2H), 3.64-3.62 (m, 4H), 1.80-1.77 (m, 2H), 1.34-1.28 (m, 16H), 0.93-0.87 (m, 12H). ^{13}C NMR (100 MHz, $CDCl_3$): δ 170.4, 150.2, 123.2, 119.7, 115.0, 114.7, 45.9, 38.6, 30.5, 28.6, 23.9, 23.1, 14.1, 10.6. HRMS (ESI, *m/z*) Calcd. for $C_{28}H_{36}Br_2N_2O_2S_2$ $[M]^+$: 654.0579; found: 654.0586. Anal. Calcd. for $C_{28}H_{36}Br_2N_2O_2S_2$: C, 51.22; H, 5.33; N, 4.27; found: C, 50.92; H, 4.91; N, 4.13.

2-(3-oxo-4-(2-butyloctyl)-6-bromothieno[3,2-b]pyrrolino-2-ylidene)-3-oxo-4-(2-butyloctyl)-6-bromothieno[3,2-b]pyrroline (6b): Column eluent, 2:1 hexane:chloroform. Yield: 74%. ^{1}H NMR (400 MHz, $CDCl_3$): δ 6.80 (s, 2H), 3.63-3.61 (m, 4H), 1.82 (m, 2H), 1.36-1.25 (m, 32H), 0.90-0.85 (m, 12H). ^{13}C NMR (100 MHz, $CDCl_3$): δ 170.3, 150.1, 123.1, 119.6, 115.0, 114.6, 46.1, 37.2, 31.8, 31.3, 31.1, 29.6, 28.6, 26.3, 23.0, 22.6, 14.1, 14.0. HRMS (ESI, *m/z*) Calcd. for $C_{36}H_{52}Br_2N_2O_2S_2$ $[M]^+$: 766.1831; found: 766.1839. Anal. Calcd. for $C_{36}H_{52}Br_2N_2O_2S_2$: C, 56.25; H, 6.82; N, 3.64; found: C, 56.06; H, 6.56; N, 3.34.

2-(3-oxo-4-(2-hexyldecyl)-6-bromothieno[3,2-b]pyrrolino-2-ylidene)-3-oxo-4-(2-hexyldecyl)-6-bromothieno[3,2-b]pyrroline (6c): Column eluent, 2:1 hexane:chloroform. Yield: 80%. ^{1}H NMR (400 MHz, $CDCl_3$): δ 6.80 (s, 2H), 3.63-3.61 (m, 4H), 1.82 (m, 2H), 1.28-1.24 (m, 48H), 0.88-0.85 (m, 12H). ^{13}C NMR (100 MHz, $CDCl_3$): δ 170.3, 150.1, 123.1, 119.7, 115.0, 114.6, 46.1, 37.2, 31.9, 31.8, 31.3, 29.9, 29.6, 29.5, 29.3, 26.3, 22.7, 22.6, 14.1, 14.0. HRMS (ESI, *m/z*) Calcd. for $C_{44}H_{69}Br_2N_2O_2S_2$ $[M+H]^+$: 879.3162; found: 879.3179. Anal. Calcd. for $C_{44}H_{68}Br_2N_2O_2S_2$: C, 59.99; H, 7.78; N, 3.18; found: C, 60.58; H, 8.09; N, 3.07.

2-(3-oxo-4-(2-octyldodecyl)-6-bromothieno[3,2-b]pyrrolino-2-ylidene)-3-oxo-4-(2-octyldodecyl)-6-bromothieno[3,2-b]pyrroline (6d): δ 6.81 (s, 2H), 3.63-3.61 (m, 4H), 1.83 (m, 2H), 1.28-1.24 (m, 64H), 0.89-0.85 (m, 12H). ^{13}C NMR (100 MHz, $CDCl_3$): δ 170.3, 150.2, 123.2, 119.7, 115.0, 114.6, 46.1, 37.2, 32.0, 31.9, 31.4, 30.0, 29.7, 29.6, 29.5, 29.4, 29.3, 26.4, 22.7, 22.6, 14.1. HRMS (ESI, *m/z*) Calcd. for $C_{52}H_{85}Br_2N_2O_2S_2$ $[M+H]^+$: 991.4414; found: 991.4441. Anal. Calcd. for $C_{52}H_{84}Br_2N_2O_2S_2$: C, 62.88; H, 8.52; N, 2.82; found: C, 62.98; H, 8.52; N, 2.82.

Synthesis of thienooxypyrroline small molecules.

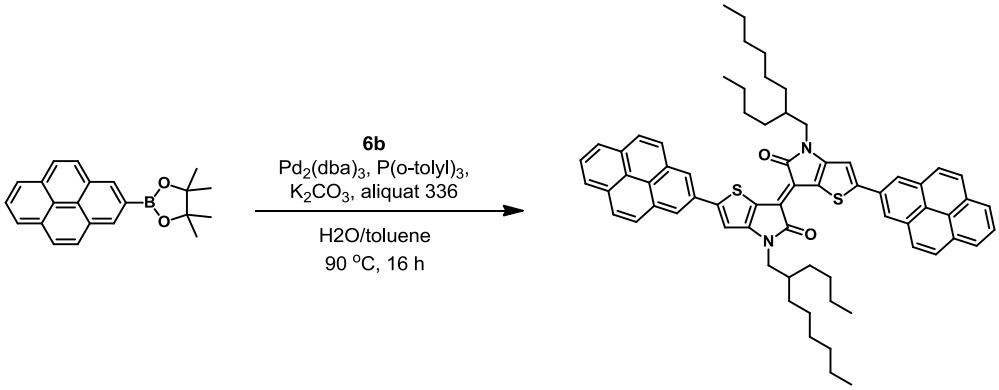

7

Bis(5-pyren-2-yl)-2-(3-oxo-4-(2-butyloctyl)thieno[3,2-b]pyrrolino-2-ylidene)-3-oxo-4-(2-butyloctyl)thieno[3,2-b]pyrroline (7): A 25 mL Schlenk tube charged with **6b** (100 mg, 0.130 mmol), 4,4,5,5-tetramethyl-2-(pyren-2-yl)-1,3,2-dioxaborolane[41] (89.6 mg, 0.273 mmol), bis(dibenzylideneacetone)palladium (2.38 mg, 2 mol %), tri-*o*-tolylphosphine (3.17 mg, 8 mol %), anhydrous K_2CO_3 (146 mg, 1.06 mmol), and 1 drop of aliquat 336 was evacuated and backfilled with nitrogen 3 times, and then toluene (2.75 mL) and water (0.5 mL) were added. The reaction mixture was placed in an oil bath preheated at 90 °C for 16 h before being precipitated into 250 mL of MeOH. The precipitates were filtered through a 20 μm nylon membrane, dissolved in chloroform, and concentrated. Purification by silica gel chromatography (1:1 hexanes:chloroform) yielded 96 mg (73%) of the desired product as a blue-green solid. ^{1}H NMR (400 MHz, C_6D_6): δ 8.45 (s, 4H), 7.97-7.94 (d, 4H), 7.83-7.74 (m, 12H), 3.92 (d, 4H), 2.20 (m, 2H), 1.53-1.36 (m, 32H), 1.03-0.97 (m, 12H). MS (FAB, *m/z*) Calcd. for $C_{68}H_{70}N_2O_2S_2$ $[M]^+$: 1010.488; found: 1010.6. Anal. Calcd. for $C_{68}H_{70}N_2O_2S_2$: C, 80.75; H, 6.98; N, 2.77; found: C, 80.78; H, 7.05; N, 2.63.

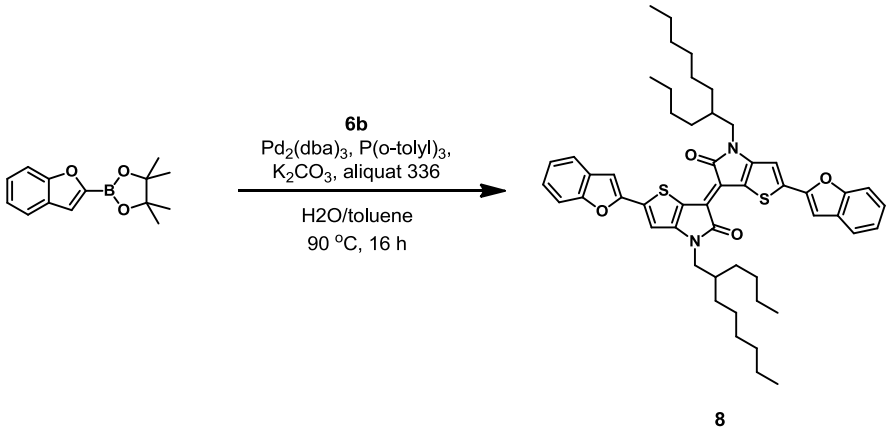

8

Bis(5-pyren-2-yl)-2-(3-oxo-4-(2-butyloctyl)thieno[3,2-b]pyrrolino-2-ylidene)-3-oxo-4-(2-butyloctyl)thieno[3,2-b]pyrroline (8): Reaction conditions and workup were the same as for **7,** except **6b** (96 mg, 0.125 mmol), 2-benzofuranboronic acid (42.3 mg, 0.261 mmol), bis(dibenzylideneacetone)palladium (2.29 mg, 2 mol %), tri-*o*-tolylphosphine (3.04 mg, 8 mol %), anhydrous K_2CO_3 (146 mg, 1.06 mmol), 1 drop of aliquat 336, toluene (2.75 mL) and water (0.5 mL) were used. Purification by silica gel chromatography (1:1 hexanes:chloroform) yielded 123 mg (84%) of the desired product as a metallic blue solid. ^{1}H NMR (400 MHz, $CDCl_3$): δ 7.60-7.57 (d, 2H), 7.51-7.48 (d, 2H), 7.32-7.25 (m, 4H), 7.15 (s, 2H), 7.07 (s, 2H), 3.76 (d, 4H),

1.98 (m, 2H), 1.37-1.27 (m, 32H), 0.93-0.86 (m, 12H). HRMS (ESI, *m/z*) Calcd. for $C_{52}H_{62}N_2O_4S_2$ $[M]^+$: 842.4146; found: 842.4167. Anal. Calcd. for $C_{52}H_{62}N_2O_4S_2$: C, 74.07; H, 7.41; N, 3.32; found: C, 73.86; H, 7.39; N, 3.54.

Synthesis of thienooxyprroline polymers.

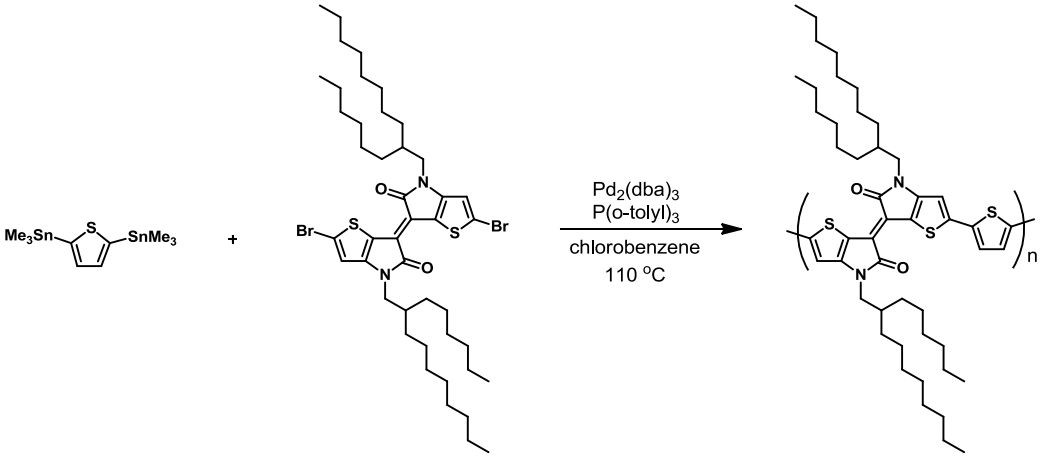

P1

PTOPT: A 25 mL Schlenk tube was charged with **6c** (133 mg, 0.151 mmol), 2,5-bis(trimethylstannyl)thiophene (61.9 mg, 0.151 mmol), and 5 mL chlorobenzene. Nitrogen was bubbled through the solution via a needle inserted through the septum for 30 min while the arm, with a stopcock in the closed position, was evacuated and backfilled with nitrogen three times. After 30 min, the stopcock was opened, the septum was removed, bis(dibenzylideneacetone)palladium (2.75 mg, 2 mol %) and tri-*o*-tolylphosphine (3.68 mg, 8 mol %) were added under positive nitrogen pressure, and a new septum was inserted. The mixture was then immediately inserted in an oil bath preheated to 90 °C. After 5 min, the temperature was increased to 110 °C for 18 h. The reaction was allowed to then cool to 55 °C, 15 mL of $CHCl_3$ was added, and the complexing ligand *N*,*N*-diethylphenylazothioformamide, a palladium scavenger, was added (4.86 mg, 20 mol %). The resulting mixture was stirred for 1 h, and precipitated into methanol (200 mL). The precipitate was filtered through a Soxhlet thimble and extracted with methanol for 2 h, hexanes for 16 h, and collected with chloroform. The chloroform solution was concentrated by evaporation, precipitated into methanol (200 mL), and filtered off as a dark solid (122 mg).

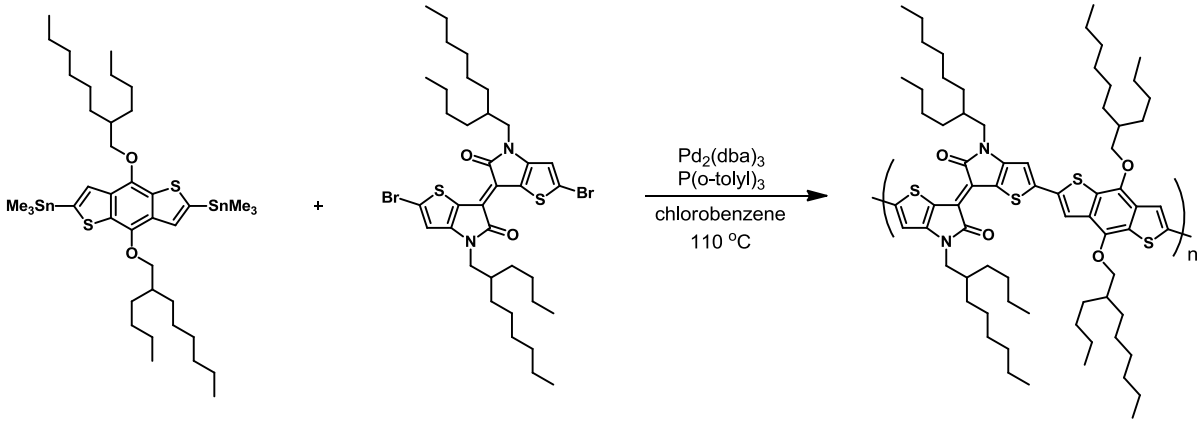

PTOPBDT: 2,6-bis(trimethylstannyl)-4,8-bis((2-ethylhexyl)oxy)benzo[1,2-b:4,5-b']dithiophene was prepared as previously described.[14,42] The same polymerization and

purification protocols as those described for **PTOPT** were followed. **PTOPBDT** was collected as a dark solid (73 mg).

References

(1) Arias, A. C. MacKenzie, J. D. McCulloch, I. Rivnay, J.; Salleo, A. *Chem. Rev*. **2010**, *110*, 3-24.
(2) Hains, A. W. Liang, Z. Woodhouse, M. A.; Gregg, B. A. *Chem. Rev*. **2010**, *110*, 6689-6735.
(3) Thompson, B. C.; Fréchet, J. M. J. *Angew. Chem*. **2008**, *47*, 58-77.
(4) Chen, H.-Y. Hou, J. Zhang, S. Liang, Y. Yang, G. Yang, Y. Yu, L. Wu, Y.; Li, G. *Nat. Photonics*. **2009**, *3*, 649-653.
(5) Blouin, N. Michaud, A. Gendron, D. Wakim, S. Blair, E. Neagu-Plesu, R. Belletête, M. Durocher, G. Tao, Y.; Leclerc, M. *J. Am. Chem. Soc*. **2008**, *130*, 732-42.
(6) Huo, L. Hou, J. Chen, H.-Y. Zhang, S. Jiang, Y. Chen, T. L.; Yang, Y. *Macromolecules*. **2009**, *42*, 6564-6571.
(7) Liang, Y. Feng, D. Wu, Y. Tsai, S.-T. Li, G. Ray, C.; Yu, L. *J. Am. Chem. Soc*. **2009**, *131*, 7792-7799.
(8) Scharber, M. C. Mühlbacher, D. Koppe, M. Denk, P. Waldauf, C. Heeger, A. J.; Brabec, C. J. *Adv. Mater*. **2006**, *18*, 789-794.
(9) Zoombelt, A. P. Fonrodona, M. Wienk, M. M. Sieval, A. B. Hummelen, J. C.; Janssen, R. A. J. *Org. Lett*. **2009**, *11*, 903-906.
(10) Mondal, R. Ko, S. Norton, J. E. Miyaki, N. Becerril, H. A. Verploegen, E. Toney, M. F. Brédas, J.-L. McGehee, M. D.; Bao, Z. *J. Mater. Chem*. **2009**, *19*, 7195-7197.
(11) Cates, N. C. Gysel, R. Beiley, Z. Miller, C. E. Toney, M. F. Heeney, M. McCulloch, I.; McGehee, M. D. *Nano. Lett*. **2009**, *9*, 4153-4157.
(12) Ma, W. Yang, C. Gong, X. Lee, K.; Heeger, A. J. *Adv. Func. Mater*. **2005**, *15*, 1617-1622.
(13) Mayer, A. C. Toney, M. F. Scully, S. R. Rivnay, J. Brabec, C. J. Scharber, M. Koppe, M. Heeney, M. McCulloch, I.; McGehee, M. D. *Adv. Func. Mater*. **2009**, *19*, 1173-1179.
(14) Piliego, C. Holcombe, T. W. Douglas, J. D. Woo, C. H. Beaujuge, P. M.; Fréchet, J. M. J. *J. Am. Chem. Soc*. **2010**, *132*, 7595-7597.
(15) Blouin, N. Michaud, A.; Leclerc, M. *Adv. Mater*. **2007**, *19*, 2295-2300.
(16) Liang, Y. Xu, Z. Xia, J. Tsai, S.-T. Wu, Y. Li, G. Ray, C.; Yu, L. *Adv. Mater*. **2010**, *22*, E135-E138.
(17) Svensson, M. Zhang, F. Veenstra, S. C. Verhees, W. J. H. Hummelen, J. C. Kroon, J. M. Inganäs, O.; Andersson, M. R. *Adv. Mater*. **2003**, *15*, 988-991.
(18) Wang, E. Wang, L. Lan, L. Luo, C. Zhuang, W. Peng, J.; Cao, Y. *Appl. Phys. Lett*. **2008**, *92*, 033307.
(19) Zhang, F. Mammo, W. Andersson, L. M. Admassie, S. Andersson, M. R.; Inganäs, O. *Adv. Mater*. **2006**, *18*, 2169-2173.
(20) Roncali, J. *Accounts Chem. Res*. **2009**, *42*, 1719-1730.
(21) Walker, B. Kim, C.; Nguyen, T.-Q. *Chem. Mater*. **2011**, *23*, 470-482.
(22) Loser, S. Bruns, C. J. Miyauchi, H. Ortiz, R. P. Facchetti, A. Stupp, S. I.; Marks, T. J. *J. Am. Chem. Soc*. **2011**, *133*, 8142-8145.
(23) Walker, B. Tamayo, A. B. Dang, X.-D. Zalar, P. Seo, J. H. Garcia, A. Tantiwiwat, M.; Nguyen, T.-Q. *Adv. Func. Mater*. **2009**, *19*, 3063-3069.
(24) Tamayo, A. B. Dang, X.-D. Walker, B. Seo, J. Kent, T.; Nguyen, T.-Q. *Appl. Phys. Lett*. **2009**, *94*, 103301.
(25) Wienk, M. M. Turbiez, M. Gilot, J.; Janssen, R. A. J. *Adv. Mater*. **2008**, *20*, 2556-2560.
(26) Zou, Y. Gendron, D. Neagu-Plesu, R.; Leclerc, M. *Macromolecules*. **2009**, *42*, 6361-6365.
(27) Bronstein, H. Chen, Z. Ashraf, R. S. Zhang, W. Du, J. Durrant, J. R. Shakya Tuladhar, P. Song, K. Watkins, S. E. Geerts, Y. Wienk, M. M. Janssen, R. A. J. Anthopoulos, T. Sirringhaus, H. Heeney, M.; McCulloch, I. *J. Am. Chem. Soc*. **2011**, *133*, 3272-3275.
(28) Zhou, E. Yamakawa, S. Tajima, K. Yang, C.; Hashimoto, K. *Chem. Mater*. **2009**, *21*, 4055-4061.
(29) Zhou, E. Wei, Q. Yamakawa, S. Zhang, Y. Tajima, K. Yang, C.; Hashimoto, K. *Macromolecules*. **2010**, *43*, 821-826.
(30) Bijleveld, J. C. Zoombelt, A. P. Mathijssen, S. G. J. Wienk, M. M. Turbiez, M. Leeuw, D. M. de; Janssen, R. A. J. *J. Am. Chem. Soc*. **2009**, *131*, 16616-16617.
(31) Allard, N. Aïch, R. B. Gendron, D. Boudreault, P.-L. T. Tessier, C. Alem, S. Tse, S.-C. Tao, Y.; Leclerc, M. *Macromolecules*. **2010**, *43*, 2328-2333.
(32) Liu, B. Zou, Y. Peng, B. Zhao, B. Huang, K. He, Y.; Pan, C. *Polym. Chem*. **2011**, *2*, 1156-1162.
(33) Mei, J. Graham, K. R. Stalder, R.; Reynolds, J. R. *Org. Lett*. **2010**, *12*, 660-663.

(34) Lei, T. Cao, Y. Fan, Y. Liu, C.-J. Yuan, S.-C.; Pei, J. *J. Am. Chem. Soc*. **2011**, *133*, 6099-6101.
(35) Stalder, R. Mei, J.; Reynolds, J. R. *Macromolecules*. **2010**, *43*, 8348-8352.
(36) Zhang, G. Fu, Y. Xie, Z.; Zhang, Q. *Macromolecules*. **2011**, *44*, 1414-1420.
(37) Wang, E. Ma, Z. Zhang, Z. Henriksson, P. Inganäs, O. Zhang, F.; Andersson, M. R. *Chem. Commun*. **2011,** *47*, 4908-4910.
(38) Lu, Z. Twieg, R. J.; Huang, S. D. *Tet. Lett*. **2003**, *44*, 6289-6292.
(39) Hennessy, E. J.; Buchwald, S. L. *J. Am. Chem. Soc*. **2003**, *125*, 12084-5.
(40) Wienk, M. M. Kroon, J. M. Verhees, W. J. H. Knol, J. Hummelen, J. C. Hal, P. A. van; Janssen, R. A. J. *Angew. Chem*. **2003**, *42*, 3371-3375.
(41) Lee, O. P. Yiu, A. T. Beaujuge, P. M. Woo, C. H. Holcombe, T. W. Millstone, J. E. Douglas, J. D. Chen, M. S.; Frechet, J. M. J. Submitted to *Adv. Mater*.
(42) Hou, J. Park, M.-H. Zhang, S. Yao, Y. Chen, L.-M. Li, J.-H.; Yang, Y. *Macromolecules*. **2008**, *41*, 6012-6018.